

Extreme winds and sea-surges in climate models

Extreme winden en stormvloed en in klimaatmodellen

(met een samenvatting in het Nederlands)

PROEFSCHRIFT

ter verkrijging van de graad van doctor aan de Universiteit Utrecht
op gezag van de Rector Magnificus Prof. dr. W.H. Gispen
ingevolge het besluit van het College voor Promoties
in het openbaar te verdedigen op
14 maart 2005 des middags te 14.30 uur

door

Hendrik Willem van den Brink

geboren op 5 januari 1974, te Amersfoort

promotor: Prof. Dr. Ir. J.D. Opsteegh
Faculteit Natuur- en Sterrenkunde, Universiteit Utrecht
co-promotor: Dr. G.P. Können
Koninklijk Nederlands Meteorologisch Instituut (KNMI), De Bilt

ISBN

This study was performed at the Royal Dutch Meteorological Institute (KNMI) in De Bilt, the Netherlands, with financial aid from the National Institute for Coastal and Marine Management (RIKZ).

Hoedanig een is Deze, dat ook de winden en de zee
Hem gehoorzaam zijn!

(Matth. 8:27)

...aan mijn Joëlla & Lilian

Contents

Introduction and Overview	1
1 The reliability of extreme surge levels, estimated from observational records of order hundred years	3
van den Brink, H.W., G.P. Können, and J.D. Opsteegh, 2003: The reliability of extreme surge levels, estimated from observational records of order hundred years. <i>Journal of Coastal Research</i> , 19 , 376–388.	
2 Uncertainties in extreme surge level estimates from observational records	27
van den Brink, H.W., G.P. Können, and J.D. Opsteegh, 2004: Uncertainties in extreme surge level estimates from observational records. <i>Philosophical Transactions of the Royal Society of London Series A</i> , in press.	
3 Statistics of extreme synoptic-scale wind speeds in ensemble simulations of current and future climate	39
van den Brink, H.W., G.P. Können, and J.D. Opsteegh, 2004: Statistics of extreme synoptic-scale wind speeds in ensemble simulations of current and future climate. <i>Journal of Climate</i> , 17 , 4564–4574	
4 Improving 10⁴-year surge level estimates using data of the ECMWF seasonal prediction system	61
van den Brink, H.W., G.P. Können, and J.D. Opsteegh, 2004: Improving 10 ⁴ -year surge level estimates using data of the ECMWF seasonal prediction system. <i>Geoph. Res. Lett.</i> , 31 , L17210, doi:10.1029/2004GL020610	
5 Estimating return periods of extreme events from ECMWF seasonal forecast ensembles	73
van den Brink, H.W., G.P. Können, J.D. Opsteegh, G.J. van Oldenborgh, and G. Burgers, 2004: Estimating return periods of extreme events from ECMWF seasonal forecast ensembles. <i>Int. Jour. of Climatology</i> , in press	

6 Increased evidence for the existence of 'superstorms'	87
Summary	97
Bibliography	101
Samenvatting	109
Dankwoord	113
Curriculum Vitae	115

Introduction and Overview

The history of The Netherlands has been influenced by floodings for many centuries. Well-known floodings are the St Elisabeth Flood (18–19 Nov 1421) and the 1953 flood (31 Jan–1 Feb 1953). By lack of knowledge about the occurrence frequency of extreme sea levels, for a long time the dike design height was taken as the largest recorded sea water level plus about one meter (Battjes and Gerritsen 2002).

Scientific research to extreme surges along the Dutch coast was largely intensified after the disastrous flooding in 1953, in which 1835 people died. Shortly after this disaster, the so-called Delta committee ('Delta commissie') was established. Its first task was to determine basic levels ('basispeilen') of the sea dikes along the Dutch coast. From economical and societal arguments the committee recommended to define this basic level to the level that has a flooding probability of 1% per century, i.e., a return period of 10^4 years (Deltacommissie 1960).

It may be clear that it is hard to find the sea water levels that correspond to such a very small probability from observational sea level records, as the latter covered only 70 years at the publication of the Report of the Delta committee in 1960 (and still a mere 100 years for the reanalysis, done by Dillingh et al. in 1993). Hence the calculations imply extrapolations over no less than two orders of magnitude in probability.

The calculations of the design heights are traditionally based on extreme value analysis. The reason for this approach is that the theory of extreme value statistics states that many distributions converge for their extremes to one of the three types of the Generalized Extreme Value (GEV) distribution (see e.g., de Haan 1976). This powerful theorem implies that the determination of extreme value distributions does not require exact knowledge about the far tail of the parent distribution. The price paid to get this theorem at work is the gigantic thinning of the data required for extreme value analysis: commonly only the largest value in each year is used. As a consequence, a large statistical uncertainty is introduced in the estimates from the short observational records.

This thesis explores the use of an alternative data source, i.e., data produced by long runs of weather- and climate models. The model records used are considerably

longer (≈ 1500 – 10000 years) than the observational records, allowing for a semi-empirical study of the statistical properties of model extremes. At the moment, the quality of the climate models has reached the level that the sea-surge output (calculated from the large-scale wind) describe the statistics of the observations correctly. This gives confidence to consider also the model results for very large return periods as faithful substitutes for real observations.

Currently, the long model records enable the examination of questions like:

- How large is the uncertainty in the surge level estimate with an exceedance probability of 10^{-4} yr^{-1} if based on the observations?
- What is the appropriate extreme value distribution to describe the surge extremes?
- Is it possible to describe the wind- and surge extremes in the extra-tropics by a single GEV distribution up to 10^4 -year return periods? Or, equivalently, is there any indication that the systems causing 10^4 -year events are of another nature ('superstorms') than those causing the moderate extremes?
- Is it possible to improve the estimates of the basic levels by use of weather- and climate models?

The exploration of these questions is the topic of this thesis.

To obtain answers to the various questions, we applied in this study three types of numerical climate models. In the chapters dealing with the first three questions, the low-resolution climate model ECBilt-Clío was used (chapters 1–3).

The potential improvement of the basic level estimate by using model data is explored with the seasonal forecasts of the European Centre for Medium-range Weather Forecasts (ECMWF). Combination of all archived seasonal forecasts results in a large data set of high quality, that is suitable for improving the 10^4 -year surge estimates (chapter 4).

Finally, in a preliminary study on the subject of wind related events, the existence of the 'superstorms', detected in chapters 1 and 3, is confirmed in ensemble experiments with the NCAR GCM (chapter 6). This result from a more sophisticated model brings the existence of 'superstorms' closer to reality.

This thesis is likely to represent only a first step in this hitherto unexplored approach to extreme value estimates. With the improvement of models and the availability of records from very long runs, more and more meteorological parameters may come in the reach of this approach. Chapter 5 gives a flavor of the spectrum of future applications of model runs in extreme value analyses.

Chapter 1

The reliability of extreme surge levels, estimated from observational records of order hundred years

Abstract

General Circulation Model-generated surges are analyzed with the Generalized Extreme Value distribution to study the uncertainty in surge level estimates with a return period of 10^4 years, derived from observational records of order hundred years.

Ensemble simulations with a total length of 5336 years were generated with the KNMI General Circulation Model ECBilt-Clio, coupled with a simple surge model to transform the wind field over the North Sea to the surge level at Delfzijl (NL). The 46 estimated surge levels with a return period of 10^4 years, calculated from sets of 116 year each, vary between 4.5 and 17 meters, with a median of 8.5 meter. The 10^4 -year estimate of the 118-year observational Delfzijl record (5.8 meter) fits well among these subsets, but this surge level is considerably lower than the median of the ensemble estimate. For an estimate of the 10^4 -year return level of the surge within an uncertainty of 10 %, a record length of about 10^3 years is required.

CO₂-doubling does not have a detectable influence on the mean wind speed over the North Sea in ECBilt-Clio. However, the model hints on the excitation of severe storms, with a frequency lower than once in 250 year. In ECBilt-Clio, these severe storms tend to dominate the 10^4 -year return value of the wind speed over the North Sea.

1.1 Introduction

Protection of the Netherlands against flooding from the sea is a matter of continuous concern. In coastal protection, a probability of 10^{-4} per year for flooding from the sea

is used as baseline (Deltacommissie 1960). The determination of the corresponding design height of the dikes requires knowledge about the tides and surges. Tides are deterministic, but surges are wind-driven, and hence stochastic.

Several problems arise when the 'accepted risk' has to be translated into the surge level being exceeded (on average) only once in 10^4 years. First, as the observational records of skew surges are only 10^2 years in length, the surge level with an average return period of 10^4 years requires an extrapolation of two orders of magnitude. It is unclear how reliable the estimate from such an extrapolation is. Second, various probability functions can be fitted to the observational records of extreme surges, leading to different results in the 10^4 -year return levels (Dillingh et al. 1993; de Haan 1990). Third, extrapolation from observational records does not contain information about surges in a greenhousegas-induced changing climate.

These problems can be explored by using a long surge record (in the order of 10^4 years) generated by a climate model. From this record, the most adequate extreme-value distribution can be determined, as well as its parameter values and the 10^4 -year surge level (within the context of the model). This most adequate distribution can then be applied to subsets of the long record, each with a time length equal to the available observational records (~ 100 years). The variation in the estimated parameter values and in the 10^4 -year surge level among the subsets provides information about the uncertainty of the estimate from the observational record.

This procedure has been applied using current climate data of the KNMI climate model ECBilt-Clio. We have concentrated on the model grid point best representing the wind field over the North Sea, and applied the surge model to the coastal station Delfzijl (NL). The effect of an increased greenhousegas concentration on extreme wind speeds is preliminary investigated.

Our study can be regarded to be complementary to studies on changing wind climate using state of the art GCMs (Kharin and Zwiers 2000; Beersma et al. 1997; Knippertz et al. 2000; Schubert et al. 1998; Hall et al. 1994). These studies have in common that they are based on output of limited length (typical 5 to 50 years), an unavoidable consequence of the complexity of these models. The limited length prevents examination of a possible change in extremes of return periods of thousands of years. In the present study, a simpler model is used, which enabled us to generate $5 \cdot 10^3$ years for the greenhouse climate at CO_2 doubling, and to explore the properties of the extreme value statistics up to return periods of 10^4 year within the context of this model, but using a meteorological parameter (surge) that is generated by a wind field of time and spatial scales comparable with the (coarse) grid distance of that model.

The paper is structured as follows: Section 1.2 describes the models used, and Section 1.3 the theoretical and experimental design. The validation of the data and

models used is given in Section 1.4. Section 1.5 gives the results, and Section 1.6 the discussion and conclusions.

1.2 Model descriptions

a. climate model

The wind data are produced by a General Circulation Model (GCM) of intermediate complexity. A GCM calculates the time evolution of a large number of weather variables on a discrete grid. For this calculation, the equations of fluid flow on a rotating earth are solved on this grid, while sub-grid physical processes are parameterized. In this way, meteorological quantities can be derived for very long periods. Because of the chaotic nature of the atmosphere, the results do not have deterministic forecast-value, but the sub-daily output does provide statistical information about the climate properties of the model.

In this study, the GCM of the KNMI, called ECBilt-Clio, was used. The atmospheric component of ECBilt-Clio is a spectral T21 global 3-level quasi-geostrophic model. The T21-resolution corresponds (for the latitudes of interest) with a grid point distance of approximately 500 km. The atmospheric time step is 4 hours. The atmospheric component of the model is coupled to a simple ocean-GCM and a thermodynamic sea-ice model. ECBilt-Clio is two orders of magnitude faster than state-of-the-art GCMs, providing the possibility of studying climate dynamics on time scales of thousands of years. For a detailed description of ECBilt-Clio we refer to Opsteegh et al. (1998, 2001).

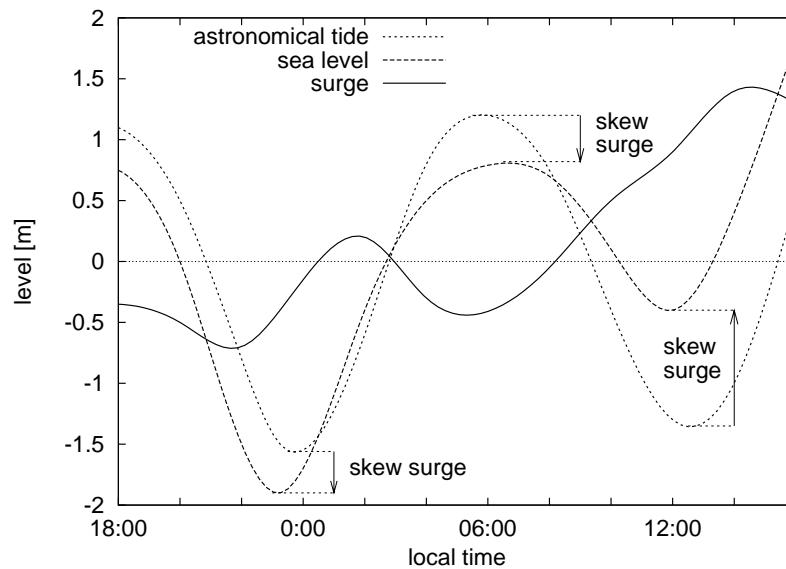
b. surge model

The sea level at a certain position and time is determined by a combination of two effects: the astronomical tide and the surge. The surge is the difference between the actual level and the astronomical tide. Neglecting resonances and other second-order effects, the surge is determined by the wind and the pressure. Whereas the astronomical tide is deterministic, the meteorological effect is stochastic.

Usually, calculated (or forecasted) surges are verified against observations of the so-called skew surge. The skew surge at high (low) tide is the difference between the astronomical high (low) tide and the observed high (low) tide. Due to hydraulic effects, the observed and astronomical high tides do not necessarily occur at the same moment (see Figure 1.1), particularly when the surges are large. Most surge models do not take this effect into account. The problems arising in the calculation of the surge from time-lagged astronomical tidal curves are bypassed by verification on

the skew surge. Usually, the high tide (rather than the low tide) skew surges are considered, restricting the number of verification moments to two per day. In practice,

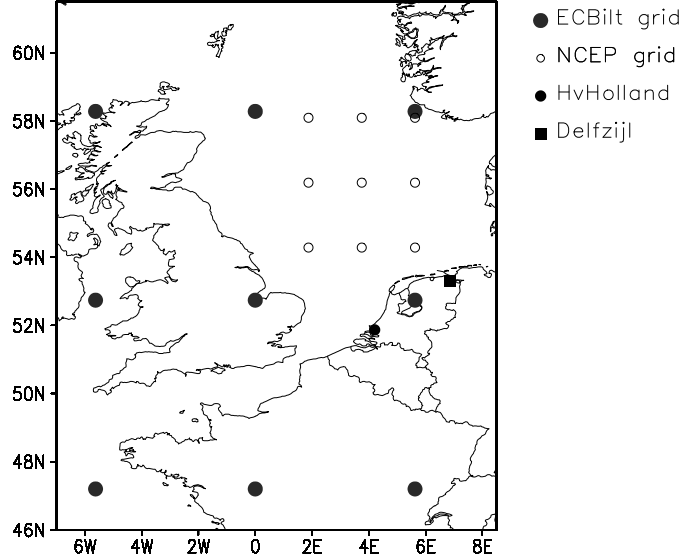
Figure 1.1: The surge (solid line) is the difference between observed sea level and astronomical tide at each moment. Due to hydraulic effects, the tidal curve may be shifted with respect to the astronomical tide. This leads to spurious effects in the surge. Surge predictions are therefore verified against the skew surge, which is the difference between the astronomical high (low) tide and the associated observed high (low) tide, which need not to take place at the same moment. In the figure the skew surges at the first low tide (0:00) and the high tide (6:00) are negative, whereas the second low tide skew surge (12:00) is positive (indicated with arrows). Shown is the situation at Delfzijl from 21 Feb 2002 18:00 to 22 Feb 2002 16:00 local time.



the observed skew surge is compared with the calculated surge for the moment of astronomical high tide. In the validation of our model, we adopted this procedure.

The relation we used to model the skew surge is based on the semi-empirical Timmerman model (Timmerman 1977). This surge model was used for many years at KNMI for operational surge forecasting. We simplified this model by neglecting time- and space-dependencies, and assuming a sinusoidal dependence on the wind

Figure 1.2: The grid points of ECBilt-Clio and NCEP. From the NCEP grid, only the grid points used for validation are shown. The Dutch coastal stations Hoek van Holland and Delfzijl are indicated.



direction. This results in the following relation for the skew surge:

$$\text{skew surge} = \gamma u^2 \cos(\phi - \beta) + \frac{1013 - p}{100.5} [m] \quad (1.1)$$

The first term is the wind effect, with u the wind speed and ϕ the clockwise wind direction with respect to north. The station-dependent parameters γ and β are determined by fitting Eq. 1.1 to the time- and space-averaged values, given by Timmerman (1977) for the station considered. For Delfzijl, $\gamma = 5.5 \cdot 10^{-3} \text{ s}^2\text{m}^{-1}$ and $\beta = 321^\circ$. So, the surge is maximal for North Western winds. For extreme surges, the second term in Eq. 1.1, which is the barometric pressure effect, is neglected, as it has a constant value of only 10 cm (see Section 1.4a.). The station pressure p is in mbar.

The surge is calculated every 12 hours from the wind averaged over the last 3 time steps (of 4 hours) of the ECBilt-Clio model. The choice for averaging over 12 hours has three reasons. First, the mean time lag between the wind over the North Sea and the surge at the coast is 6 hours, being of the same order. Second, the Timmerman model also uses time-averaged values, to incorporate the inertia of the surge phenomenon. Third, the periodicity of the tide is close to 12 hours.

Calculations are also done with the NCEP reanalysis wind data. Figure 1.2 shows the ECBilt-Clio and NCEP grid points.

We found that, for our experimental set-up, the intermediate complexity of ECBilt-Clio lends itself optimally to the calculation of the 10^4 -year surge level, as on the one hand ECBilt-Clio is fast enough to generate thousands of years of wind data, and on the other hand it provides the large-scale wind, which drives the surge.

1.3 Methodology

a. Generalized Extreme Value distribution

We applied the Generalized Extreme Value (GEV) distribution to the set of annual maxima of the surge and the wind speed to describe the statistical properties of the extremes. The distribution of normalized extremes approaches asymptotically to this GEV distribution (see e.g. de Haan (1976), Galambos (1978) and Kotz and Nadarajah (2000)), which is described analytically by:

$$F(y) = e^{-e^{-x}} \quad (1.2)$$

where x is a substitute for:

$$x = \ln \left(1 - \frac{\theta}{\alpha}(y - \mu) \right)^{-1/\theta} \quad (1.3)$$

with μ the location parameter, α the scale parameter, θ the shape parameter, and y the variable considered (Jenkinson 1955). These parameters are indicated in Figure 1.3. Depending on the sign of θ , 3 types are distinguished:

1. $\theta = 0$; The Gumbel or Fisher-Tippett I distribution
2. $\theta < 0$; The Fisher-Tippett II distribution, having a lower limit
3. $\theta > 0$; The Fisher-Tippett III distribution, with an upper limit

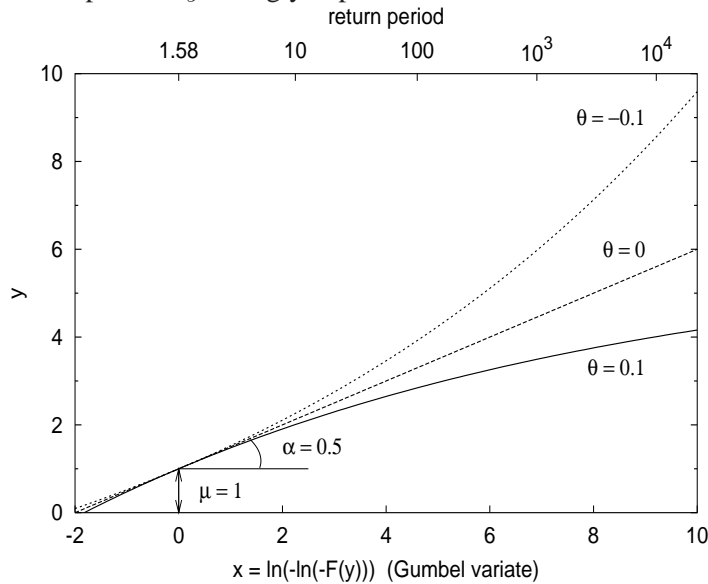
For the Gumbel distribution ($\theta = 0$), Eq. (1.3) can be simplified to:

$$x = \frac{y - \mu}{\alpha} \quad (1.4)$$

The probability of exceedance of a certain level is usually expressed in terms of the return period T . The *return period* T is the average number of years between two succeeding exceedances of the corresponding *return level* y :

$$T(y) = \frac{1}{1 - F(y)} = \frac{1}{1 - e^{-e^{-x}}} \quad (1.5)$$

Figure 1.3: The parameters of the GEV distribution. The location parameter μ is the value corresponding with $x = 0$ and $T = 1.58$. The scale parameter α is the slope at $x = 0$, and the shape parameter θ is the curvature. For large return periods, y strongly depends on θ .



Plotting y against the Gumbel variate $x = -\ln(-\ln(F(y)))$ (a so-called Gumbel plot) will result in a straight line if the distribution obeys the Gumbel distribution, or in a curved line - convex for type II and concave for type III (see Figure 1.3). For a more comprehensive description we refer to Kotz and Nadarajah (2000).

An estimate of $F(y)$ is obtained by using the ordered extremes $y_1 \leq y_2 \leq \dots \leq y_n$. The n extremes divide the total range between 0 and 1 into $n + 1$ equally spaced intervals, and thus $E\{F(y_i)\} = i/(n + 1)$ (van Montfort 1969). We used the slightly different (unbiased) estimate $E\{F(y_i)\} = (i - 0.35)/n$ (Hosking et al. 1985). Convergence of extremes to the GEV distribution can be regarded as an analogue of the well-known central limit theorem. The central limit theorem states that under very general conditions the distribution of the sample mean converges to the normal distribution as the sample becomes large; the limit represented by Eq. 1.2 holds for the extremes of large samples.

To determine the distribution of the extremes, usually the annual maxima are taken. However, this is only a good choice if the number of independent realizations within the sampling period (one year) can be considered as asymptotically large, the extremes are independent and identically distributed. As Cook (1982) shows,

one may expect that the squared wind speed converges faster than the wind speed itself to the GEV distribution. This assumes a fast convergence for the surge (as it is proportional to u^2).

The method of Probability Weighted Moments was used for estimating the three parameters. The covariance matrix of the estimated parameters is given by Hosking et al. (1985), from which the uncertainty in \hat{y} (i.e. the estimated value of y) was estimated by use of the following estimator:

$$\begin{aligned} \sigma^2(\hat{y}_T) = & \left(\frac{\partial y}{\partial \mu}\right)^2 \sigma^2(\hat{\mu}) + \left(\frac{\partial y}{\partial \alpha}\right)^2 \sigma^2(\hat{\alpha}) + \left(\frac{\partial y}{\partial \theta}\right)^2 \sigma^2(\hat{\theta}) \\ & + 2 \frac{\partial y}{\partial \mu} \frac{\partial y}{\partial \alpha} \sigma(\hat{\mu}, \hat{\alpha}) + 2 \frac{\partial y}{\partial \mu} \frac{\partial y}{\partial \theta} \sigma(\hat{\mu}, \hat{\theta}) + 2 \frac{\partial y}{\partial \alpha} \frac{\partial y}{\partial \theta} \sigma(\hat{\alpha}, \hat{\theta}) \end{aligned} \quad (1.6)$$

with $\sigma^2(\hat{\mu})$ variance of $\hat{\mu}$ and $\sigma(\hat{\mu}, \hat{\alpha})$ the covariance between $\hat{\mu}$ and $\hat{\alpha}$. The derivatives of y follow from the inverse of Eq. 1.3:

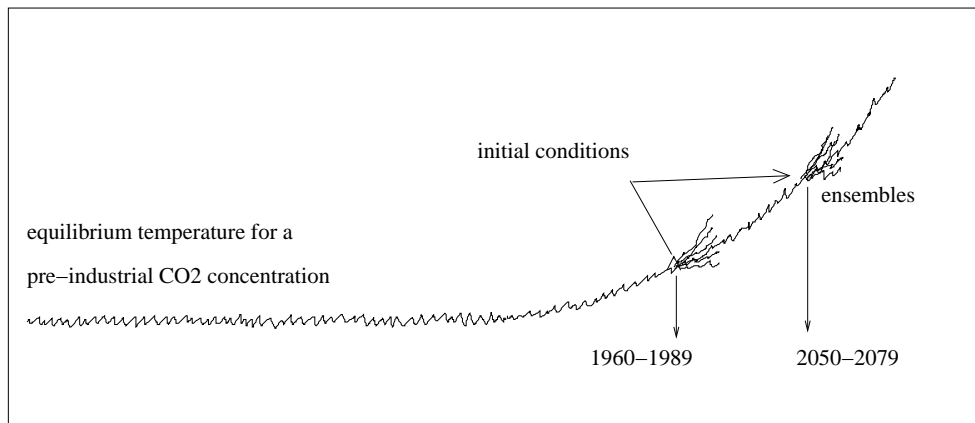
$$y_T = \mu + \frac{\alpha}{\theta} (1 - e^{-\theta x}) \quad (1.7)$$

and are evaluated at $(\hat{\mu}, \hat{\alpha}, \hat{\theta})$ for a given return period T .

b. Set-up of the numerical experiment

184 runs of 30 years each were generated, with a CO₂ concentration according to the period 1960-1989. This is called the 'control run'. For each of these ensemble runs, the same initial condition is used for the ocean and the atmosphere except for a random perturbation in the initial potential vorticity field of the atmosphere. This leads to different realizations after several days and hence to other 30-year series representative of the 1960-1989 period (see Figure 1.4). With the control run, we tested the uncertainty in the extrapolation of the extreme surges for Delfzijl. This was done by deriving the annual extremes from each year, hence one event per year. To ensure independence of the extreme events in two consecutive years, the annual periods run from 1 July to 30 June, giving 29 extremes per ensemble member, and 5336 extremes for the control run. The statistical analysis was performed in three steps: First, the GEV distribution was applied to the total set of 5336 years. From this is was determined whether the full set of the annual surge extremes could be described by a Gumbel distribution ($\theta = 0$) or a GEV distribution with $\theta \neq 0$. Second, the GEV distribution was fitted to the 46 subsets of 116 years each, as the same was done with the observational (118 year) Delfzijl surge record. Third, all 46 estimated 10⁴-year surge levels, and the estimate of the observations, are compared with the estimate of the total set.

Figure 1.4: Generating 30-year ensemble runs for two initial conditions. To create the ensembles, small perturbations were applied to the initial conditions. The one set corresponds to observed CO₂ concentrations during 1960-1989 and make the control run, and the other to projected values for 2050-2079, making the greenhouse run.



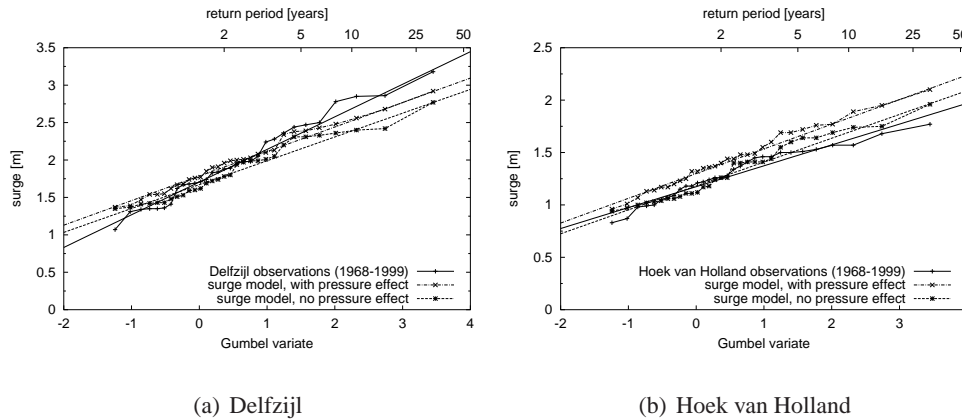
Besides the control run, we also generated ensemble runs of 30 year with estimated CO₂ concentrations according to the period 2050-2079 (following the SRES A1 CO₂ emission scenario (Nakicenovic et al. 2000)). This emission scenario results in approximately doubled CO₂ concentration in 2050-2079 (620 ppm on average) with respect to the control run (320 ppm). This ensemble is called the 'greenhouse run'. Like the control run, it has a total length of 5336 years. We compared the full greenhouse run with the full control run to investigate a possible influence of increased greenhousegas concentrations on the wind climate over the North Sea.

1.4 Validation of surge model and ECBilt-Clio

a. Wind and surge

For verification of the surge model, we used the reanalysis dataset of the National Center of Environmental Prediction (NCEP), USA (Kalnay et al. 1996). This dataset provides the weather variables on a global 2.5° x 2.5° grid every 6 hours from 1948 up to the present. The NCEP wind at 10 meter is not a directly measured quantity, but derived via a dynamical atmospheric model from the surface pressure and upper layer measurements. The grid point value is representative of the area around the grid

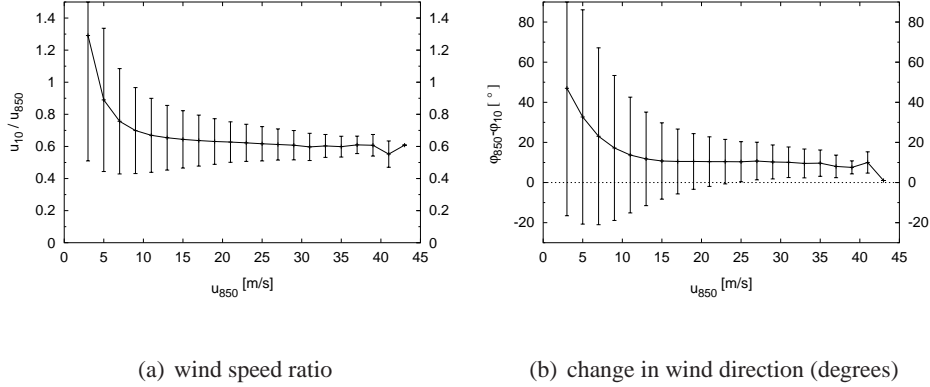
Figure 1.5: Gumbel plots for the surge in Delfzijl (a) and Hoek van Holland (b), calculated with the surge model (Eq. 1.1) from the average wind in the North Sea representing NCEP grid points, with and without the local pressure effect. Used is the period 1968-1999. The thick lines represent the fit to the observations.



point. We verified the statistics of the NCEP wind with the statistics of Dutch coastal stations. It was found that the differences in the distribution of the daily mean wind speed and direction in winter according to the (3.75E,52.4N) NCEP grid point and the average of two Dutch coastal stations (Hoek van Holland and Vlissingen, both within the area of this NCEP grid point) were not larger than the differences between the stations itself. We conclude that the NCEP wind data is good enough to rely on for this study.

The validity of the surge model is tested for Delfzijl and Hoek van Holland by feeding Eq. 1.1 with the 12-hourly NCEP wind averaged over 9 grid points over the North Sea (indicated with open circles in Figure 1.2). These 9 grid points in NCEP cover the same area as a single grid point in ECBilt-Clio (bold dots in Figure 1.2). The Gumbel distribution was applied to the computed annual (July-to-July) surge extremes, and compared with the distribution of the observed extremes. Both records cover the period 1968-1999. Figure 1.5 shows that, despite all simplifications, the surge model correctly estimates the parameters of the fitted Gumbel distribution. Illustrative is the fact that the model indicates for more than 50 % of the years the correct day at which the annual maximum occurred. Figure 1.5 also shows that the effect of pressure on the extreme surges has indeed a constant value of only 10 cm throughout the entire range of the extremes. This justifies the neglect of the pressure effect in Eq. 1.1.

Figure 1.6: Ratio of the wind speed at 10 m u_{10} to that at 850 hPa level u_{850} (a) and change in wind direction ϕ (b) over sea for the surge-relevant wind directions, for Northern mid-latitudes as derived from NCEP data. The bars indicate the estimated standard deviations.



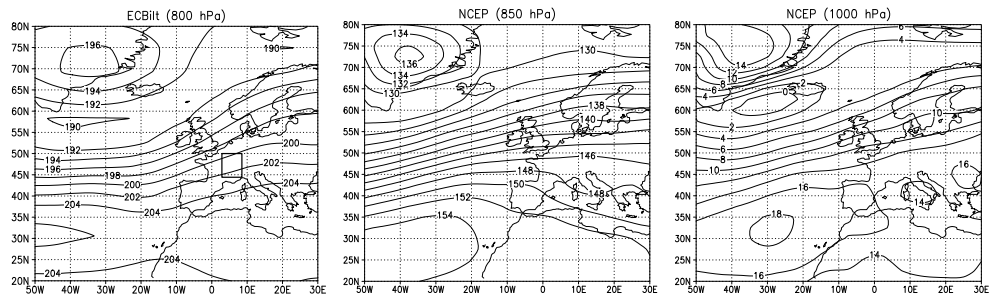
b. ECBilt-Clio winds

The lowest level of the ECBilt-Clio output is 800 hPa (corresponding with a mean height of 2 km), whereas the surge model assumes 10 meter winds. With the NCEP dataset, we empirically studied the relation between these winds by considering the relation at all NCEP ocean grid points between 40° and 60° North for daily-averaged winds. Figure 1.6(a) shows the relation between the wind speed at 850 hPa u_{850} and the wind speed ratio u_{10}/u_{850} for the winds between West and North (the relevant directions for positive surges). Figure 1.6(b) gives the difference in the wind direction between those levels. Both figures indicate a constant value for $u_{850} > 15$ m/s. This constant is 0.6 for the wind speed ratio and 10° for the difference in wind direction, in accordance with Garratt (1992). From this we conclude that the use of 800 hPa winds instead of 10 meter winds does not influence the shape parameter θ of the GEV distribution, but only the location parameter μ and the scale parameter α .

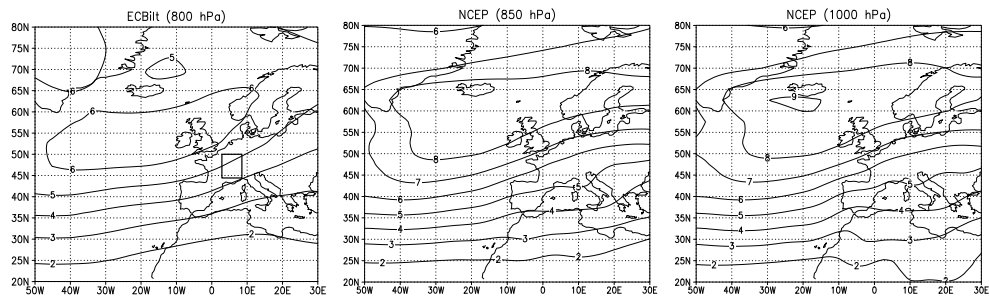
Figure 1.7(a) shows the mean geopotential height-field over Europe in winter (Dec-Mar), both for the ECBilt-Clio model at 800 hPa and for the NCEP data at 850 hPa and 1000 hPa. There is fair agreement between the ECBilt-Clio 850 hPa pattern and the NCEP 1000 hPa pattern, except that the ECBilt-Clio pattern is shifted to the south over $5-10^\circ$. This shift, which is also visible in the standard deviation of the geopotential height (Figure 1.7(b)), suggests that the wind field over the North Sea is better represented in ECBilt-Clio by a somewhat more southerly grid point than

by the actual North Sea grid point. Therefore, in our study of surges from the North

Figure 1.7: Mean geopotential height over Europe in winter (Oct-Mar) according to a 30-year run of ECBilt-Clio at 800 hPa for the control climate, and 30 years of NCEP data at 850 hPa and 1000 hPa (a), with the standard deviation for ECBilt-Clio and NCEP (b). The path of the maximum standard deviation is an indicator of the location of the storm track. The grid box in ECBilt-Clio, best representing the wind field over the North Sea, is indicated.



(a) geopotential height (dam) for ECBilt-Clio at 800 hPa and NCEP at 850 hPa and 1000 hPa



(b) standard deviation of the geopotential height (dam) for ECBilt-Clio at 800 hPa and NCEP at 850 hPa and 1000 hPa

Sea we considered the grid point (6E,47N), indicated in the ECBilt-Clio pictures of Figure 1.7 (see also Figure 1.2). The fact that this grid point is over land is assumed to be of minor importance, as the ECBilt-Clio wind is at 800 hPa, and at that level boundary layer effects can be neglected.

Figure 1.8: Comparison between the considered ECBilt-Clio grid point and the North Sea representing NCEP area for the wind speed (a) and the direction (threshold 10 m/s) (b). The wind speed distribution is represented as a Weibull plot. Considered is the winter season (Oct-Mar).

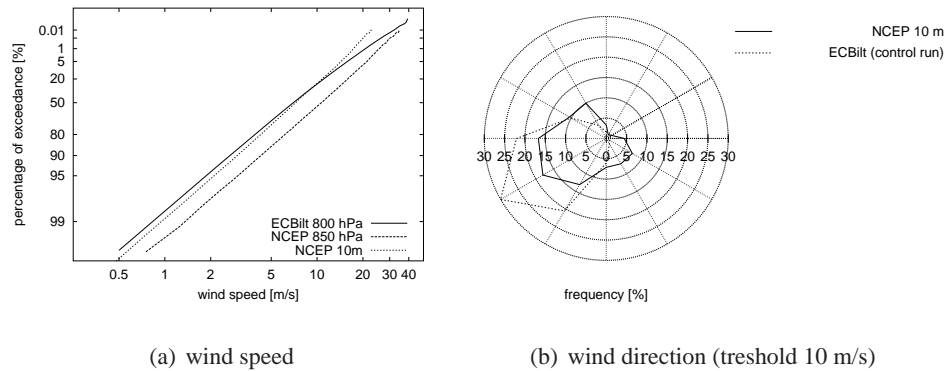


Figure 1.8(a) compares the distribution of the 800 hPa wind speed and direction (threshold 10 m/s) for this ECBilt-Clio grid point of interest (Figure 1.7) with the North Sea representing NCEP area at 10 meter (open circles in Figure 1.2). The distribution of the wind speed is represented as a Weibull plot, which results in a straight line if the distribution is described by the Weibull distribution: $F(u) = 1 - \exp(-u/a)^k$. The agreement with the NCEP wind speed is good for the wind up to 10 m/s, but deviates for larger wind speeds. This deviation will lead to a larger location and scale parameter of the GEV distribution in ECBilt-Clio. The agreement in direction distributions is less, although the effect of the discrepancy on the surge in Delfzijl (determined by North Western winds) is small. This discrepancy does not play a role in the investigation of the wind speed.

We conclude from this evaluation that the combination ECBilt-Clio-surge model seems adequate for the purpose of this study, i.e. to explore the uncertainties that are inherent to the determination of 10^4 -year return levels from observational series of 10^2 -year length.

1.5 Results

a. Uncertainty of estimated surge levels

Figure 1.9 shows the Gumbel plot of the 5336 annual surge extremes of the control run, as calculated from the ECBilt-Clio winds by the surge model. The distribution of the annual surge extremes can be described by the Fisher-Tippett II GEV distribution (upward curved, $\theta < 0$), although the largest extremes fluctuate considerably around the fitted line. Up to a return period of 10 years, the extreme surges from ECBilt-Clio correspond well with those of the 1881-1999 observational record of Delfzijl. However, the estimated 10^4 -year return level from ECBilt-Clio is considerably higher (8.5 m) than from the observational record (5.8 m). This is mainly due to the difference in estimated shape parameters θ (the values are given in Table 1.1 on page 21). Figure 1.9 clearly indicates that a GEV distribution ($\theta \neq 0$) rather than a Gumbel distribution is required to describe accurately the annual surge extremes in ECBilt-Clio for the grid point of interest.

Figure 1.9: Gumbel plots and fits of the surges for the 5336-year control run in ECBilt-Clio for the North Sea representing grid point (6E,47N) and for the observational record in Delfzijl (118 years). Both the GEV and the Gumbel distribution are fitted to the control run.

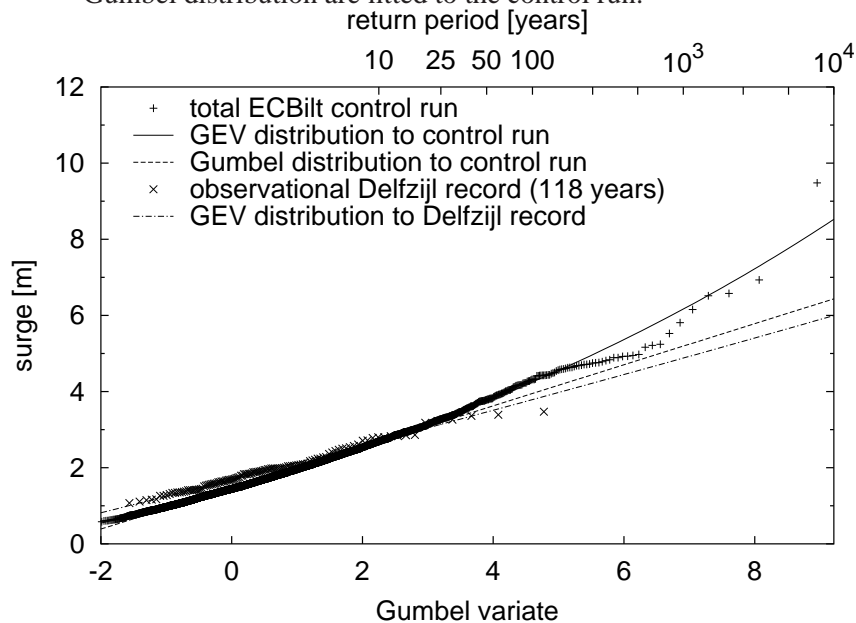


Figure 1.10: Histograms of the estimated GEV parameters θ , α and μ from the 46 sets of 116 years each from the control run. The arrows indicate the estimates from the 1881-1999 observational set of Delfzijl.

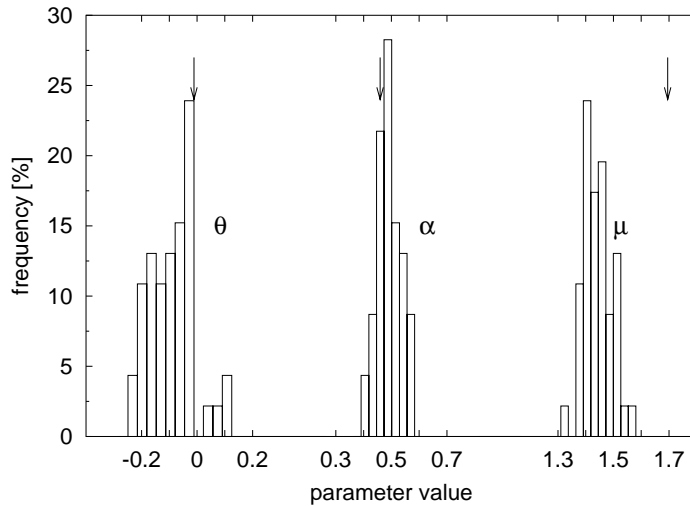
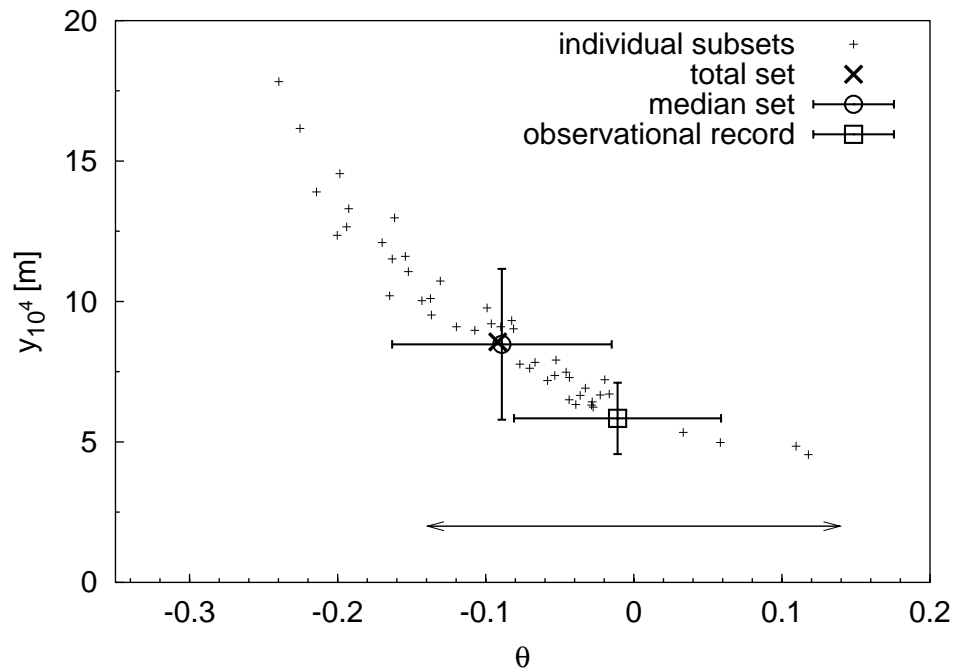


Figure 1.10 shows the histograms of the estimated parameters of the GEV distribution of surges in Delfzijl from all 46 subsets of 116 years of the control run. The mean estimate of the location parameter μ is about 25 cm too low, compared with the observations, which can partly be attributed to the neglect of the pressure effect for the ECBilt-Clio extremes. The other parameters of the observational record are in the range of the ECBilt-Clio parameters. Noticeable is the wide range in estimated parameters - clearly an effect of sampling. The influence of θ on the estimated 10^4 -year return level is depicted in Figure 1.11, which shows for all 46 subsets the estimated 10^4 -year surge level y_{10^4} as a function of the shape parameter θ . The wide range in θ results in estimated return levels between 4.5 and 17 meters, with an average of 9.2 meter, and a standard deviation of 3.1 meter. These values correspond well with those for the median set ($y_{10^4} = 8.5 \pm 2.7$ m) and the total set ($y_{10^4} = 8.5 \pm 0.4$ m), using Eq. 1.6 for estimating the standard deviations.

The observational record fits well in the plot, suggesting that this record can be regarded as a realistic subset among all other subsets.

Although Figure 1.9 indicated that the Gumbel distribution ($\theta = 0$) is not able to describe adequately the annual surge extremes, for 70% of the subsets the hypothesis $H_0: \theta = 0$ is not rejected (at 5% level, according to Hosking et al. (1985)). For most of these situations, the 10^4 -year surge level will be underestimated, giving an average

Figure 1.11: The estimated 10^4 -year return level for the surge as a function of the corresponding θ , together with the estimate from the total control run of 5336 years, and the estimate from the 1881-1991 observational set of Delfzijl, with its standard deviations of θ and the 10^4 -year surge level according to Eq. 1.6. Also shown is the median set for y_{10^4} . The arrow indicates the range for which the hypothesis $H_0: \theta = 0$ for the subsets is not rejected (5% level).



estimate of 8.3 meter instead of 9.2 meter.

In order to find the length of the record required to estimate the 10^4 -year surge level of 8.5 m with an accuracy of 1 meter, we extended two subsets until their estimated 10^4 -year surge levels differed no more than 2 meter. As Figure 1.12 shows, in this case the record length should be larger than 10^3 years for an accuracy of 1 meter in the 10^4 -year surge level estimate. Note that also the required record length depends on θ . This dependence is shown in Figure 1.13 for a relative uncertainty $\frac{\sigma(y_{10^4})}{y_{10^4} - \mu}$ of 10 %. This relative uncertainty is independent of α and μ .

We conclude that the uncertainty in the estimate of the 10^4 -year surge level from a record of 10^2 years is mainly determined by the uncertainty in the shape parameter θ .

Figure 1.12: Estimated surge level as a function of the number of years in the data set used for the fit. Shown are two independent realizations from the control run. The estimated value from the total run of 5336 years (8.5 m) is indicated by a solid line. An estimate with an uncertainty of 1 m (dashed lines) requires a record length of order 1000 years.

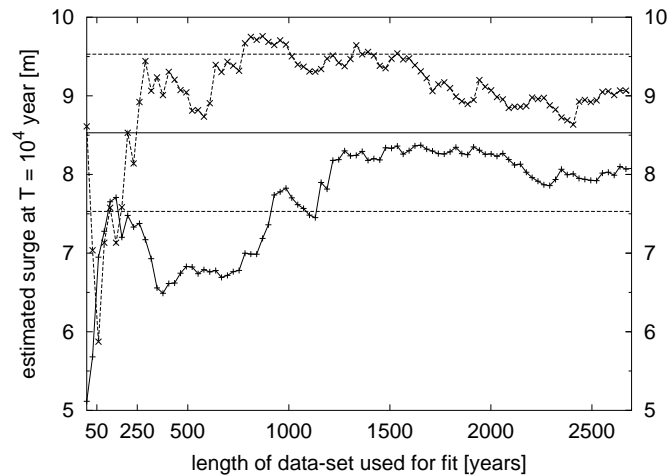


Figure 1.13: Required record length as a function of the shape parameter θ for a relative uncertainty $\frac{\sigma(y_{10^4})}{y_{10^4} - \mu}$ of 10 %, according to Eq. 1.6. The vertical scale is logarithmic. The required record length decreases quadratically with the relative uncertainty.

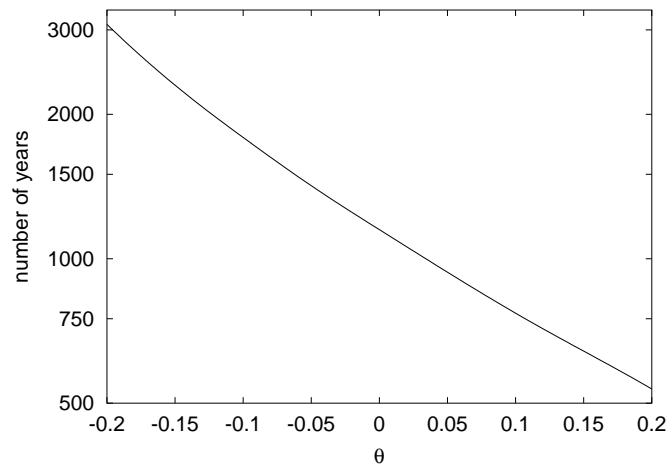
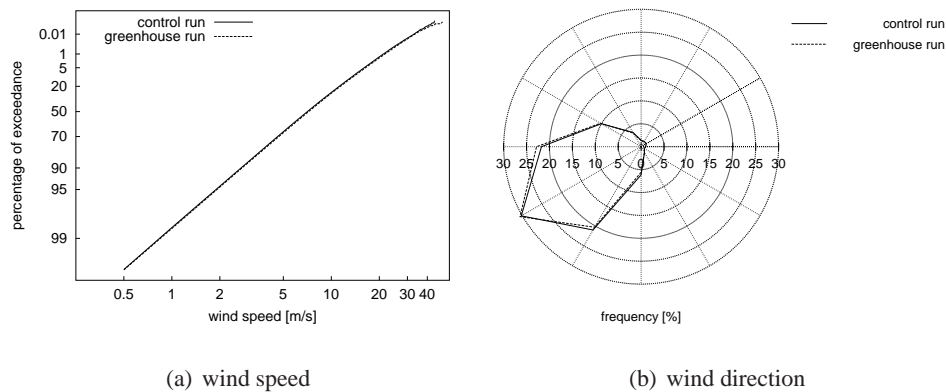


Figure 1.14: Distributions for the wind speed (a) and the wind direction (b) for the control run and the greenhouse run for the North Sea representing ECBilt-Clio grid point (6E,47N).



This uncertainty stems from sampling effects, and leads to an uncertainty of a factor two in the 10^4 -year surge level if determined from the observational record. In practice, a record of order thousand years is required for an uncertainty of 10 %.

b. Greenhouse effect on surge and wind

Figure 1.14(a) shows a Weibull plot of the distributions of the wind speed for the control run and the greenhouse run for the North Sea representing grid point in ECBilt-Clio (6E,47N). The distributions are virtually identical. The distributions of the wind direction are depicted in Figure 1.14(b). There is a slight increase in westerly- and a decrease in southerly winds, resulting in increasing frequency of positive surge in Delfzijl.

Table 1.1 compares the parameters of the GEV distributions for the control run and the greenhouse run and the corresponding 10^4 -year surge and wind levels. Figure 1.15 and Table 1.1(a) show an increase in the location parameter μ of 8 %, and in the scale parameter α of 6 % for the surge. The shape parameter θ remains unchanged. This results in an increase of the 10^4 -year surge level of 0.6 meter; this increase is not statistically significant at the 5 % level.

The influence of the greenhouse climate on the extreme wind speed is shown in Figure 1.16 and Table 1.1(b). Following Cook (1982), the GEV distribution is fitted to u^2 . Like as for the surge, also for the extreme wind speed the location parameter μ

Figure 1.15: Gumbel plots and fits of the surges for the 5336-year control- and greenhouse runs in ECBilt-Clio for the North Sea representing grid point (6E,47N).

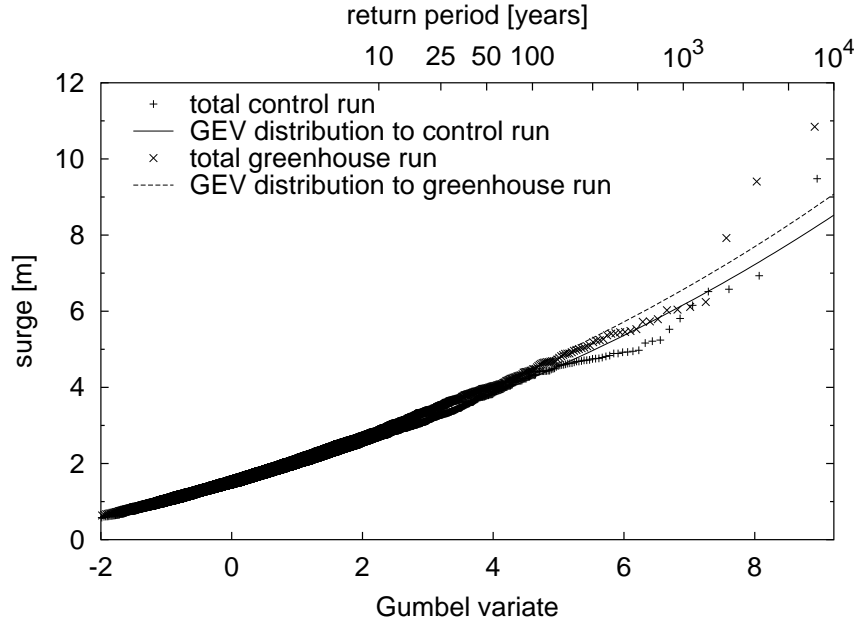


Table 1.1: GEV-parameters for the fits to the surge (a) and wind speed (b), with the estimated 10^4 -year levels and their uncertainty according to Eq. 1.6 for the North Sea representing grid point (6E,47N) in ECBilt-Clio and for the observational record of Delfzijl. See Section 1.6a for comments on the uncertainty of the observational record.

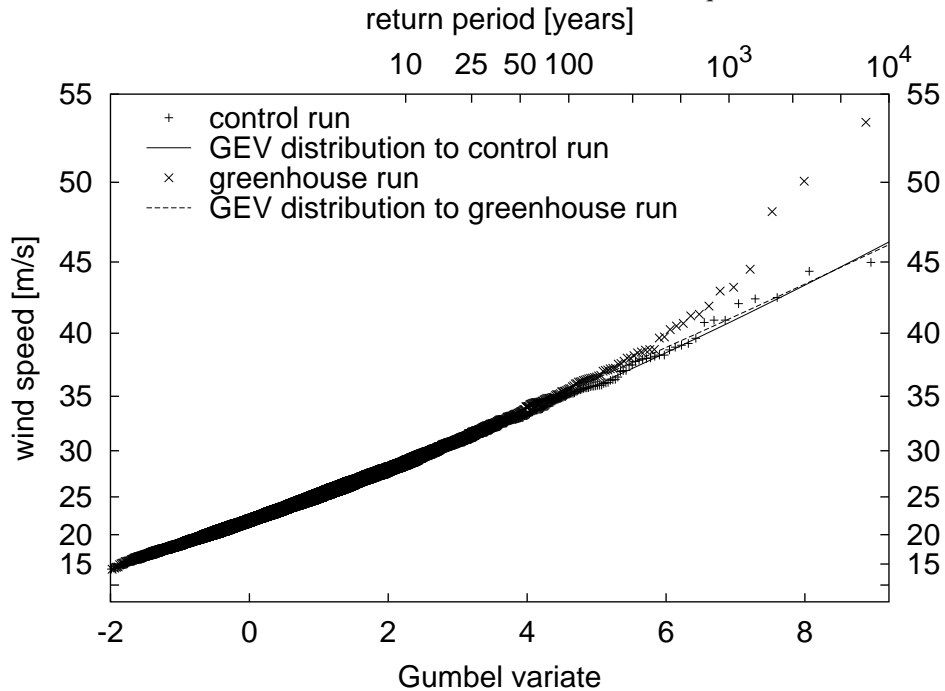
	μ [m]	α [m]	θ [-]	10^4 -year surge [m]
control run	1.45 ± 0.01	0.49 ± 0.01	-0.091 ± 0.01	8.5 ± 0.4
greenhouse run	1.57 ± 0.01	0.52 ± 0.01	-0.092 ± 0.01	9.1 ± 0.4
Delfzijl record	1.69 ± 0.05	0.43 ± 0.03	-0.011 ± 0.07	5.8 ± 1.3

(a) surge

	μ [m^2s^{-2}]	α [m^2s^{-2}]	θ [-]	10^4 -year wind [m/s]
control run	462 ± 2	140 ± 2	-0.069 ± 0.01	47.5 ± 1.0
greenhouse run	493 ± 2	149 ± 2	-0.053 ± 0.01	47.6 ± 1.0

(b) wind speed (fitted to u^2)

Figure 1.16: Gumbel plots and fits of the 12-hourly averaged wind speed for the control- and greenhouse runs in ECBilt-Clio for the North Sea representing grid point (6E,47N). The kink at a return period of 250 years in the greenhouse run suggests the presence of a double population in the extreme wind distribution. The vertical scale is quadratic.



and the scale parameter α increase, both with 6 %. The (not significant at 5 % level) decrease of the shape parameter θ cancels the increase due to μ and α for a return period of 10⁴ years.

Figure 1.16 shows for the greenhouse run a systematic deviation with respect to the fitted distribution for wind speeds with return periods more than 250 years. The kink in the graph, caused by severe events, suggests the existence of a second population in the extreme wind distribution. The fit to the total set is not influenced by these severe events, due to the large number of points before the kink. However, if the sampling period is increased from one year to a century, the parameters of the GEV distribution are predominantly determined by these severe events. Extrapolating from this severe-events-dominated GEV distribution results in a considerably higher 10⁴-year return value for the wind speed than extrapolation of the total set of annual extremes.

1.6 Discussion and conclusions

a. Uncertainty in extrapolation

The climate model ECBilt-Clio indicates that the surge extremes of the control climate can be described with a GEV distribution up to the return period of interest: 10^4 years. However, the estimates from 46 records of 116 years (like in the observational record) vary between half and twice the median value. This range is also obtained for neighboring grid points, indicating that only a crude estimate can be made with a single record of order hundred years.

For a practical useful uncertainty range of about 10 %, one needs 10^3 years of surge extremes. To improve the confidence in the absolute value of the calculated return level, a more complex General Circulation Model has to be used to generate 10^3 years of data for a realistic estimate of the 10^4 -year return level of the surge.

Our results suggest that the observational record can be regarded as a realistic subset among all other subsets (Figure 1.10). The considerable lower estimate of the uncertainty range for the observational record ($\sigma(y_{10^4}) = 1.3$ m) than for the ECBilt-Clio median set ($\sigma(y_{10^4}) = 2.7$ m) is caused by the non-linearity of the of y_{10^4} with respect to θ . In the situation of small records (making $\sigma(\theta)$ large) and large return periods (making $\frac{\partial y}{\partial \theta}\sigma(\theta)$ dominant over $\frac{\partial y}{\partial \mu}\sigma(\mu)$ and $\frac{\partial y}{\partial \alpha}\sigma(\alpha)$), a better uncertainty estimate is obtained by determining the upper and lower bounds as $y(\hat{\mu}, \hat{\alpha}, \hat{\theta} - 2\sigma(\hat{\theta}))$ and $y(\hat{\mu}, \hat{\alpha}, \hat{\theta} + 2\sigma(\hat{\theta}))$ respectively. Estimating the uncertainty interval in this way results for the observational record of Delfzijl in an upper bound of 9.2 m, against 8.4 m according to Eq. 1.6. Monte Carlo simulation gives 9.4 m for the parameters of the observational record. So, Eq. 1.6 underestimates the upper bound of the estimated return level in the situation of short records and large return periods.

The different extrapolation methods, applied to the record for Delfzijl in Dillingh et al. (1993) show a mutual difference of not more than 10 %, whereas the estimates from different records differ up to 200 %. This indicates that the method used for extrapolation is of minor importance with respect to accuracy than the representativity of the underlying dataset.

b. Convergence rate to GEV distribution

In this paper we fitted the GEV distribution to the surge and to u^2 . However, it is not known beforehand if these variables are the best choices with respect to their convergence rate to the asymptotic distribution. While theory shows that (for any $k > 0$) the extremes of the Weibull distribution $F(u) = 1 - \exp(-u/a)^k$ converge asymptotically to the Gumbel distribution (Embrechts et al. 1997), the convergence rate depends on k . Fast convergence is expected if one fits u^k , with k derived from

the tail of wind speed (practically: u larger than Weibull constant a). The reason is that this transforms the Weibull distribution into an exponential distribution, which has a fast convergence to the Gumbel distribution. We therefore recommend to fit u^k , where k can be obtained from Weibull analysis. If a different power n is chosen, then incomplete convergence (due to the finite series length) may result in an over-estimation of θ if $n < k$ and vice versa.

The Weibull distribution of the wind (Figure 1.14) suggests that in the tail $k \sim 1.5$, which is somewhat smaller than the $k=2$ -value proposed by Cook (1982). This implies that for wind $u^{1.5}$, or equivalently for surge $y^{0.75}$, has to be extrapolated to get optimal convergence. The incomplete convergence due to the choice u^2 leads to a θ -estimate that is too small. The results on the 10^4 -year level are a 3 % smaller wind speed and a 6 % smaller surge.

We advise a careful evaluation of the variable to be fitted to obtain fast convergence to the expected extreme value distribution. In any case, one should be careful to interpret $\theta > 0$ as the result of an upper limit, as long as the level of convergence is unclear.

c. Severe events

ECBilt-Clio hints on the excitation of 'superstorms' in the greenhouse climate, defined as storms with more extreme winds than expected from extrapolation of less extreme events. If these severe events are real, and if they are part of a second population that becomes apparent for high return periods only, than the kink at a return period of ~ 250 year in the Gumbel plot of Figure 1.16 means that these 'superstorms' dominate the extreme value statistics at frequencies lower than once in 250 years.

It is tempting to find an interpretation for these superstorms. Preliminary analysis indicates that a part of them may originate from the amalgamation of two precursor cyclones. Cyclogenesis by Wave-Merging is regularly observed above North America (Gaza and Bosart 1990) but seem rarer above Europe. Merging cyclones are known to result in extreme winds and core pressures (Hakim et al. 1995a,b).

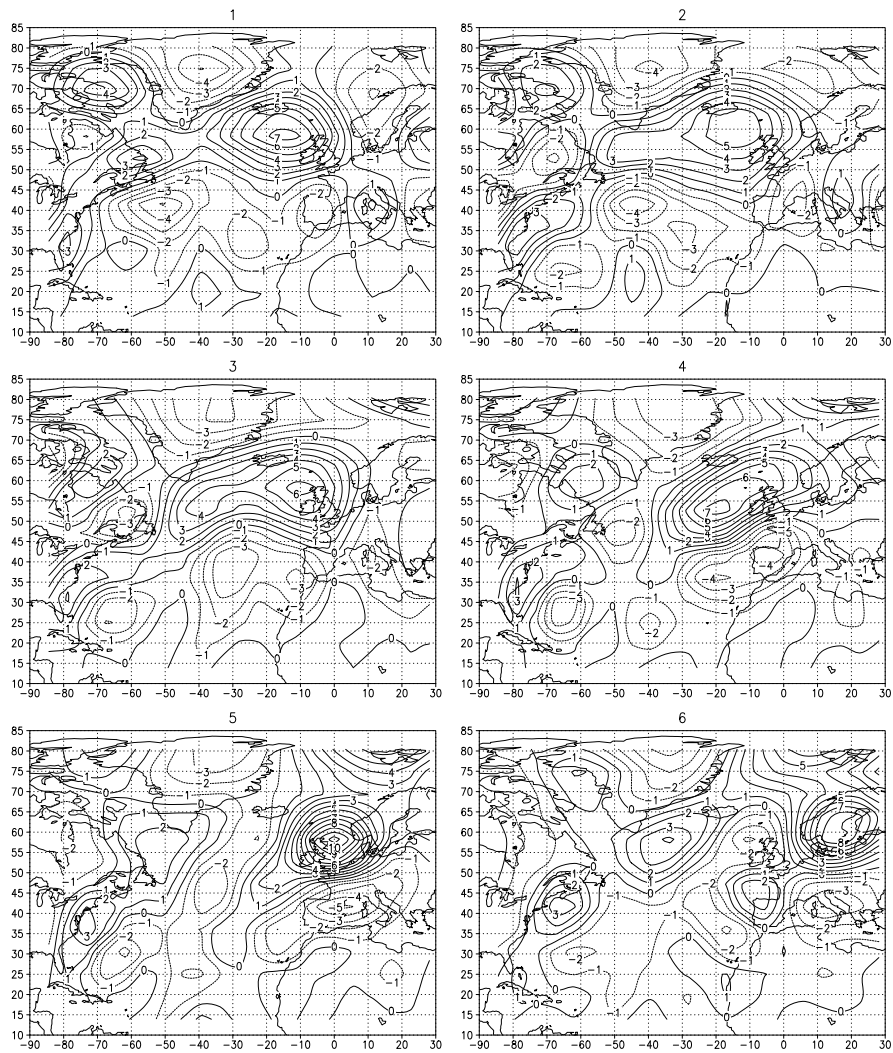
We speculate at the moment that the changing climate results in a seldom occurrence of these Wave-Mergers over North-western Europe. It may be that this mechanism is also possible in the control climate, but that its rarity is so extreme that it does not show up in the Gumbel plot of order 10^4 year. If this conjecture is true, than the occurrence of superstorms in a greenhouse climate can be regarded to be the result of an increased probability of these events under the changed CO_2 conditions. The time-evolution of the relative vorticity during one of these severe events is shown in Figure 1.17 (Appendix 1.A). It clearly shows the merging of two cyclones, and the explosive increase in relative vorticity and wind speed.

The reason for this merging, and its relation to the greenhousegas concentration, has to be investigated, as well as the physical reliability of these superstorms. This future research will concentrate on the analysis of the synoptic situations leading to the severe events, and on changes in the spatial distribution of wind extremes due to the greenhouse effect.

1.A Meteorological situation during a severe event

Figure 1.17 shows the situation from 4 days before till 1 day after the day with the largest wind speed in the ECBilt-Clio greenhouse run. The evolution of the daily-averaged vertical component of the relative vorticity at 800 hPa indicates that two storms (with their centers at (55E,52N) and (15E,57N) on day 1), interact and merge during day 2 to 5. This results in a explosive increase in relative vorticity and wind speed. The situation in the simulation of Figure 1.17 resulted in a 12-hourly wind speed over the North Sea of 53 m/s, and a surge level in Delfzijl of 7.9 m.

Figure 1.17: Meteorological situation of a severe ECBilt-Clio event. Shown is the daily-averaged vertical component of the relative vorticity (in 10^{-5} m/s^2) at 800 hPa. Panel 5 shows the most extreme situation. The event resulted in a wind speed of 53 m/s, and a surge level in Delfzijl of 7.9 m.



Chapter 2

Uncertainties in extreme surge level estimates from observational records

Abstract

Ensemble simulations with a total length of 7540 years are generated with a climate model, and coupled to a simple surge model to transform the wind field over the North Sea to the skew surge level at Delfzijl (NL). The 65 constructed surge records, each with a record length of 116 years, are analyzed with the Generalized Extreme Value (GEV) and the Generalized Pareto distribution (GPD) to study both the model and sample uncertainty in surge level estimates with a return period of 10^4 years, as derived from 116-year records.

The optimal choice of the threshold, needed for an unbiased GPD-estimate from Peak-Over-Threshold (POT) values, cannot be determined objectively from a hundred-year data set. This fact, in combination with the sensitivity of the GPD-estimate to the threshold, and its tendency towards too low estimates, leaves the application of the GEV distribution to storm-season maxima as the best approach. If the GPD-analysis is applied, the exceedance rate λ should be chosen not larger than 4.

The climate model hints at the existence of a second population of very intense storms. As the existence of such a second population can never be excluded from a hundred-year record, the estimated 10^4 -year wind speed from such records has always to be interpreted as a lower limit.

2.1 Introduction

In The Netherlands, a probability of 10^{-4} per year for flooding from the sea is used as baseline for dike design (Deltacommissie 1960). Several problems arise when translating this 'accepted risk' into the sea level being exceeded (on average) only

once in 10^4 years. First, as the observational records of tidal stations are only 10^2 years in length, the surge level with an average return period of 10^4 years requires an extrapolation of two orders of magnitude. It is unclear how reliable the estimate from such an extrapolation is. Second, various probability functions can be fitted to the observational records of extreme surges, leading to different results in the 10^4 -year return levels (Dillingh et al. 1993; de Haan 1990). Third, extrapolation from observational records does not contain information about surges in a greenhouse gas induced changing climate. Fourth, a second population of rare but intense storms, originating from a different kind of meteorological system, would result in higher return values than estimated from standard extreme value analysis of the available short records.

These problems are explored by analyzing two very long surge records for the Dutch coastal station Delfzijl, which were generated by a climate model. One series refers to the present-day climate; the second to the future (doubled greenhouse gas concentration) conditions. The length of these series (order 10^4 years) allow for exploring the far tail of the distribution, as well as for uncertainty estimates of the return values if calculated from much shorter (order 10^2 years) subsets.

2.2 Model descriptions

Wind data are generated by the General Circulation Model (GCM) ECBilt-Clio, consisting of an ocean model Clio (Goosse and Fichefet 1999) and an atmospheric model ECBilt (Opsteegh et al. 1998, 2001). ECBilt is a spectral T21 global 3-level quasi-geostrophic model, with a time step of 4 hours. The T21-resolution corresponds (for the latitudes of interest) with a grid point distance of approximately 500 km.

The surge model we used is a simplified version of the Timmerman model (Timmerman 1977). It is described and validated in van den Brink et al. (2003). We calculated a surge level every 12 hours.

2.3 Methodology

a. Extreme Value distributions

There are two commonly applied approaches in extreme value statistics: In the first approach, 'block maxima' are considered, to which the Generalized Extreme Value (GEV) distribution is applied. The GEV distribution function is given by:

$$\text{GEV} = P(Y \leq y) = \exp \left(- \left[1 - \frac{\theta}{\alpha}(y - \mu) \right]^{1/\theta} \right) \quad (2.1)$$

with μ the location parameter, α the scale parameter, θ the shape parameter, and y the block maximum of the considered variable (de Haan 1976).

In the second approach, all values above a certain threshold u are considered. To these 'Peak over Threshold' (POT) values, the Generalized Pareto Distribution (GPD) is applied. The GPD distribution function is given by:

$$\text{GPD}_\lambda = P(Y - u \leq y | Y > u) = 1 - \left[1 - \frac{\theta}{\alpha}(y - \mu)\right]^{1/\theta} \quad (2.2)$$

with μ the location parameter, α the scale parameter, θ the shape parameter, and y the variable above a chosen threshold u . We follow the common approach to choose μ equal to the threshold u (Palutikof et al. 1999). The exceedance rate λ , which depends on the threshold u , is estimated as the average number of exceedances over the threshold u per 'block'. From both approaches, the level belonging to a given probability of exceedance can be estimated by inverting equations 2.1 and 2.2.

The shape parameters θ of the GEV and the GPD distributions are equal if the threshold is large enough (Katz et al. 2002).

In order to come to an optimal estimate, it is desirable that the estimate is both unbiased (i.e., with the right expected value) and efficient (i.e., with a small uncertainty). The uncertainty depends mainly on the number of samples that are considered, whereas a systematic bias will be introduced if a wrong distribution is used to describe the data. As both the GPD and the GEV distribution describe only the 'tail' of the parent distribution, a bias will be introduced if samples that do not belong to this 'tail' are also considered. Which samples belong to the tail, in the sense that they can be described with the same parameters as the more extreme events, depends on the convergence rate of the parent distribution to the asymptotic extreme value distribution. For the 'block maxima' approach, this convergence is assumed beforehand, whereas for the POT-approach, this question is commonly answered empirically, making use of the fact that for the 'tail', the estimated shape parameter θ should be independent of the threshold u , and thus of the exceedance rate λ . This can be explored by plotting the estimated shape parameter θ as a function of the threshold u or the exceedance rate λ . The chosen λ is then the largest one for which θ is stable (de Haan 1990; Coles 2001). If there are strong fluctuations or trends in the estimated θ , quantile estimates are difficult to obtain (see e.g. Brabson and Palutikof 2000).

So, the larger sample set that is considered in the POT-approach (if $\lambda > 1$) makes this method more efficient than the 'block maxima' approach. On the other hand, the POT-approach is more likely to be biased, as samples less far in the tail of the distribution are also used.

For a further overview of the advantages and disadvantages of the POT-approach and the 'block maxima' approach, we refer to Palutikof et al. (1999)

b. Set-up of the numerical experiment

With ECBilt-Clio, 260 runs of 30 years each were generated, with a CO₂ concentration according to the period 1960-1989 (320 ppm on average). In addition to the control run, we also generated 233 ensemble runs of 30 years with estimated CO₂ concentrations according to the period 2050-2079 (following the SRES A1B CO₂ emission scenario (Nakicenovic et al. 2000)). This emission scenario results in approximately doubled CO₂ concentration (620 ppm on average) in 2050-2079 with respect to the control run.

As every 30-year run contains 29 storm season periods, we have $260 \times 29 = 7540$ 'block maxima' for the control run, and 6902 for the greenhouse run.

c. Data handling

To remove dependent events from the POT-selection, we require a minimal time separation between selected events of 96 hours, as in de Haan (1990).

We concentrate on storm season events (October till March) to improve homogeneity of the data set (de Haan 1990). We applied the surge model to the ECBilt-Clio grid point (6E,47N). This grid point best represents the North Sea winds (van den Brink et al. 2003).

We calculated the parameters of the GEV and GPD distributions via the method of Maximum Likelihood (Coles 2001). The 95%-confidence levels were estimated from the profile likelihood (Coles 2001).

Figure 2.1 shows the number of exceedances λ as a function of the threshold u for the observations and the ECBilt-Clio data. ECBilt-Clio has somewhat less exceedances over a given threshold than the observations. In this study, we compare both record for situations with equal exceedance rate λ , which means that for the observational record a higher threshold is chosen than for the ECBilt-Clio record.

Figure 2.2 shows a return level plot for the observational set and the ECBilt-Clio set. The extremes of ECBilt-Clio are in reasonable agreement for return periods up to 50 years. For return periods larger than 50 years, the extremes in ECBilt-Clio are higher than in the observational set.

2.4 Results

a. Dependence of 10^4 -year estimate on model choice

With the control run, we tested the uncertainty in the extrapolation of the extreme surges for Delfzijl. We applied the GPD distribution to the 116-year observational surge record of Delfzijl (1883-1999), to 65 subsets of 116 years each of ECBilt-Clio, and to the total set of 7540 years, all for several choices of λ . We also ap-

Figure 2.1: Number of exceedances λ per storm season (October to March) as a function of the threshold u for the observations and the ECBilt-Clio data. The vertical scale is logarithmic.

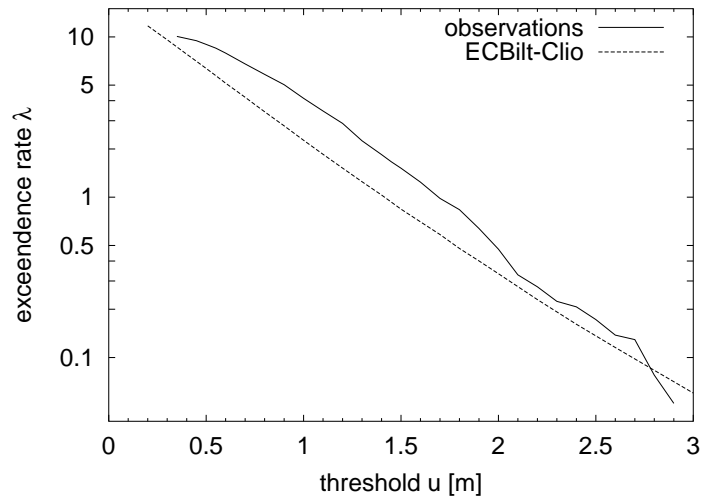


Figure 2.2: Return level plot for the observational set and the ECBilt-Clio set. The lines are GEV- and GPD-fits with exceedance rate $\lambda = 3$ to both sets. The horizontal scale is logarithmic.

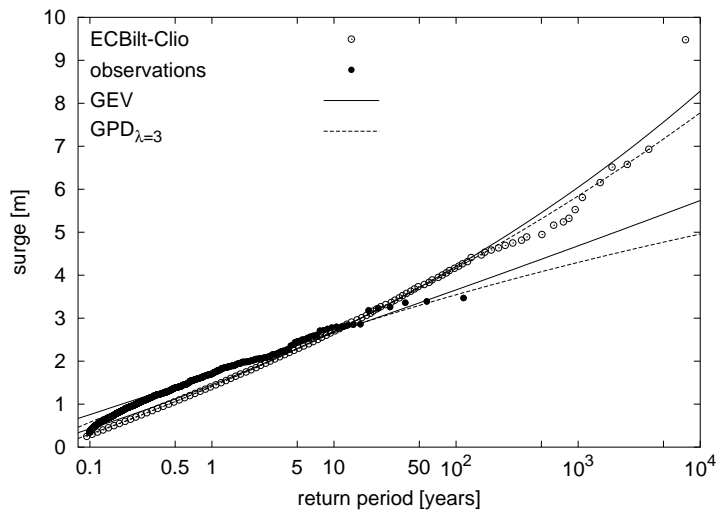
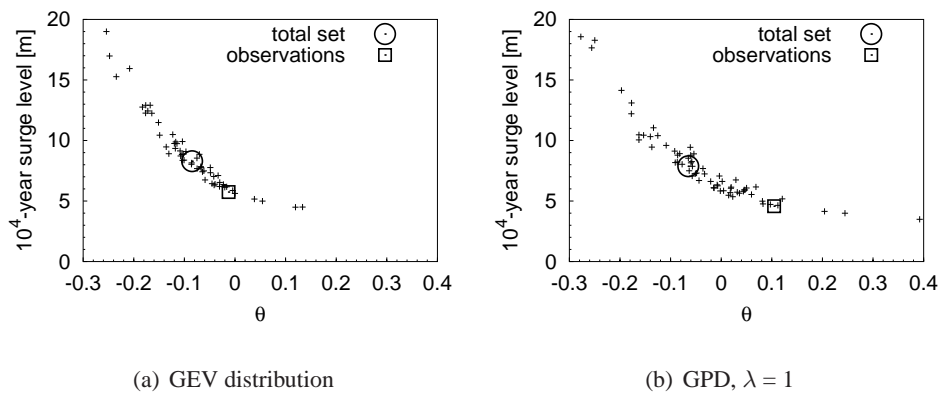
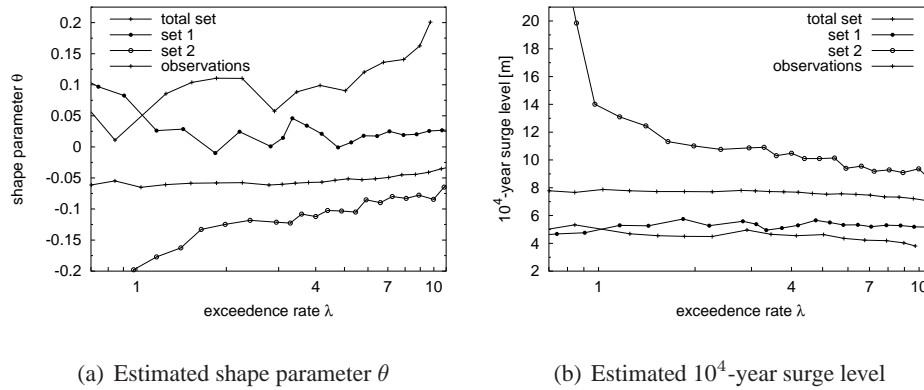


Figure 2.3: The estimated 10^4 -year return level for the surge as a function of the corresponding shape parameter θ for 65 subsets (each of 116 years length) from the ECBilt-Clio control run. Shown are the GEV-estimates (a) and the GPD-estimates for exceedance rate $\lambda = 1$ (b). Also shown are the estimates from the total ECBilt-Clio control run of 7540 storm seasons (circle), and the estimate from the 1883-1999 observational set of Delfzijl (square).



plied the GEV distribution to the storm season block-maxima of all these sets. The 10^4 -year estimates are shown in Figure 2.3 as a function of the estimated shape parameter θ from the GEV distribution (panel a) and from the $\text{GPD}_{\lambda=1}$ distribution (panel b). Figure 2.3 shows the following features: First, both panels resemble the strong correlation between the estimated shape parameter θ and the estimated 10^4 -year return level. Second, the 10^4 -year estimate from the total 7540-year ECBilt-Clio set are similar for the GEV (8.29 m (7.21,10.9)) and the $\text{GPD}_{\lambda=1}$ estimate (7.87 m (7.28,8.62)) (the values between brackets are the lower- and upper 95%-confidence levels). Third, the lower $\text{GPD}_{\lambda=1}$ estimate (4.66 m (3.70,8.95)) than the GEV estimate (5.85 m (4.17,11.5)) indicates that the two approaches can result in considerably different 10^4 -year estimates (although they do not differ significantly in this case). Fourth, the 10^4 -year estimates of the 116-year ECBilt-Clio subsets vary considerably, between 4 and 20 m, both for the GEV- and the $\text{GPD}_{\lambda=1}$ estimates.

Figure 2.4: (a) Estimated shape parameters θ of the GPD-distribution for the surge in Delfzijl according to the total 7540-year ECBilt-Clio set as a function of the exceedance rate λ . Also shown are estimates from two arbitrarily chosen 116-year ECBilt-Clio subsets (set 1, set 2), and the observational set. (b) The corresponding 10^4 -year surge levels. The horizontal axes are logarithmic.



b. Dependence of GPD 10^4 -year estimate on exceedance rate

We now want to explore if $\lambda > 1$ makes application of the GPD distribution more efficient than the GEV distribution. Figure 2.4 shows the estimated GPD shape parameters and 10^4 -year return levels as a function of λ . Figure 2.4(a) shows the estimates from the total 7540-year set, two arbitrarily chosen 116-year ECBilt-Clio sets and the observational set. Figure 2.4(b) gives the estimated 10^4 -year surge levels for the same sets.

Figure 2.4 gives the following information: First, if $\lambda < 1$, the estimate of θ (and thus the 10^4 -year estimate) from a 116-year subset is very sensitive to λ , which is undesired. Second, also for $\lambda > 1$, considerable fluctuations in the estimated shape parameter θ remain in 116-year sets, as both the two ECBilt-Clio sets and the observational set show. This fact, together with the different 'stable' regions for θ of the two ECBilt-Clio 116-year subsets, make it difficult or even impossible to choose an optimal value of λ from a 116-year record. Third, the two 116-year ECBilt-Clio subsets remain for all λ 's either below, or above the estimate of the total 7540-year ECBilt-Clio set. Fourth, even the estimates of the total 7540-year ECBilt-Clio set are not threshold-independent. This suggests that the upward slope of θ (for $\lambda > 4$) in Figure 2.4(a) (and the corresponding decreasing 10^4 -year estimate in Figure 2.4(b))

is a bias, caused by samples that do not belong to the tail of the parent distribution. Fifth, the fact that the estimates from the observational set are within the ECBilt-Clio range for the GEV and the GPD distribution for $\lambda \lesssim 3$, but outside that range for $\lambda \gtrsim 3$, might indicate that the observational set is even more biased for large values of λ than the ECBilt-Clio set.

We conclude that λ should be in the range between 1 and 4 to have a more or less unbiased 10^4 -year surge estimate. However, such a range can only be determined from an extremely long data set. Data sets of order hundred years are too short to determine a maximal choice of λ (and thus of the minimal threshold) that results in an unbiased estimate. The strong dependence of the GPD-estimates on the choice of λ makes it difficult, or even impossible, to obtain reliable unbiased GPD-estimated 10^4 -year surge levels from 10^2 -year records.

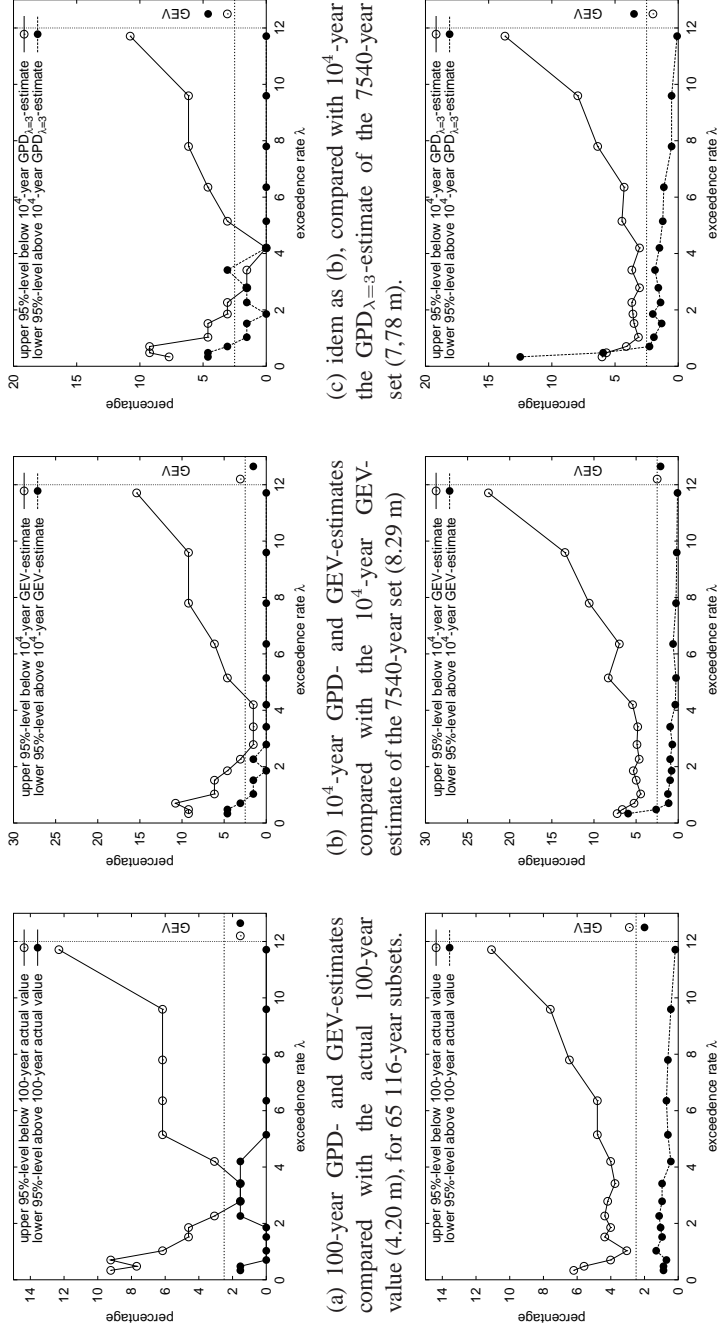
c. *Optimal choice for threshold*

In order to investigate the bias in more detail, we determine the fraction of the 65 subsets for which the actual value lies outside the 95%-confidence interval. These percentages are shown in Figure 2.5(a) for a return period of 100 years, split out to the lower- and upper 95%-confidence level. The actual 100-year value is 4.20 m (according to Figure 2.2). The open circles in Figure 2.5(a) show that the fraction of upper 95%-confidence levels is larger than 2.5% for all exceedance rates, except between 2 and 4. For $\lambda \geq 5$, the number of subsets for which the upper 95%-confidence levels is below the actual value is large, whereas for none of the 65 subsets the actual value is below the the lower 95%-confidence levels. This indicates the existence of bias towards too low values.

Fitting a GEV-distribution to the 65 subsets gives one subset for which the 100-year upper 95%-confidence level is lower than the actual value, and one subset for which the lower 95%-confidence level is higher than the actual 100-year value. The corresponding percentages are plotted at the right side of Figure 2.5(a).

To highlight the effects of Figure 2.5(a), the calculations are repeated, but now based on 1000 116-years subsets, obtained by randomly sampling from the total ECBilt-Clio set, in order to decrease the noise. The results for a return period of 100 years are shown in Figure 2.5(d). This confirms the findings of Figure 2.5(a) that there is a bias in the GPD_λ -estimates. Whereas Figure 2.5(a) did not indicate a bias for $\lambda = 3$, Figure 2.5(d) shows that there is a small bias for $\lambda < 4$, which strongly increases for $\lambda > 4$. Figure 2.5(d) indicates no bias in the GEV-estimates (about 2.5% of the upper 95%-confidence intervals is lower than the actual value, and about 2.5% of the lower 95%-confidence intervals is above the actual value).

Figure 2.5: Percentages of the number of sets that do not contain the 'real' value within its 95%-confidence intervals, estimated with the GPD_λ -distribution for different exceedance rates λ , and with the GEV-distribution. The 'real' value is chosen to be the actual 100-year value of the 7540-year set in (a,d), the 10^4 -year GEV-estimate of the 7540-year set in (b,e), and the 10^4 -year $GPD_{\lambda=3}$ -estimate of the 7540-year set in (c,f). Upper: 65 116-year subsets; Lower: 1000 116-year sets, randomly sampled from the total ECBilt-Clio set.



(a) idem as (a), for 1000 sampled sets.

(b) idem as (b), for 1000 sampled sets.

(c) idem as (c), for 1000 sampled sets.

For the 10^4 -year return periods, the percentages exceeding the upper- and lower 95%-confidence intervals are depicted in Figure 2.5(b,c,e,f). In this case, i.e., for 10^4 -year return periods, the 'real' value for the 10^4 -year return value has to be chosen, as it can not be determined directly from Figure 2.2. As possible 'real' values we considered both the GEV- and the $\text{GPD}_{\lambda=3}$ -estimates, as obtained from the total 7540-year set. The reason for considering $\lambda = 3$ in the GPD-estimate is that this value of the exceedance rate λ turns out to be the best, according to Figure 2.5(a). Another reason is that the $\text{GPD}_{\lambda=3}$ -estimate is correct for a 100-year return period (Figure 2.2).

Figures 2.5(b,c) show the results for the 65 subsets, respectively taking the 10^4 -year GEV-estimate (8.29 m) as 'real' value, and the 10^4 -year $\text{GPD}_{\lambda=3}$ -estimate (7.78 m). Figures 2.5(e,f) show the results for the 1000 sampled subsets.

We see an even stronger bias towards too low values for the 10^4 -year return periods than for the 100-year return periods for the GPD-estimates if $\lambda > 4$ (note the different vertical range of Figures 2.5(b,c,e,f) with respect to Figures 2.5(a,d)). No bias is detected for the GEV-estimates in the situation that the 10^4 -year GEV-estimate is taken as 'real' value (Figures 2.5(e)), and for the GPD-estimates if $1 < \lambda < 4$ in the situation that the 10^4 -year $\text{GPD}_{\lambda=3}$ -estimate is taken as 'real' value (Figures 2.5(f)), as expected from consistency.

We conclude from Figure 2.5 that the GPD-estimates are more sensitive to bias than the GEV-estimates, especially if the exceedance rate $\lambda > 4$. The GEV-estimates are unbiased. This leaves the GEV analysis as the preferred method.

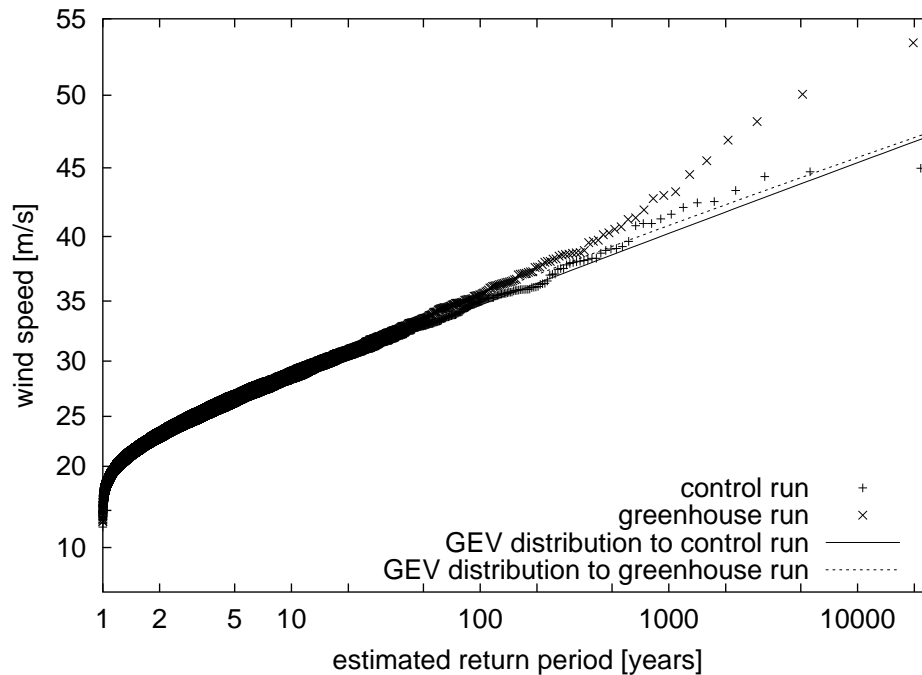
d. Greenhouse effect on wind

The effect of the greenhouse doubling on the extreme wind speed in ECBilt-Clio for the North Sea grid point is shown in Figure 2.6. Up to return periods of ≈ 100 years, no effect is apparent. However, for wind speeds with return periods of more than 250 years, the greenhouse run deviates systematically from the fitted GEV distribution. This suggests the existence of a second population in the extreme wind distribution. Fitting the GEV distribution to the deviating extremes only, results in a considerably higher 10^4 -year return value for the wind speed than fitting to the total set. For a more comprehensive description, we refer to van den Brink et al. (2004a).

2.5 Discussion and conclusions

The variance in the GEV-estimates from 65 records of 116 years indicates that only a crude estimate of the 10^4 -year surge level can be made from a single record with a length of the order of a hundred years. The GPD-estimates give lower 95%-confidence intervals for exceedance rates $\lambda > 1$ than the GEV-estimates, but the

Figure 2.6: Return level plot of the observed and GEV-estimated 12-hourly averaged wind speeds for the control- and greenhouse runs in ECBilt-Clio for the North Sea representing grid point (6E,47N). The kink at a return period of 250 years in the greenhouse run suggests the presence of a double population in the extreme wind distribution.



total 7540-year ECBilt-Clio set shows that these GPD-estimates are biased toward lower 10^4 -year values.

For the ECBilt-Clio data, the percentage of the 95%-confidence levels containing the actual value can be determined for a return period of 100 years, and estimated for a return period of 10^4 years. This analysis points out that application of the GPD-analysis to the ECBilt-Clio data leads to estimates that are biased towards too low values. We emphasize that this analysis can only be done for extremely long sets, and thus not for the short observational sets.

The unknown optimal value of the exceedance rate λ for the observational set, combined with the sensitivity of the GPD-estimate to the choice of λ , and the tendency towards too low estimates, leaves in our opinion the GEV analysis as the preferred method to apply to the observational data, despite of its large uncertainty. If the GPD-analysis is applied, λ should be chosen not larger than 4.

In the future, output of more advanced climate- and surge models will be used to calculate the 10^4 -year surge level and its uncertainty. Another possibility may be to apply the optimal λ , as obtained from the climate model, to the observational data and still estimate the 10^4 -year surge level and its uncertainty from the observations.

ECBilt-Clio hints at the excitation of extratropical 'superstorms', defined as storms with more extreme winds than expected from extrapolation of less extreme events. The fact that this second population is only apparent in the greenhouse run for this grid point indicates that regions where second populations exist, can be shifted, enhanced or generated by climate change. The reality of this model-induced second population has still to be shown (van den Brink et al. 2004a). Due to their extreme rarity, they are not detectable from records of only hundred years in length. Reversing this argument implies that extrapolations from 100-year records to 10^4 -year return levels are only valid under the condition that the extreme value distribution is single populated. As this condition can never be proved from 100-year records, the GEV- or GPD- (or any other distribution) estimated 10^4 -year wind speed from 100-year records has always to be interpreted as a lower limit.

Chapter 3

Statistics of extreme synoptic-scale wind speeds in ensemble simulations of current and future climate

Abstract

Statistical analysis of the wind speeds, generated by a climate model of intermediate complexity, indicates the existence of areas where the extreme value distribution of extratropical winds is double populated, the second population becoming dominant for return periods of order 10^3 years. Meteorological analysis of the second population shows that it is caused when extratropical cyclones merge in an extremely strong westerly jet stream, conditions are generated which are favorable for occurrence of strong diabatic feedbacks. Doubling of the greenhouse gas concentrations changes and enlarges the areas of second population, and increases its frequency. If these model results apply to the real world, then in the exit areas of the jet stream the extreme wind speed with centennial to millennial return periods is considerably larger than extreme value analysis of observational records implies.

3.1 Introduction

Motivated by safety and dike design demands, much statistical research with observational data has been done on the estimation of extreme wind speeds and storm surges (Cook 1982; Simiu et al. 2001; de Haan 1990) for return periods up to 10^4 years. Although a wide variety of methods has been developed (see e.g. Palutikof et al. (1999) for an overview), all practical applications hamper from the restricted length of the observational series (order hundred years), on which the statistical extrapolations are based.

Several assumptions underly the statistical estimate of the wind speed with a

return period of 10^4 years. The most important one, i.e. that all extratropical extremes (up to return periods of 10^4 years) belong to the same population, is hard to verify from the available short observational sets.

We evaluated this problem within the context of a climate model of intermediate complexity. We have generated ensemble runs (consisting of 3509 years in total) with a climate model, both for the current climate (~ 1975) and for a climate at doubled CO_2 concentrations (~ 2065). With these long records we searched for double populations in the extreme value distributions of annual wind extremes for return periods up to 10^4 years. In addition, we explored the effect of increased greenhouse gas concentrations on the mean annual wind and on the double populations. Finally, we analyzed the meteorological conditions of the small but violent second population of extreme winds.

The paper is structured as follows: Section 3.2 describes the theoretical statistical basis, and Section 3.3 the data handling of the model output and the detection of double populations from extreme value distributions. Section 3.4 describes the climate model used, and Section 3.5 the statistical results. Section 3.6 analyzes the second population in meteorological sense, and Section 3.7 gives the discussion and conclusions.

3.2 Extreme Value Analysis

a. General arguments

Let M_m be the maximum of m independent observations $\xi_1, \xi_2, \dots, \xi_m$ from distribution $F(x)$:

$$M_m = \max(\xi_1, \xi_2, \dots, \xi_m) \quad (3.1)$$

then the distribution of M_m is given by:

$$P(M_m \leq x) = P(\xi_1 \leq x)P(\xi_2 \leq x)\dots P(\xi_m \leq x) = F^m(x) \quad (3.2)$$

Extreme Value theory states that the distribution of maxima of many probability distributions $F(x)$ (properly normalized with α_m and μ_m) approaches asymptotically to a specific class of functions $G(x)$:

$$\lim_{m \rightarrow \infty} P\left(\frac{M_m - \mu_m}{\alpha_m} \leq x\right) = \lim_{m \rightarrow \infty} F^m(\alpha_m x + \mu_m) = G(x) \quad (3.3)$$

where $G(x)$ is given by:

$$G(x) = e^{-(1-\theta x)^{1/\theta}} \quad (3.4)$$

with the parameter $\theta \in \mathbb{R}$ determining the nature of the function (see e.g. de Haan (1990) and Kotz and Nadarajah (2000)). A special case of $G(x)$ is the Gumbel distribution, which is $G(x)$ with $\theta = 0$. Then, interpreting $\theta = 0$ as the limit $\theta \rightarrow 0$, (3.4) reduces to:

$$G(x) = e^{-e^{-x}} \quad (3.5)$$

There are many examples of parent distributions $F(x)$ whose normalized extremes converge to the Gumbel distribution, e.g. the normal distribution, the exponential distribution and the Weibull distribution (Embrechts et al. 1997).

b. Generalized Extreme Value (GEV) distribution of wind data

We rewrite m in (3.1) as rp , with r the average number of independent daily averaged wind speeds in a year, and p the sample period in years from which the maxima M_p are extracted. If we suppose that the distribution of the normalized p -year wind maxima follows $G(x)$ for $p \geq 1$, we can write (3.4) in the form of the so-called Generalized Extreme Value (GEV) distribution $G_p(u)$: (Jenkinson 1955):

$$G_p(u) \equiv P(M_p \leq u) = e^{-e^{-x_p}} \quad (3.6)$$

with M_p the p -year wind maxima, $G_p(u)$ the GEV distribution resulting from p -year sampling, and x_p a substitute for:

$$x_p = \ln \left(1 - \theta \frac{u - \mu_p}{\alpha_p} \right)^{-1/\theta} \quad (3.7)$$

in which μ_p is the location parameter, α_p the scale parameter, θ the shape parameter, and u the wind speed. The location parameter μ_p can be interpreted as the wind speed exceeded on average once during the sample period p (Buishand and Velds 1980). For $\theta > 0$, u is bounded by an upper limit of value $\mu_p + \alpha_p/\theta$; for $\theta \leq 0$, u can approach infinity.

The Gumbel distribution ($\theta = 0$) is interpreted as the limit of (3.7) as $\theta \rightarrow 0$, leading to:

$$x_p = \frac{u - \mu_p}{\alpha_p} \quad (3.8)$$

Extreme value distributions are often plotted as a so called Gumbel plot, where the variable u is on the ordinate, and the abscissa is transformed into the Gumbel Variate:

$$\text{Gumbel Variate} = -\ln(-\ln(F^m(u))) \quad (3.9)$$

On a Gumbel plot, a Gumbel distribution is represented by a straight line, whereas a GEV distribution ($\theta \neq 0$) is curved, downwardly for $\theta > 0$ and upwardly for $\theta < 0$.

Using that that $[G_1(u)]^p = G_p(u)$ (Leadbetter et al. 1983, p. 8), from (3.6) follows:

$$x_p = x_1 - \ln p \quad (3.10)$$

Substituting (3.10) into (3.7) gives:

$$\begin{aligned} \mu_p &= \mu_1 + \alpha_1 \frac{1 - p^{-\theta}}{\theta} \\ \alpha_p &= \alpha_1 p^{-\theta} \end{aligned} \quad (3.11)$$

In the special case of the Gumbel distribution, the right hand sides of (3.11) are $\mu_1 + \alpha_1 \ln p$ and α_1 , respectively.

In extreme value studies, the probability of exceedance of a certain value u is usually expressed in terms of the *return period* T . The return period T is the average number of years between two succeeding exceedances of the corresponding *return value* u :

$$T(u) \equiv \frac{1}{1 - G_1(u)} \approx p e^{x_p} \quad \text{for } T \gg p \quad (3.12)$$

c. Two Component Extreme Value (TCEV) distribution

The local wind can be caused by two meteorological systems a and b of different physical nature, each of them generating its own distribution $F_a(u)$ and $F_b(u)$. Then, the parent distribution $F_{a,b}(u)$ is said to be mixed, and can be decomposed into:

$$F_{a,b}(u) = (1 - \epsilon)F_a(u) + \epsilon F_b(u) \quad (3.13)$$

with $0 < \epsilon < 1$. An interpretation of (3.13) is that of every m samples, $(1 - \epsilon)m$ originates from mechanism a , and ϵm from b . Especially interesting is the case in which $\epsilon \ll 1$, and where the far tail of $F_b(u)$ is heavier than that of $F_a(u)$. Then $F_{a,b}(u) \approx F_a(u)$, and $F_b(u)$ can not easily be detected from the parent distribution. However, the extremely large events will originate from system b , which existence may be detected from the observed distribution of the extremes.

If $F_a^{(1-\epsilon)m}(u) \rightarrow G_a(u)$ and $F_b^{\epsilon m}(u) \rightarrow G_b(u)$, then the distribution of the extremes $G_{a,b}(u)$ of the mixed distribution is given by (Cook et al. 2003):

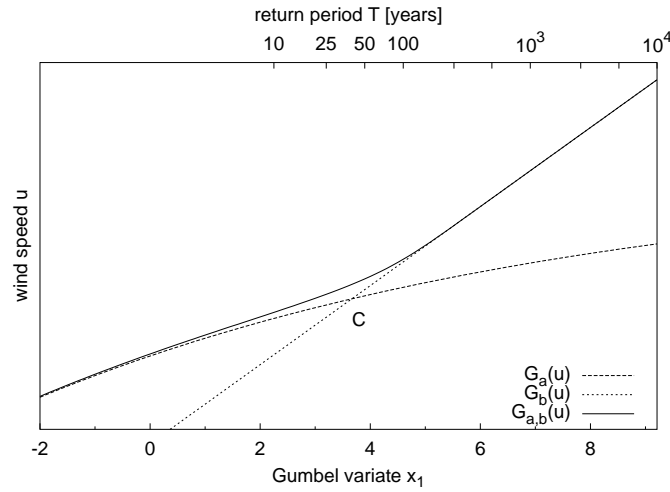
$$G_{a,b}(u) \equiv F_a^{(1-\epsilon)m}(u) F_b^{\epsilon m}(u) \rightarrow G_a(u) G_b(u) \quad (3.14)$$

where the subscripts a, b of $G(u)$ refer to the populations of systems a and b .

The simplest case of $G_{a,b}(u)$ represents the multiplication of two Gumbel distributions $G_a(u)$ and $G_b(u)$, which Rossi et al. (1984) calls the Two Component Extreme Value (TCEV) distribution:

$$G_{a,b}(u) = \exp\left(-e^{-\frac{u-\mu_a}{\alpha_a}} - e^{-\frac{u-\mu_b}{\alpha_b}}\right) \quad (3.15)$$

Figure 3.1: A Generalized Extreme Value (GEV) distribution $G_a(u)$ and a Gumbel distribution $G_b(u)$, with the corresponding Generalized Two Component Extreme Value (GTCEV) distribution $G_{a,b}(u)$. The intersection point C of $G_a(u)$ and $G_b(u)$ is in this example at $x_1 = 3.67$, corresponding with a return period T_C of 40 year. The distributions are shown on a Gumbel plot.



If transformed into the Gumbel variate, (3.9) becomes for the TCEV distribution:

$$\text{Gumbel variate} = -\ln\left(e^{-\frac{u-\mu_a}{\alpha_a}} + e^{-\frac{u-\mu_b}{\alpha_b}}\right) \quad (3.16)$$

which shows that a Gumbel plot of extremes from a mixed distribution $G_{a,b}(u)$ results in a smooth transition from the asymptote of the distribution of the extremes $G_a(u)$ originating from the dominant population a , to the distribution of the violent extremes $G_b(u)$, originating from the rare population b . The intersection point C of $G_a(u)$ and $G_b(u)$ marks the sampling period T_C where the probability for sampling an extreme from population a or b is the same.

Figure 3.1 illustrates this behavior for the second-simplest case of a Two Component Extreme Value distribution, which is the case that $G_a(u)$ in (3.14) is allowed to generalize to a GEV distribution, but $G_b(u)$ remains a Gumbel distribution. We denote this type of Two Component distribution, which we shall concentrate on in this paper, by the Generalized Two Component Extreme Value (GTCEV) distribution, of which the Two Component Extreme Value distribution is a special case. The reason for analyzing the second-simplest case is that the the simplest case is not appropriate, as population a can not be described by a Gumbel distribution. The combination of

two GEV distributions is not suitable, as population b is too small to estimate the shape parameter θ .

For a GTCEV distribution to become apparent in the data, three conditions have to be fulfilled. First, the series length in years Y should amply exceed the return period T_C of the crossing point C . Second, the sampling period p should be sufficiently large to achieve convergence for the extremes of both populations a and b to their respective limits $G_a(u)$ and $G_b(u)$. Third, the sampling period p should be much smaller than T_C , since in the opposite case $G_a(u) \rightarrow 1$ and hence the GTCEV approaches $G_b(u)$, which is the ultimate extreme value limit of both $G_b(u)$ and $G_{a,b}(u)$. Note however, that the detection of the presence of a GTCEV distribution is easiest for $\theta_a > 0$, as in the opposite case $G_a(u)$ curves upwardly so that the GTCEV distribution becomes more difficult to distinguish from a single component GEV distribution with $\theta_a < 0$. Figure 3.1 may help to illustrate these points.

3.3 Data Handling

In empirical studies, the parameters of the GEV distribution $G_p(u)$ are obtained from a series with a finite length of Y years. Taking the maxima of every p years, n values remain to fit, with

$$n = \frac{Y}{p} \quad (3.17)$$

Traditionally, the GEV distribution is applied to the annual maxima, so with sample period $p = 1$, giving $n = Y$ values to fit. This practice implicitly assumes that convergence to the GEV limit (Eq. 3.3) is achieved for $m = r$, with $r \approx 50 \ll 365$ the average number of independent daily averaged wind speeds in a year (Coles 2001, p. 98). It depends on the mathematical form of the parent distribution $F(u)$ whether the annual maxima have indeed converged to the asymptotic distribution $G_{p=1}(u)$ for $m \approx 50$. If the convergence is too incomplete for $p = 1$ to achieve a meaningful GEV analysis, one remedy is to increase the sampling period p . However, this leads to a proportionally decreased number of points n on which the GEV fit is based, and hence to increased sampling noise and standard errors in the parameter estimations of the GEV distribution. In our analysis, we apply an alternative method, namely to improve convergence by transforming the data in such a way that they become distributed according to a faster converging parent distribution. The method makes use of the fact that, for extratropical wind speeds, the Weibull distribution is well established as the parent distribution:

$$F(u) = 1 - e^{-(u/a)^k} \quad (3.18)$$

with u the wind speed, a the Weibull scale parameter and k the Weibull shape parameter. Theory shows that the maxima of observations from a Weibull distribution converge asymptotically (for any $k > 0$) to the Gumbel distribution, with the convergence rate depending on k , being largest for the exponential distribution ($k = 1$) (Embrechts et al. 1997; Cook and Harris 2001). Hence, improved convergence to the Gumbel distribution can be obtained if u^k instead of u is the fitted parameter, as this transforms the Weibull distribution into an exponential distribution. We made use of this property, and determined k in the tail of the parent distribution, after which the parameter u^k was fitted to a GEV distribution (Eqs. 3.6, 3.7). The underlying conjecture is that, even if deviations from the Weibull distribution in the far tail would lead to convergence to the GEV distribution instead of to the Gumbel distribution, the convergence rate to that GEV distribution is still faster for u^k than for u .

In the analysis of wind maxima, we restrict ourself to the storm-season (Oct-Mar) instead of to the annual maxima, assuming better homogeneity of the parent distribution within the storm season (Dillingh et al. 1993).

a. GEV parameter estimation

The parameters of the GEV distribution were estimated by the method of Probability Weighted Moments (Hosking et al. 1985). We also used his estimate of the plot positions:

$$x^i = -\ln\left(-\ln\left(\frac{i - 0.35}{n}\right)\right) \quad (3.19)$$

with x^i the plot position of the i^{th} maximum in the set of n ordered maxima. Eq. 3.19 can be regarded as a discrete version of (3.9). The estimated return value of the wind speed $u_{p,T}$ for a given x (which is determined by the sample period p and return period T via (3.12)) follows from inverting (3.7) and back-transforming u^k to u :

$$u_{p,T} = \left(\mu_p + \frac{\alpha_p}{\theta}(1 - e^{-\theta x_p})\right)^{1/k} \quad (3.20)$$

with k the Weibull shape parameter. Neglecting the sampling error in the Weibull shape parameter k , the standard error $\sigma_{u,p,T}$ in the estimated return value $u_{p,T}$ is calculated by the so-called delta method (see e.g. Coles 2001, p. 33):

$$\sigma_{u,p,T}^2 = \nabla \mathbf{u}^T \mathbf{V} \nabla \mathbf{u} \quad (3.21)$$

with

$$\nabla \mathbf{u} = \left[\frac{\partial u}{\partial \mu}, \frac{\partial u}{\partial \alpha}, \frac{\partial u}{\partial \theta} \right]^T$$

and \mathbf{V} the variance-covariance matrix

$$\mathbf{V} = \begin{pmatrix} \sigma_{\mu}^2 & \sigma_{\mu\alpha} & \sigma_{\mu\theta} \\ \sigma_{\mu\alpha} & \sigma_{\alpha}^2 & \sigma_{\alpha\theta} \\ \sigma_{\mu\theta} & \sigma_{\alpha\theta} & \sigma_{\theta}^2 \end{pmatrix}$$

with σ_{μ} the standard error of μ etc. The values of \mathbf{V} are given by Hosking et al. (1985).

b. Detection of Two Component Extreme Value distributions

The statistical analysis was performed in four steps: First, the Weibull parameters a and k were determined for each grid point on the Northern Hemisphere. These parameters a and k were obtained by least mean square fitting all daily wind speeds with $u > a$ (i.e. the upper e^{-1} part of the distribution, to exclude the influence of the lower wind speeds) in the winter season in a 150-year record, hence 9932 daily values per grid point. Second, the GEV distribution was fitted to the set of 3509 annual maxima u^k for each grid point, so with $p = 1$ and $n = Y = 3509$. The third step was to identify possible GTCEV distributions, i.e. locations where the extreme value distribution originates from populations a and b . In that procedure, we assume that the data are GTCEV-distributed if the 10^4 -year return value as obtained from the GEV fit to p -yearly sampled maxima $u_{p,10^4}$ exceeds the 10^4 -year return value as obtained from the GEV fit to annual maxima $u_{1,10^4}$ by more than two standard deviations. Expressed in a signal-to-noise ratio SN

$$SN \equiv \frac{u_{p,10^4} - u_{1,10^4}}{\sqrt{\sigma_{u,p,10^4}^2 + \sigma_{u,1,10^4}^2}} \quad (3.22)$$

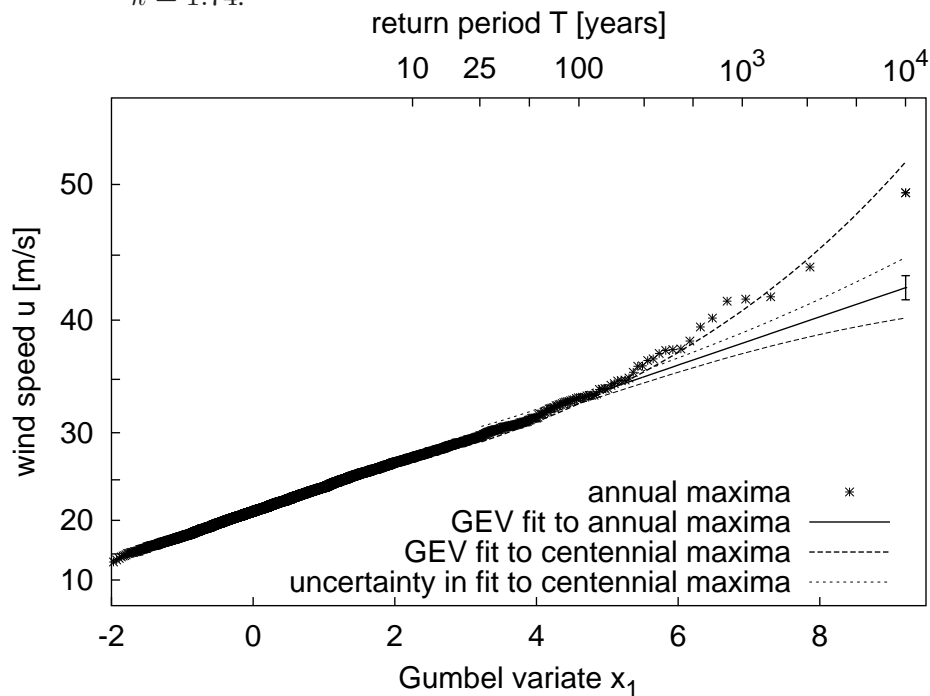
the criterion reads:

$$SN > 2 \quad (3.23)$$

where $\sigma_{u,1,10^4}$ is the sampling uncertainty in $u_{1,10^4}$, and $\sigma_{u,p,10^4}$ the standard error in $u_{p,10^4}$ when fitting a GEV distribution to p -yearly sampled maxima originating from $G_{p=1}(u^k)$ (using (3.11) to calculate μ_p and α_p). In our situation, the criterion (3.23) corresponds to a probability of less than 5% that the wind is single populated (this probability is, due to the skew distribution of rare return levels, somewhat larger than the 2.5% corresponding with a normal distribution). This process is visualized in Figure 3.2, which shows 3509 annual maxima with the fitted GEV distributions to the annual ($p = 1$) and centennial maxima ($p = 100$). We will apply (3.22) to annual and centennial maxima, although the outcome is rather robust for other choices of p .

The fourth step was to estimate the GTCEV distribution $G_{a,b}(u)$ for specific grid points where $SN > 2$. Here, we assumed that $F_b(u)$ is also Weibull distributed with

Figure 3.2: Visualization of the procedure to detect Generalized Two Component Extreme Value distributions. The 10^4 -year return value $u_{100,10^4}$, estimated by fitting the GEV distribution to the centennial maxima, is compared to the 10^4 -year return value $u_{1,10^4}$, estimated by fitting the GEV fit to the annual maxima. $G_a(u^k)$ is the estimate of the maxima of population $F_a(u)$ and $G_b(u^k)$ the estimate of population b . For this case $u_{1,10^4} = 42.5$ m/s and $u_{100,10^4} = 51.6$ m/s, and $\sigma_{u,1,10^4} = 0.9$ m/s (indicated by the bar). The uncertainty in the fit to centennial maxima $\sigma_{u,100,10^4} = 2.1$ m/s, giving $SN = 3.9$. According to (3.23), this implies detection of a GTCEV distribution, and hence of a double population in the extreme winds. Shown is a set of 3509 daily averaged annual maxima from the greenhouse run at (47N,6E). The vertical axis is linear in u^k , with $k = 1.74$.



the same shape parameter k as $F_a(u)$. $G_b(u)$ was estimated from the maxima which deviate considerably from the GEV fit to annual maxima, and $G_a(u^k)$ by adjusting μ_a , α_a and θ_a iteratively in such a way that fitting a GEV distribution to the given distribution $G_{a,b}(u^k)$ (assuming that $G_b(u^k)$ is correctly estimated from the deviating maxima) results in the same GEV parameters as the original data set. From $G_a(u^k)$ and $G_b(u^k)$, the intersection point C and the corresponding return period T_C were derived.

3.4 ECBilt-Clio Model description

The Climate Model used in this study is a coupled atmosphere-ocean-sea ice model of intermediate complexity, called ECBilt-Clio. The atmospheric component "EC-Bilt" is a spectral T21 global 3-level quasi-geostrophic model. The atmospheric time step is 4 hours. It is coupled to a dynamic ocean model "Clio", which has a dynamic sea-ice component and a relatively sophisticated parameterization of vertical mixing (Goosse and Fichefet 1999). For a more detailed description of the model, we refer to Opsteegh et al. (1998); Goosse and Fichefet (1999) and Schaeffer et al. (2002).

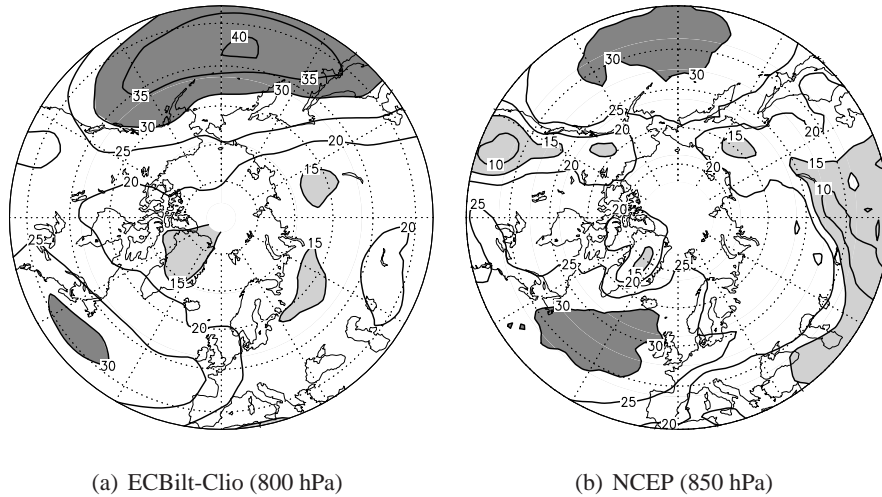
a. Experimental setup

A transient run was generated for the period 1860 to 2080, using historical greenhouse forcings for 1860 to 2000, and the SRES A1 CO₂ emission scenario (Houghton et al. 2001) for 2000 to 2050. This emission scenario results in approximately doubled CO₂ concentrations in 2050 (550 ppm) with respect to the emission in 1860 (290 ppm).

An ensemble of 121 runs of 30 years each was generated, starting from the situation in 1960 of the transient run. The set of all 121 runs for the period 1960-1989 is called the 'control experiment'. For each grid point, vector-averaged daily mean extreme wind speeds were sampled from each October-to-March period in the set, giving 29 extremes per ensemble member and grid point, and 3509 extremes per grid point for the entire control experiment. Note that we often refer to annual extremes, whereas only storm season extremes are sampled. For five ensemble runs, also all 27000 daily-averaged wind speeds in each grid point in the storm season were archived.

We also generated 121 ensemble runs of 30 years starting from the situation in 2050 of the transient run. This set for the period 2050-2079 is called the 'greenhouse experiment'. As before, the series from which the extremes are sampled has a total length Y of 3509 years, and the sub-series for which all daily values were archived was 150 years.

Figure 3.3: Location parameter $\mu_{p=1}$ of the annual wind speeds, estimated from fitting a GEV distribution to the ECBilt-Clio control experiment (3509 years) and to the NCEP data set (36 years). The location parameter $\mu_{p=1}$ represents the wind speed which is exceeded on average once a year. Values larger than 30 ms^{-1} and smaller than 15 ms^{-1} are shaded.

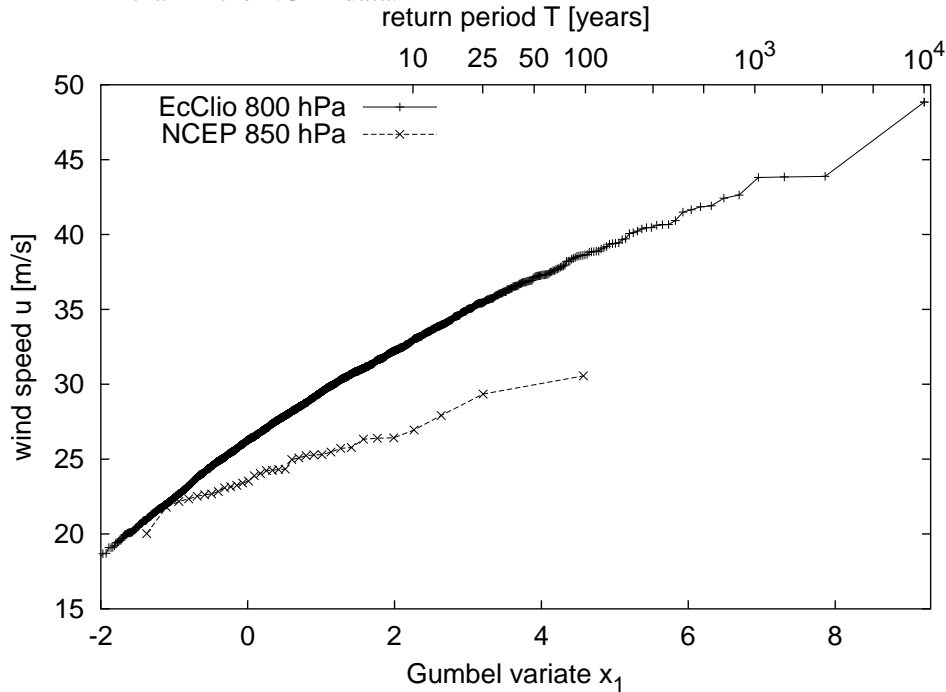


b. Validation of extreme statistics

For validation of the extreme wind distribution in ECBilt-Clio, we used the Reanalysis Dataset of the National Center of Environmental Prediction (NCEP) (Kalnay et al. 1996). This dataset provides the wind on a global $2.5^\circ \times 2.5^\circ$ grid every 6 hours. We used the July 1965 - June 2002 NCEP data. By lack of a 1000 hPa layer in ECBilt-Clio, we sampled wind speeds at 800 hPa (~ 2 km height) instead, being the lowest wind level in ECBilt-Clio. Comparison of the wind distributions at 850 and 1000 hPa for ocean grid points within the NCEP data shows similarity between the extreme value distributions (van den Brink et al. 2003). So, we assume that the ECBilt-Clio 800 hPa extreme winds have the same behavior as the extreme surface winds.

A suitable parameter to illustrate the ability of generating extremes is the GEV location parameter $\mu_{p=1}$, as it represents the wind speed that is exceeded on average once a year. Figure 3.3 shows $\mu_{p=1}$ (back transformed from u^k to the wind u) as estimated from the 3509 annual wind extremes in the control experiment of ECBilt-Clio at 800 hPa and from the 36 annual wind extremes in the NCEP data set at 850 hPa,

Figure 3.4: Distribution of the annual maxima at (65W,47N) in ECBilt-Clio and NCEP. The variability in extremes in ECBilt-Clio is considerably larger than in the NCEP data.

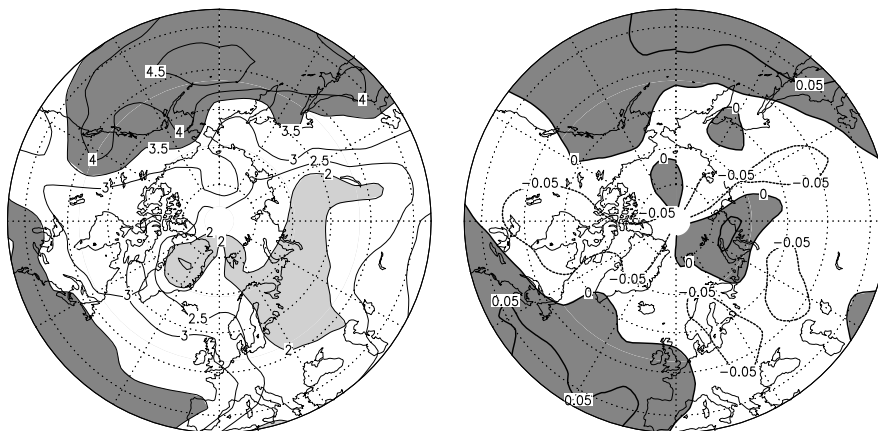


respectively. Figure 3.3 shows an overall agreement in the patterns over sea, although the position of the storm tracks in ECBilt-Clio and NCEP are slightly different, with the Pacific storm track in ECBilt-Clio being too strong. Enhanced land-sea gradients and underestimations over land are apparent in ECBilt-Clio, probably caused by the simplified parameterizations of the boundary layer over land and the extremely low vertical resolution.

The wind speeds with return periods longer than 10^2 years are considerably larger in ECBilt-Clio than in NCEP. This is illustrated in Figure 3.4 for grid point (65W,47N), for which ECBilt-Clio and NCEP have comparable estimates of the annual wind $\mu_{p=1}$, but differ considerably for larger return periods. Apparently, the variability in extremes is much larger in ECBilt-Clio than in the NCEP data.

In conclusion, it is clear that in the verification of ECBilt-Clio, considerable differences emerge. This is to be expected from models of intermediate complexity like ECBilt-Clio. Despite of these shortcomings, the ECBilt-Clio values seem close enough to reality to justify studies like the present one, i.e. exploration of the sta-

Figure 3.5: Estimated GEV scale parameter $\alpha_{p=1}$ (back transformed from u^k to u) and shape parameter $\theta_{p=1}$ of the daily averaged wind speed for the ECBilt-Clio control experiment at 800 hPa as derived from 3509 annual maxima of u^k . The standard error σ_θ according to Hosking et al. (1985) is between 0.012 and 0.015.



(a) scale parameter $\alpha_{p=1}$. Values larger than 3.5 and smaller than 2.0 are shaded

(b) shape parameter $\theta_{p=1}$. Positive values are shaded

tistical nature of extreme winds, like the potential existence of a double population. However, it should be emphasized that the question of the reality of specific features generated in ECBilt-Clio can only be answered with results of models of higher complexity.

3.5 Results

a. Spatial distribution of GEV parameters in the control experiment

The estimated GEV scale parameter $\alpha_{p=1}$ and shape parameter $\theta_{p=1}$ of the daily averaged annual maxima of the wind speed for the ECBilt-Clio control experiment at 800 hPa are shown in Figure 3.5. All three GEV parameters are largest over the oceanic storm tracks. In these regions, $\theta_{p=1}$ is lightly positive, i.e. downwardly curved on a Gumbel plot. A possible reason might be that here there is a physical upper limit to the wind speed (although this limit is far beyond the 10^4 -year wind). The small range of absolute values of θ in Figure 3.5(b) indicates that the annual

Figure 3.6: Signal-to-noise ratio SN for $|SN| > 1.5$ in the control experiment. According to our criterion (Eq. 3.23), $SN > 2$ indicates the existence of a double population.

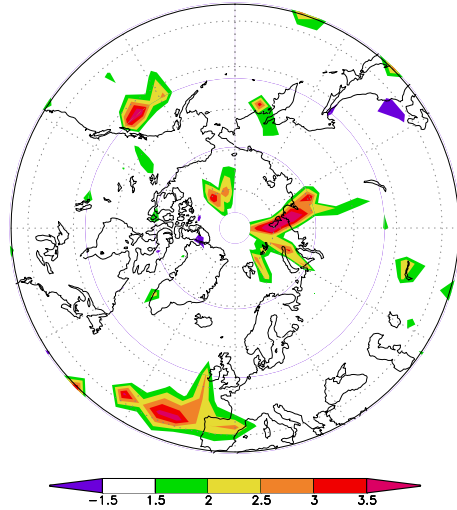
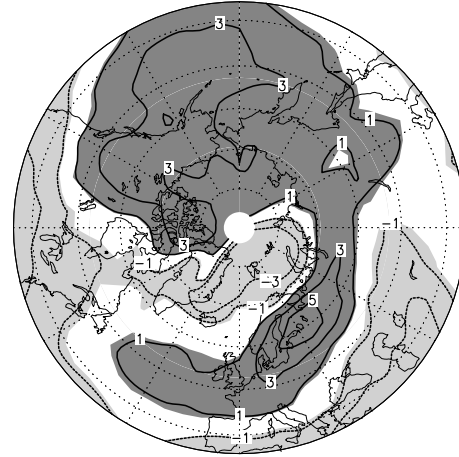


Figure 3.7: Relative changes (in %) in the GEV location parameter $\mu_{p=1}$ due to the greenhouse effect. The shaded areas are significant at 5% level.



maxima of u^k in ECBilt-Clio do not strongly deviate from the Gumbel distribution.

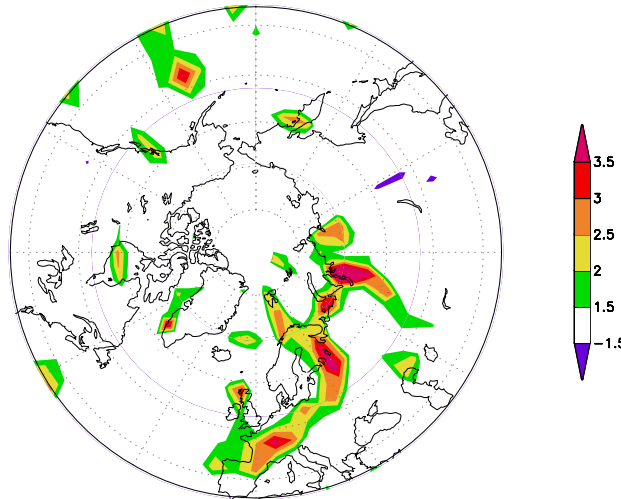
b. Two Component Extreme Value distributions in the control experiment

The spatial distribution of SN is shown in Figure 3.6 for $|SN| > 1.5$. Only patterns of large *positive* signal-to-ratios SN are detected. This indicates the reality of the patterns, as only situations with positive SN can be attributed to second populations. For 9.4 % of the area shown in Figure 3.6, SN is larger than 2, which is a factor two more than the expected 5% from Monte Carlo simulations. Figure 3.6 shows patterns of SN that fulfill our criterion (Eq. 3.23) over the Atlantic, the East Pacific and Siberia, which indicates that in the control run, double populations in the extreme wind speeds are apparent at the end of both storm tracks.

c. Greenhouse effect on wind extremes

The change in the annual extreme wind due to the greenhouse effect is represented by the change in the GEV location parameter $\mu_{p=1}$, shown in Figure 3.7. It shows a significant increase of the once-a-year exceeded wind speed over the Northern Atlantic and Europe, as well as over the Pacific and North America. Maximum increase

Figure 3.8: Signal-to-noise ratio SN for $|SN| > 1.5$ in the greenhouse experiment. According to our criterion (Eq. 3.23), $SN > 2$ indicates the existence of a double population.



(5%) is found over Scandinavia. Comparison with Figure 3.3 shows a zonally more elongated storm track, which is consistent with the positive NAO-like response to enhanced greenhouse gas forcing in ECBilt-Clio (Figure 11 in Schaeffer et al. (2003)). Apparently, the change in the annual wind maxima $\mu_{p=1}$ behaves similarly to the change in the mean wind in winter.

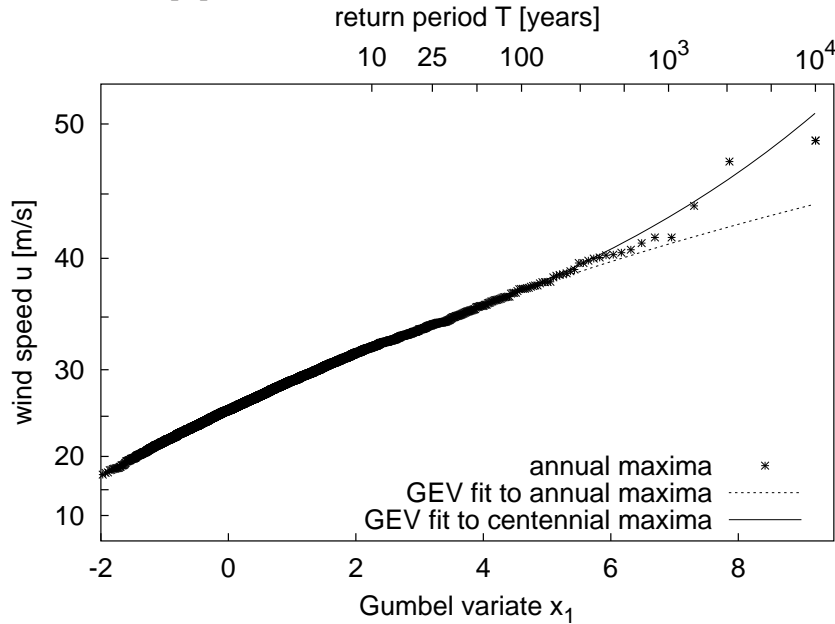
The regions where Two Component Extreme Value distributions are detected in the greenhouse experiment are shown in Figure 3.8. It shows the same patterns as in the control run, with the Atlantic region shifted to the east and elongated from Spain to Finland. For 10.6 % of the area shown in Figure 3.8, SN is larger than 2, which is a slight increase with respect to the control run.

3.6 Meteorology of the second population

Close inspection of the grid points with large positive SN reveals that the deviating extremes of neighboring grid points all originate from a restricted number of storms. Apparently, the storms are so intense, that they influence the highest extremes over a larger area during their track to the east.

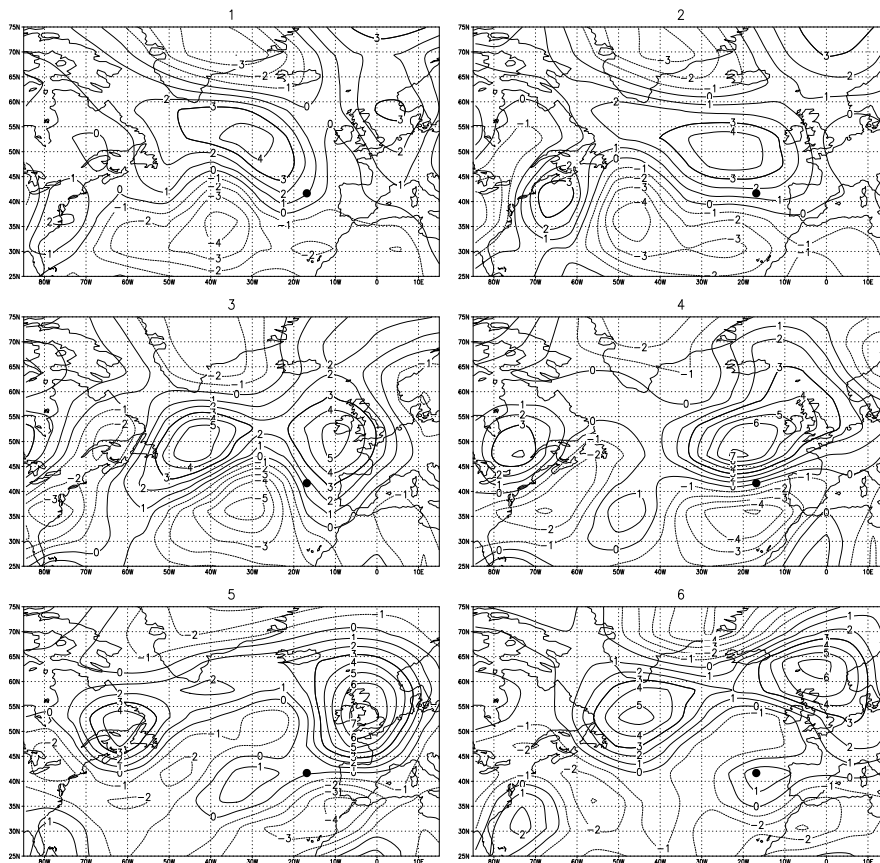
To find the meteorological circumstances responsible for this second population,

Figure 3.9: Gumbel plot for grid point (17W,42N) in the control run. The signal-to-noise ratio SN according to (3.22) is 3.8. Especially the three most severe events deviate from the fit, and are assumed to originate from the second population. The vertical scale is linear in u^k , with $k = 1.71$.



we concentrate on the events which clearly belong to that second population. We will consider grid point (17W,42N) in the control run, for which the maximum signal-to-noise ratio SN of 3.8 occurs. Figure 3.9 shows that the three most severe events substantially deviate from the fit, and thus can safely be assumed to originate from the second population. This is also apparent from the fact that SN decreases from 3.8 to $0.1 \ll 2$ if these three points are omitted from the data set, which means that there is no significant detection of a second distribution possible without the three largest events. The relative vorticity for the most extreme event is shown in Figure 3.10. In the first two days, it displays a mature cyclone which is no longer developing. However, at day 3, another cyclone is starting to merge with the original cyclone, resulting in explosive cyclogenesis and extreme wind speeds at the location of interest until day 5. After day 5, the decay phase of the eddy sets in. The importance of wave merging for the process of explosive cyclogenesis is stressed in several observational studies of cyclogenesis, e.g. Hakim et al. (1995a,b) and Gaza and Bosart (1990). In our results, merging occurs in the 1st, 2nd, 3rd and 5th most extreme events, but not

Figure 3.10: Daily averaged 800 hPa relative vorticity (10^{-5} s^{-1}) during merging. At day 4, the most extreme wind in 3509 years is reached for the indicated location (17W,42N).



in the situations of the other 10 largest extremes. We hypothesize that merging is a crucial condition for a second population of extreme wind speeds to occur.

Analysis of normal annual extremes shows that, at this location, wave merging is not exceptional. So, although important for the cyclogenesis process, it is clearly not a sufficient condition for a second population to occur. To distinguish between normal annual extremes and the merging events of the second population, we examined the anomalous time mean 500 hPa streamfunction pattern. The anomaly pattern was computed by first averaging the 500 hPa streamfunction Ψ over a period of 7 days preceding the day for which the maximum wind occurred in the grid point (17W,42N). This was done for 600 cases belonging to the first population a , and the four cases belonging to the second population b . The anomalous pattern Ψ_{an} is defined as the mean of the mentioned cases Ψ_b minus the mean of the 600 cases Ψ_a in the area between 80W and 10W and between 20N and 65N:

$$\begin{aligned}\Psi_{an} &= \Psi_b - \Psi_a & (3.24) \\ \Psi_a &= \frac{1}{600} \sum_{i=1}^{600} \Psi_{a,i} & \Psi_b = \frac{1}{4} \sum_{i=1}^4 \Psi_{b,i}\end{aligned}$$

where $\Psi_{a,i}$ is the 7-day averaged 500 hPa streamfunction pattern of case i in the first population a , and $\Psi_{b,i}$ is the same for the second population b . Figure 3.11 displays Ψ_a (a) and Ψ_{an} (b), and Figure 3.12 the corresponding zonal wind pattern.

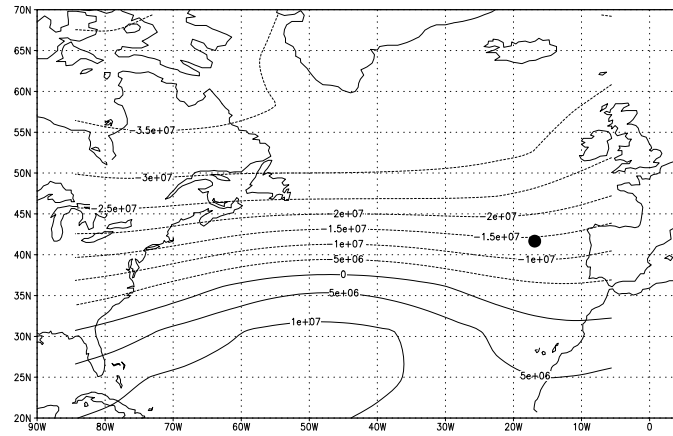
Figures 3.11 and 3.12 show that annual extremes develop in a mean circulation which is in a strong westerly phase, with maximum time mean zonal winds of 24 m/s. The anomaly pattern of the second population has a large positive amplitude in the model's version of the North Atlantic Oscillation pattern, and leads to a much stronger jet than normal annual extremes (up to 31 m/s). The pattern has an extension in easterly direction. We have computed the probability that the anomaly pattern of a member in the first population projects just as strong on the Ψ_{an} pattern as the four members of the second population. For the projection we used the squared norm:

$$p_i = \frac{\langle \Psi_{a,i} - \Psi_a, \Psi_{an} \rangle}{\langle \Psi_{an}, \Psi_{an} \rangle} \quad (3.25)$$

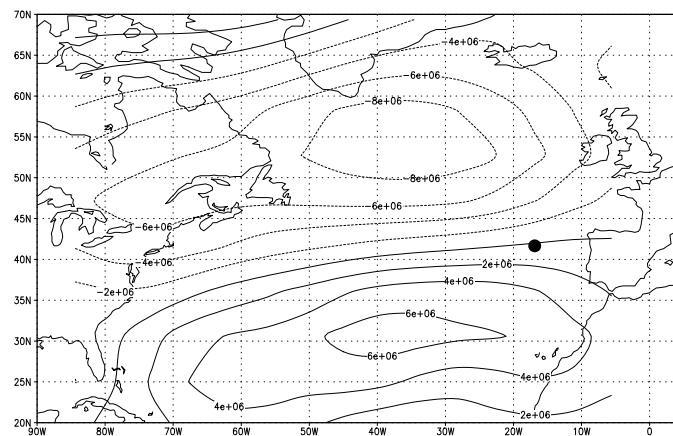
The events of population a will have an average projection of zero, and population b of one.

There are only six events of the 600 with a projection larger than unity, which means that the location and intensity of the jet stream of the second population has a frequency of order once in 10^2 years. Another striking feature of the second population is that the events are accompanied by extreme precipitation, where large scale precipitation and convective precipitation contribute equally. All four events of the

Figure 3.11: Mean streamfunction Ψ_a of the first population a (a) and the difference Ψ_{an} between the second population b and the first population a (b).

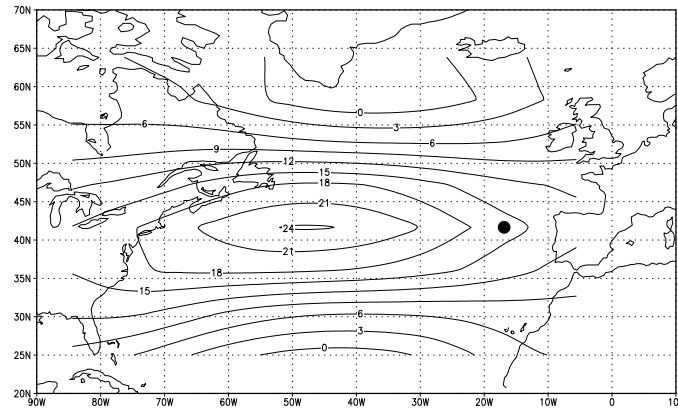


(a) mean 7-day averaged 500 hPa streamfunction Ψ_a of the first population a

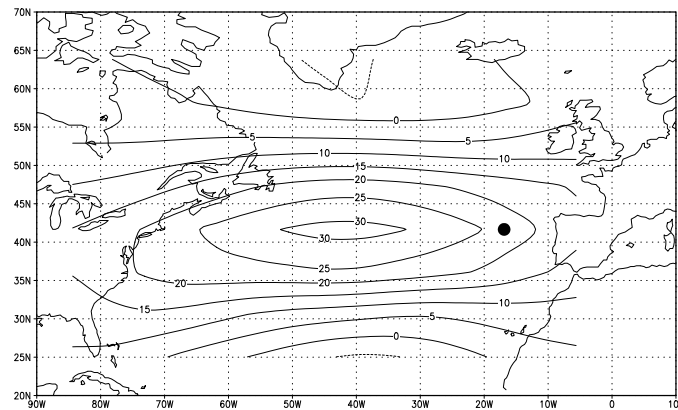


(b) difference Ψ_{an} in the mean streamfunction of the second population Ψ_b with that of the first population Ψ_a

Figure 3.12: Time mean zonal wind at 500 hPa of the first population (a), the second population (b), and their difference (c).



(a) mean 7-day averaged 500 hPa zonal wind speed of the first population *a*

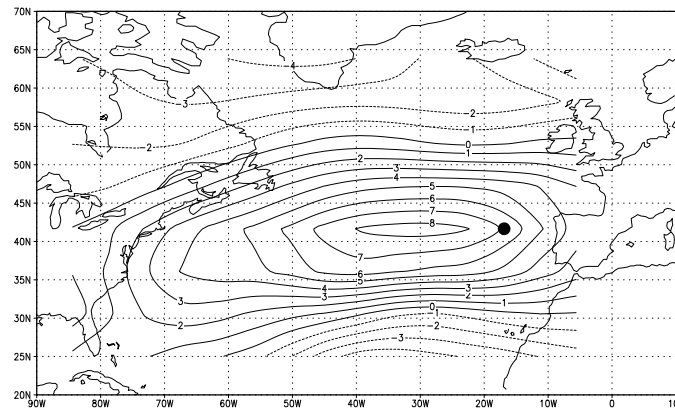


(b) mean 7-day averaged 500 hPa zonal wind speed of the second population *b*

second population have daily precipitation rates which have return periods of order 10^3 years.

We tentatively conclude that an extremely strong jet stream in which wave merging occurs can generate conditions which are favorable for the occurrence of strong

Figure 3.12 (continued): (c) difference of (a) and (b)



diabatic feedbacks. This leads to anomalously strong cyclogenesis and the generation of a second population of wind extremes.

We checked this hypothesis with the data from the greenhouse experiment. We consider grid point (5E,47N), which has a maximum in the signal-to-noise ratio SN of 3.9. Here, the 1st to 7th and 10th largest extremes belong to cyclones that originated after merging. Skipping the 7 largest events from the data set reduces SN from 3.9 to $0.35 \ll 2$. So, again, the detection is only significant when the merging events are incorporated.

Projection on the area between 80W and 10E and between 20N and 65N shows an increase of the maximum mean zonal wind from 22 to 31 m/s. Once in 56 years, the projection is larger than unity. Also the precipitation rates are extraordinary. For 6 of the 7 events, the return periods of the precipitation rates are of order 10^3 years. So, our hypothesis based on the control experiment is confirmed by the results of the greenhouse experiment.

We conclude that the extreme wind speed belongs to a second population if the following three conditions are fulfilled: First, there is an intense jet stream, corresponding with a positive NAO. Second, two cyclones merge to a single intense cyclone. Third, the cyclone is accompanied by extreme precipitation.

3.7 Discussion and conclusions

The climate model ECBilt-Clio shows preferred regions for the extratropics in which the annual wind extremes with return periods of order 10^3 years belong to another

population than the more frequent annual winds. One consequence of this result is that in such regions, the 10^4 -year wind speed can not be estimated from annual extremes in observed series with timelengths of order hundred years. Only a lower limit of the 10^4 -year wind can be estimated from such a series, as the existence of a second population in the extremes always increases the 10^4 -year wind. Another, closely related, consequence is that this low frequency of the second population prevents detection from single-station observational records.

We found that the second population in EcBilt-Clio exists of merging cyclones embedded in a strong jet stream, and that they are accompanied with extreme precipitation. The robustness of these results has to be confirmed by analyzing the results of more advanced models.

Doubling of the greenhouse gas concentrations has two important effects on the second population in the wind speed. The first is that the regions change for which second populations appear. This implies that regions, which are single-populated in the current climate, may be double-populated in a 2CO_2 climate and vice-versa. The second effect of CO_2 doubling in EcBilt-Clio is that, in double populated areas, the frequency of cyclones from the second population increases. Whereas the second population is dominant over the first population for return periods of 600 years and larger for the control run, this turning point lays at a return period of 40 years for the greenhouse run. This implies that not only the 10^4 -year winds are influenced by the second population, but also the 10^2 -year winds.

We attribute the eastward shift of the Atlantic area with double populations in the greenhouse experiment to the response in the climatological winter mean, which resembles a positive NAO pattern with largest westerly wind increase over Scandinavia (see Figure 11 in Schaeffer et al. (2003)). This response causes the eastward elongation of the storm track as shown in Figure 3.7, and consequently of the area in which a second population occurs.

Chapter 4

Improving 10^4 -year surge level estimates using data of the ECMWF seasonal prediction system

Abstract

The vulnerability of society on extreme weather has resulted in extensive research on the statistics of extremes. Although the theoretical framework of extreme value statistics is well developed, meteorological applications are often limited by the relative shortness of the available datasets. In order to overcome this problem, we use archived data from all past seasonal forecast ensemble runs of the European Centre for Medium-Range Weather Forecasts (ECMWF). For regions where the forecasts have very little seasonal skill the archived seasonal forecast ensembles provide independent sets that cumulate to over 1500 years. We illustrate this approach by estimating 10^4 -year sea-surge levels at high-tide along the Dutch coast. No physical mechanisms occur in the ECMWF model that make the distribution of very extreme surges different from what is inferred from a direct analysis of the observations. In comparison with the observational sets, the ECMWF set shows a decrease in the statistical uncertainty of the estimated 10^4 -year return value by a factor four.

4.1 Introduction

Meteorological extremes have large impacts on society. Typical examples are flooding of rivers caused by extreme precipitation, extended droughts, extreme temperatures, and flooding from the sea caused by extreme wind speeds. The higher the extremes, the more difficult it is to obtain their statistics from the observational datasets. However, these very extreme meteorological situations cause the most disastrous events. For many types of extremes, the meteorological situations causing these ex-

treme events are of synoptic scale ($O(10^3 \text{ km})$), and last for longer times (>12 hours). These properties make them appropriate to be explored with the set of ensembles of simulations generated by the ECMWF seasonal prediction system (Anderson et al. 2003). The resolution in space and time of the dataset is high enough to resolve extremes on synoptic scales.

The ECMWF seasonal forecast dataset has two properties advantageous for examining current-climate extremes. First, it combines high resolution in space (1.875° , 40 levels) and time (6-hourly output) with large record length (1569 years in total by May 2004). This length exceeds that of most high-resolution climate model runs (Kharin and Zwiers 2000; Kysely 2002; Kiktev et al. 2003). Second, the ECMWF model does not drift far from the observed climatology, as the individual forecast ensemble members are only 6 months in length. Here, we illustrate the power of the dataset by estimating extreme surge levels along the Dutch coast.

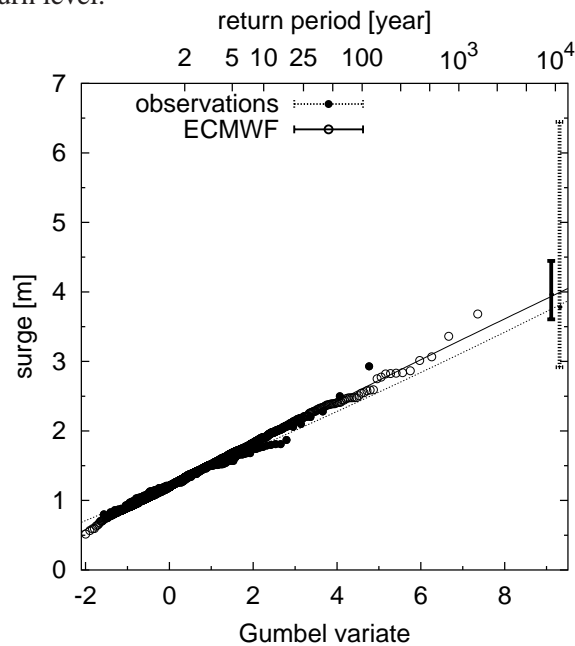
4.2 GEV analysis of observed surges

Approximately 40% of the Netherlands is below sea level. This part, with millions of inhabitants, is protected against flooding from the sea by dikes. Dutch official policy is that a flooding event is 'allowed' to happen with a probability of at most 10^{-4} per year, hence with a mean return period of 10^4 years. However, the heights of the dikes that correspond to this probability are hard to determine from Dutch observational sea level records, which cover order hundred years. So, an extrapolation over two orders of magnitude in probability is required, resulting in an 95%-confidence interval of several meters, which is considerably larger than the value of the expected sea level rise in the coming century (Church et al. 2001).

We follow the common choice in empirical studies to fit the annual maxima to the Generalized Extreme Value (GEV) distribution, and plot the results on a Gumbel plot, i.e., a plot with the ordered values on the ordinate and on the abscissa the Gumbel variate $x = -\ln(-\ln(F(x)))$, with $F(x)$ the cumulative distribution function of the variable x (see section 4.7 for further details). Figure 4.1 shows the annual maxima of the 117-years observational record for the Dutch coastal station Hoek van Holland, the fitted GEV distribution, its extrapolation to a return period of 10^4 years, and the corresponding 95%-confidence interval at this return period.

There are no known physical processes that limit the surge height to values below the estimated upper 95%-confidence level (6.44 m for Hoek van Holland). The high 95%-confidence level has large consequences for dike design. Another uncertainty in the extrapolation from the ~ 100 years of observations is the question if all surge extremes up to the 10^4 -year return period can be described by one GEV distribution with fixed parameters, a condition which is not always satisfied (van den Brink et al.

Figure 4.1: Gumbel plot for the 117 annual surge maxima of the Hoek van Holland observational set for 1887-2004 (\bullet), and for the 1569 annual maxima according to the archived data generated by the ECMWF seasonal forecast ensembles for 1987-2004 (\circ). Also shown are the GEV fits up to a return period of 10^4 years and the 95%-confidence interval of the 10^4 -year return level.



2004a).

The ECMWF dataset offers the possibility to check this condition, as well as to decrease the statistical uncertainty in the 10^4 -year estimate, due to the thirteen times larger amount of data compared to the observations.

4.3 ECMWF Model

Since August 2001 the ECMWF produces every month an ensemble of 40 global seasonal forecasts up to six months ahead, i.e., amply surpassing the 2-weeks horizon of weather predictability from the atmospheric initial state. Over the period 1987–2001, hindcasts, that is forecast runs on historical data, have been performed with smaller ensembles for calibrating the forecast system. The system consists of a coupled atmosphere-ocean model (Anderson et al. 2003). The atmospheric component

has a horizontal resolution of T95 (1.875°) and 40 levels in the vertical (Ritchie et al. 1995; Gregory et al. 2000; Anderson et al. 2003). The ocean component has a resolution of 1.4° and 29 vertical levels (Wolff et al. 1997). The ECMWF dataset provides, among other fields, global fields of 6-hourly winds and 2m-temperatures, 12-hourly sea level pressures and temperatures, and 24-hourly precipitation amounts.

We constructed 1569 calendar years by combining pairs of ensemble members with six months difference in starting date (see Table 4.1 for details), all of them generated by the so-called System-2 (Anderson et al. 2003).

Since the ECMWF model has very limited skill in predicting the NAO index (see also Palmer et al. 2004), effectively the simulations sample all different NAO situations.

The GEV location parameter μ for the annual maximum of 6-hourly wind speed (averaged between 30°N – 60°N and 90°W – 30°E) is constant within 1% for different forecast times. This indicates that the wind climatology of the system shows no detectable deterioration with forecast time.

The dependence between the ensemble members in the first weeks of the forecasts has negligible influence on the estimates of the GEV parameters of the surge.

We compared the daily-mean annual minima of the sea level pressure (SLP) at the Dutch coastal station Den Helder over 1906-2004 with the 1569 annual minima of the ECMWF SLP at the nearest sea grid point to Den Helder. The Gumbel plot is shown in Figure 4.2. There is a good agreement between the annual minima of the ECMWF data and the observations. We conclude that the ECMWF seasonal forecast system generates (deep) depressions with the same frequency and intensity as observed.

4.4 Surge Equation

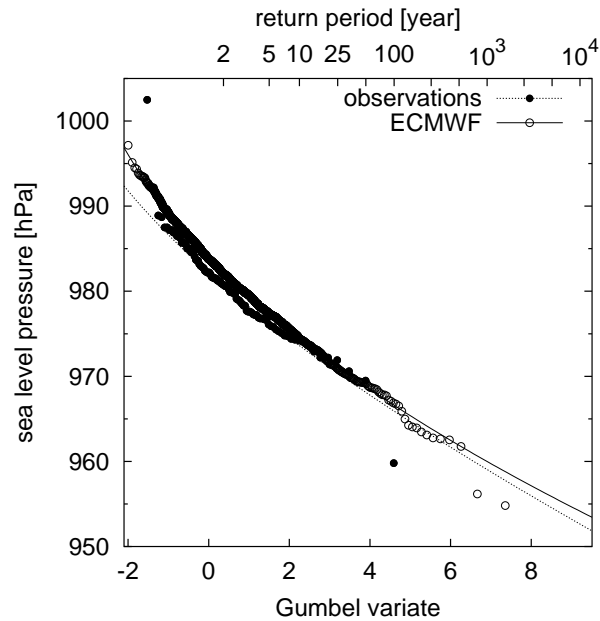
We use the following equation (van den Brink et al. 2003) to calculate from the meteorological data the surge at high-tide (i.e., the difference between the observed high tide and the calculated height of the astronomical high tide) at the coastal station Hoek van Holland:

$$\text{Surge} = A C_d u_{10}^2 \sin(\phi - \beta) + \frac{1015 - \text{SLP}}{100.5} \quad [\text{m}] \quad (4.1)$$

with C_d the drag coefficient, u_{10} the wind speed at 10 m averaged over 12 hours at a central grid box over the North Sea (depicted in Figure 4.3a), ϕ the wind direction and A and β empirically determined constants by Timmerman (1977). The second term on the right hand side of Eq. 4.1 represents the barometric pressure effect, with SLP the instantaneous sea level pressure in Hoek van Holland in hPa. Here, we describe the dependence of C_d on the wind speed u_{10} as

$$10^3 C_d = 0.738 + 0.068 u_{10} \quad (4.2)$$

Figure 4.2: Gumbel plot for the 98 annual SLP minima of the Den Helder observational set for 1996-2004 (\bullet), and for the 1569 annual SLP minima of the ECMWF dataset (\circ). The lines are the GEV fits up to a return period of 10^4 years.



where u_{10} is expressed in ms^{-1} , and in which the constants were obtained from a linear fit between the instantaneous, once-a-day available drag coefficient of the ECMWF dataset and u_{10} . To assure that Eq. 4.2 describes optimally the specific case of strong north-westerly winds, we used in the determination of the constants in Eq. 4.2 only those situations that resulted in the annual maximum surges in Hoek van Holland. In the 12-27 m/s range, which covers our range of interest, Eq. 4.2 fits closely to a Charnock relation (Charnock 1955) with parameter 0.016. Our estimate compares well with other estimates of high-speed drag over sea (e.g., Smith et al. 1992; Bonekamp et al. 2002).

The surge equation was validated by comparing the 1957-2002 observed annual extreme surges in Hoek van Holland with the annual extreme surges calculated from Eqs. 4.1 and 4.2 using the wind and pressure of the ERA40-Reanalysis data (Simmons and Gibson 2000). Table 4.3 and Figure 4.1 show good agreement between the GEV distributions fitted to the observed and calculated surges. About 1/2 of the annual extremes according to the ERA40 dataset correspond to the same storm as the

annual extremes in the observations.

4.5 Results

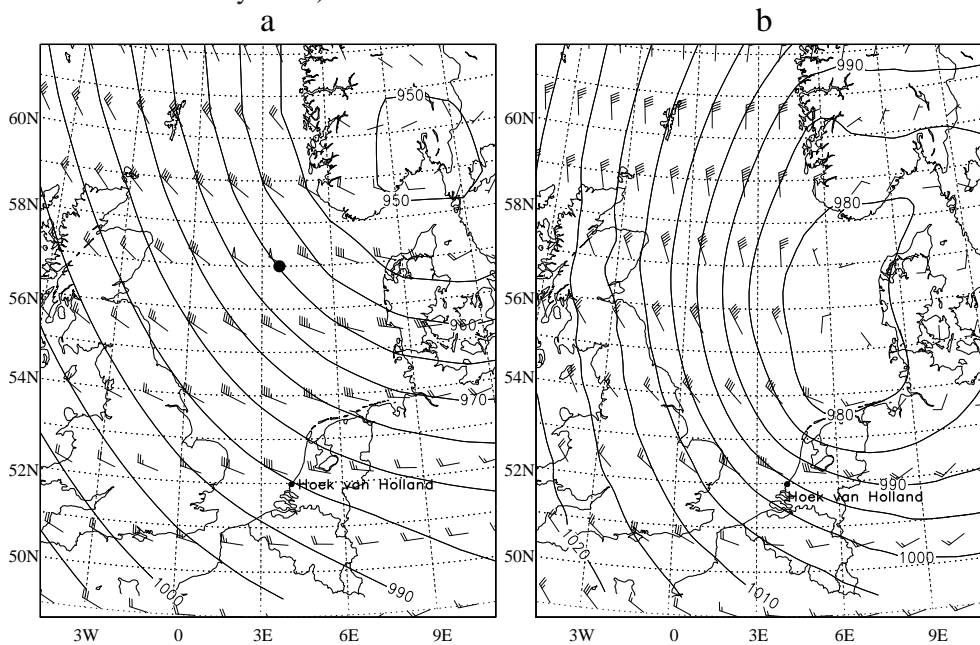
We calculated the surge at high-tide for coastal station Hoek van Holland with Eqs. 4.1 and 4.2, using SLP and u_{10} of the ECMWF dataset. The 1569 annual extremes are shown on a Gumbel plot in Figure 4.1, together with the 117 annual extremes of the 1887-2004 observational set. The following four features are apparent from Figure 4.1. First, the ECMWF-based data indicate that for extreme surges, a single GEV distribution is appropriate up to return periods of at least 10^3 years. So, the ECMWF data gives no indication that physical processes limit the strength of extreme storms, nor that the 10^3 -year winds are caused by another type of storms than 10-year winds, as in the less comprehensive model discussed in van den Brink et al. (2004a). Second, the GEV location parameter μ (representing the surge level with an exceedance probability of once a year) estimated from the ECMWF dataset equals that of the observational record within one cm (see also Table 4.4). This implies that systematic differences between the observed data and the results from the ECMWF system with the surge equation are small compared to the statistical uncertainties. Third, 10^4 -year surge level estimates from the ECMWF dataset (3.96 m) and from the observational record (3.78 m) are nearly equal. Fourth, the 95%-confidence interval of the 10^4 -year estimate reduces from 3.52 m for the observational set to 0.84 m for the ECMWF set, i.e., a reduction by a factor four.

The meteorological situation in the ECMWF data that leads to the highest surge at Hoek van Holland (3.68 m) is depicted in Figure 4.3a. For comparison, Figure 4.3b shows the meteorological situation according to the ECMWF-Reanalysis of the largest real event in the observations (2.93 m, on 1 February 1953). Both situations show a large-scale depression, generating a strong north-westerly flow over the entire North Sea. The 25 hPa deeper depression and the more north-easterly position of the depression in Figure 4.3a with respect to the situation in Figure 4.3b leads to a 0.75 m higher surge level at Hoek van Holland. Figure 4.3 shows that the largest surge from the ECMWF dataset is caused by a realistic meteorological situation.

4.6 Conclusions

The ECMWF seasonal forecast dataset can serve as a powerful tool for estimating 10^3 - 10^4 -year return values for meteorological extremes that are caused by synoptical weather systems. The statistics of extreme storm surge levels in the Netherlands in this dataset can be described well by a single GEV distribution for return periods ranging from 1 to 10^3 years. The statistical uncertainty in the 10^4 -year return surge

Figure 4.3: Wind and pressure field for the situations of highest surge at high-tide in Hoek van Holland. **a**: in the ECMWF dataset for day 57 in ensemble member 15, starting from 1 November 1987 (calculated surge in Hoek van Holland: 3.68 m). The dot is the location used for calculating the surge at high-tide via Eqs.4.1 and 4.2. **b**: ECWWMF Reanalysis, for the highest surge in the observations for Hoek van Holland (2.93 m, on 1 February 1953).



level is reduced by a factor four with respect to observations. The dataset offers potentials to estimate 10^3 - to 10^4 -year return values for wind, temperature, precipitation and related variables as surge and river discharges, with unprecedented accuracy.

4.7 Auxillary Information

This section is only part of the electronic version of the paper, and is available from <ftp://ftp.agu.org/apend/gl/2004GL020610/>.

Extreme value statistics

A fundamental theoretical result from the statistics of extremes is that any limiting distribution of so-called 'block maxima' must be in the form of the Generalized Extreme Value (GEV) distribution (Coles 2001):

$$G(x) = P(M \leq y) = e^{-e^{-x}} \quad (4.3)$$

with M the maximum over a block of standard length, $G(x)$ the GEV distribution, and x a substitute for:

$$x = \ln \left(1 - \theta \frac{y - \mu}{\alpha} \right)^{-1/\theta} \quad (4.4)$$

with μ the location parameter, α the scale parameter, θ the shape parameter, and y the variable considered. In order to eliminate the effects of the annual cycle, a common choice in empirical studies is to examine the distribution of annual maxima (Palutikof et al. 1999; Katz et al. 2002). The probability of exceedance of a certain value y is usually expressed in terms of the return period T , which is the average number of years between two succeeding exceedances of the corresponding return value y :

$$T = \frac{1}{1 - G(x)} \approx e^x \quad \text{for } T \gg 1 \quad (4.5)$$

The results in Figures 4.1 and 4.2 are plotted on a Gumbel plot, a plot with the Gumbel variate $-\ln(-\ln(F(x)))$ as abscissa ($F(x)$ being the cumulative distribution function) and the return value y as ordinate. This representation transforms a Gumbel distribution ($G(x)$ with $\theta = 0$) into a straight line.

For fitting the data to the GEV distribution, we used the maximum-likelihood procedure. The 95%-confidence values in the return value estimates were determined from the log-likelihood profile (Coles 2001).

Table 4.1: Combinations of 6-months forecasts to construct calendar years. The 1987-Aug 2001 period are hindcasts, and the Aug 2001-May 2004 are forecasts. Notation: 1st to 4th digit: year; 5th and 6th digit: month; last two digits: ensemble number.

ensemble 00-04	ensemble 05-39	ensemble 40
198707-00 ↔ 198801-00	198711-05 ↔ 198805-05	198711-40 ↔ 198805-40
198708-00 ↔ 198802-00	198811-05 ↔ 198905-05	198811-40 ↔ 198905-40
198709-00 ↔ 198803-00	198911-05 ↔ 199005-05	198911-40 ↔ 199005-40
198710-00 ↔ 198804-00	199011-05 ↔ 199105-05	199011-40 ↔ 199105-40
198711-00 ↔ 198805-00	199111-05 ↔ 199205-05	199111-40 ↔ 199205-40
198712-00 ↔ 198806-00	199211-05 ↔ 199305-05	199211-40 ↔ 199305-40
198807-00 ↔ 198901-00	199311-05 ↔ 199405-05	199311-40 ↔ 199405-40
198808-00 ↔ 198902-00	199411-05 ↔ 199505-05	199411-40 ↔ 199505-40
198809-00 ↔ 198903-00	199511-05 ↔ 199605-05	199511-40 ↔ 199605-40
198810-00 ↔ 198904-00	199611-05 ↔ 199705-05	199611-40 ↔ 199705-40
198811-00 ↔ 198905-00	199711-05 ↔ 199805-05	199711-40 ↔ 199805-40
198812-00 ↔ 198906-00	199811-05 ↔ 199905-05	199811-40 ↔ 199905-40
: ↔ :	199911-05 ↔ 200005-05	199911-40 ↔ 200005-40
: ↔ :	200011-05 ↔ 200105-05	200011-40 ↔ 200105-40
200107-00 ↔ 200201-00		
200108-00 ↔ 200202-00	200108-05 ↔ 200202-05	
200109-00 ↔ 200203-00	200109-05 ↔ 200203-05	
200110-00 ↔ 200204-00	200110-05 ↔ 200204-05	
200111-00 ↔ 200205-00	200111-05 ↔ 200205-05	
200112-00 ↔ 200206-00	200112-05 ↔ 200206-05	
200207-00 ↔ 200301-00	200207-05 ↔ 200301-05	
200208-00 ↔ 200302-00	200208-05 ↔ 200302-05	
200209-00 ↔ 200303-00	200209-05 ↔ 200303-05	
200210-00 ↔ 200304-00	200210-05 ↔ 200304-05	
200211-00 ↔ 200305-00	200211-05 ↔ 200305-05	
200212-00 ↔ 200306-00	200212-05 ↔ 200306-05	
200307-00 ↔ 200401-00	200307-05 ↔ 200401-05	
200308-00 ↔ 200402-00	200308-05 ↔ 200402-05	
200309-00 ↔ 200403-00	200309-05 ↔ 200403-05	
200310-00 ↔ 200404-00	200310-05 ↔ 200404-05	
200311-00 ↔ 200405-00	200311-05 ↔ 200405-05	

Table 4.2: Specification of the number of years constructed from the ensemble forecasts.

	#ensembles	hindcasts	forecasts	total	
ensemble 00-04	5	$14 \times 6 + 1 = 85$	16	505	years
ensemble 05-39	35	14	16	1050	years
ensemble 40	1	14	-	14	years
total				1569	years

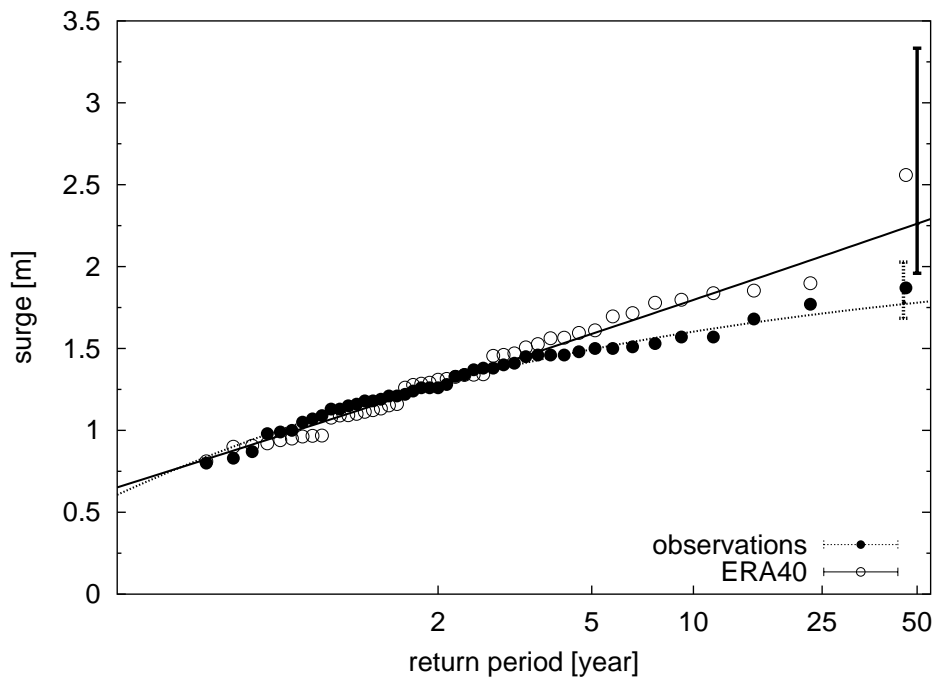
Table 4.3: GEV parameter estimates and their standard errors, and 50-year surge level estimates with the 95%-confidence values, as obtained from the observational dataset for Hoek van Holland, and from the ERA40-Reanalysis dataset using Eq. 1 and 2, both for the period 1957-2002.

	μ [m]	α [m]	θ	50-year surge [m]
ERA40	1.18 ± 0.05	0.27 ± 0.03	-0.02 ± 0.13	$2.26 \begin{smallmatrix} 3.33 \\ 1.96 \end{smallmatrix}$
observations	1.21 ± 0.04	0.23 ± 0.03	0.25 ± 0.09	$1.78 \begin{smallmatrix} 2.03 \\ 1.68 \end{smallmatrix}$

Table 4.4: GEV parameter estimates and their standard errors, and 10^4 -year surge level estimates with the 95%-confidence values, as obtained from the 1887-2004 observational dataset for Hoek van Holland, and from the 1569-year ECMWF dataset using Eq. 1 and 2.

	μ [m]	α [m]	θ	10^4 -year surge [m]
ECMWF	1.21 ± 0.01	0.31 ± 0.01	0.008 ± 0.018	$3.96 \begin{smallmatrix} 4.44 \\ 3.60 \end{smallmatrix}$
observations	1.22 ± 0.03	0.26 ± 0.02	-0.017 ± 0.06	$3.78 \begin{smallmatrix} 6.44 \\ 2.92 \end{smallmatrix}$

Figure 4.4: Gumbel plot of the observed surge in Hoek van Holland (●), and the surge calculated from the ERA40-Reanalysis dataset using Eq. 1 and 2 (○), both for the period 1957-2002. The lines are the GEV fits to the annual maxima. The 95%-confidence values are shown for a return period of 50 years.



Chapter 5

Estimating return periods of extreme events from ECMWF seasonal forecast ensembles

Abstract

Meteorological extremes have large impacts on society. The fact that approximately 40 % of The Netherlands is below sea level, makes this country especially vulnerable for floodings, both from the sea and from the rivers. This has resulted in extensive research on the statistics of extremes. However, application to meteorological and hydrological situations are always hampered by the shortness of the available datasets, as the required return levels exceed the records lengths with a factor 10 to 100. In order to overcome this problem, we use archived data from all past seasonal forecast ensemble runs of the European Centre for Medium-Range Weather Forecasts (ECMWF) since 1987 as input for extreme value statistics analysis. We make use of the fact that the seasonal forecast have little seasonal skill for The Netherlands, which implies that the ensembles can be regarded as independent sets that cumulate to over 1500 years.

We investigate the hydraulic response in the Netherlands to extreme synoptic scale weather systems by studying the extreme value distributions of sea storm surge levels, waves and river discharges. The application is detailed in four practical examples originating from coastal protection, river flooding protection, and water management problems. The long record length of the ECMWF data reduces the uncertainty in the 10^3 -year and the 10^4 -year return values considerably with respect to the results based on observational time series. The ECMWF data set gives the opportunity to explore the distribution of events that depend on several kind of extremes.

5.1 Introduction

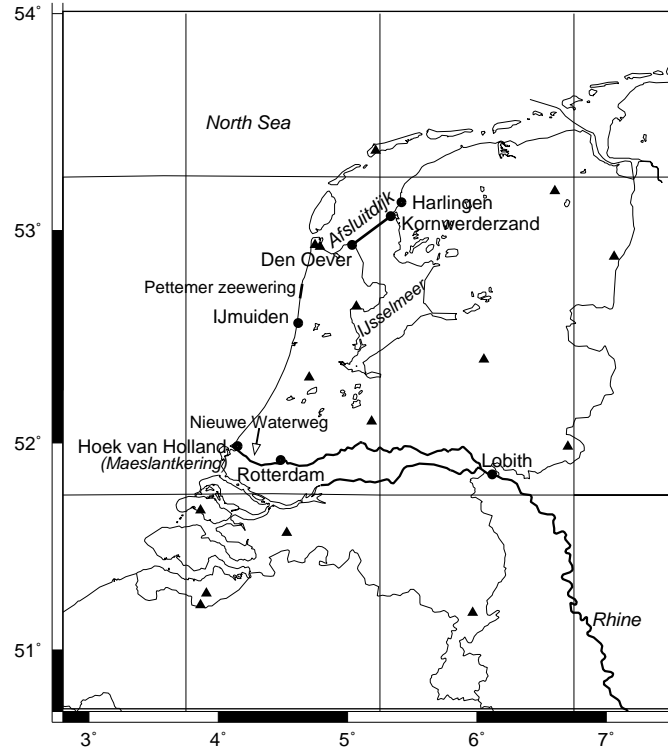
Much statistical research has been done on estimating the statistics of extremes of weather (related) variables, like precipitation, wind speed, river discharge and surge from observational records (Buishand 1991; Palutikof et al. 1999; Katz et al. 2002; de Haan 1990). To overcome the rather short length of the observational records (order hundred years), we explored an alternative data source, i.e. the archived seasonal forecast ensemble data of the European Center for Medium-Range Weather Forecasts (ECMWF) over the period 1987-2004, which cumulate to a total size of 1569 simulated years (status May 2004). Assuming that this model is a faithful representation of the climate system, these simulated years represent many realizations of the present climate on synoptic scale. Because this model dataset is an order of magnitude longer than the length of the observational sets, an improved estimate of extreme levels can be obtained. In an earlier article (van den Brink et al. 2004b) we discussed the extreme value statistics of storm surges at the Dutch coast. We found that the ECMWF model represents the statistics of large and deep depressions well. The statistical uncertainty of the height of a 10^{-4} probability storm surge was decreased by a factor four compared with the use of the historical observations, with systematic errors that appeared smaller than the statistical uncertainty. As an elaboration of van den Brink et al. (2004b), we apply in this paper the ECMWF seasonal forecast data set to four hydraulics-related situations in The Netherlands, that result from severe weather events on synoptic scale. First, to extreme Rhine river discharges at the location where it flows into the Netherlands. Second, to the duration of the spells that sea-level is too high sluicing water from the 'IJsselmeer' into the North Sea. Third, to the frequency that the big 'Maeslantkering' storm surge barrier in the 'Nieuwe Waterweg' Rhine outlet must be closed in order to prevent flooding of the densely populated Rotterdam area. The criteria for closing the barrier depend on the sea level as well as on the Rhine river discharge. Fourth, to the frequency of failure of the 'Pettemer zeewering' sea dike, which depends both on sea level elevation and wave height. See Figure 5.1 for the locations of the towns, rivers and barriers.

This paper is structured as follows: Section 5.2 describes the theoretical framework, Section 5.3 the ECMWF model and seasonal forecast ensembles, Section 5.4 the extreme value analysis of the mentioned applications, and Section 5.5 the conclusions and discussion.

5.2 Theory

A fundamental theoretical result from the statistics of extremes is that any limiting distribution of 'block maxima' must be in the form of the Generalized Extreme Value

Figure 5.1: Map of The Netherlands, with the locations that are mentioned in the text. The lines represent the physical grid to which the ECMWF data have been interpolated ($1.5^\circ \times 1.5^\circ$). The triangles are the 15 stations used for verification of the precipitation.



(GEV) distribution (e.g. de Haan 1976):

$$G(x) = P(M \leq y) = e^{-e^{-x}} \quad (5.1)$$

with M the maximum over a 'block' of standard length, $G(x)$ the GEV distribution, and x a substitute for:

$$x = \ln \left(1 - \theta \frac{y - \mu}{\alpha} \right)^{-1/\theta} \quad (5.2)$$

with μ the location parameter, α the scale parameter, θ the shape parameter, and y the considered variable. A common choice is to examine the distribution of annual maxima. In that case, the location parameter μ represents the value which is exceeded on average once a year.

In extreme value studies, the probability of exceedance of a certain value y is usually expressed in terms of the *return period* T . The return period T is the average number of years between two succeeding exceedances of the corresponding *return value* y :

$$T = \frac{1}{1 - G(x)} \approx e^x \quad \text{for } T \gg 1 \quad (5.3)$$

For fitting the data to the GEV distribution, we used the method of maximum likelihood. The 95%-confidence values in the return value estimates were determined from the log-likelihood profile (Coles 2001).

The results are plotted on a Gumbel plot, a plot of a cumulative distribution function $F(x)$ with the Gumbel variate $-\ln(-\ln(F(x)))$ as abscissa and the return value y as ordinate. This representation transforms the Gumbel distribution ($G(x)$ with $\theta = 0$) into a straight line.

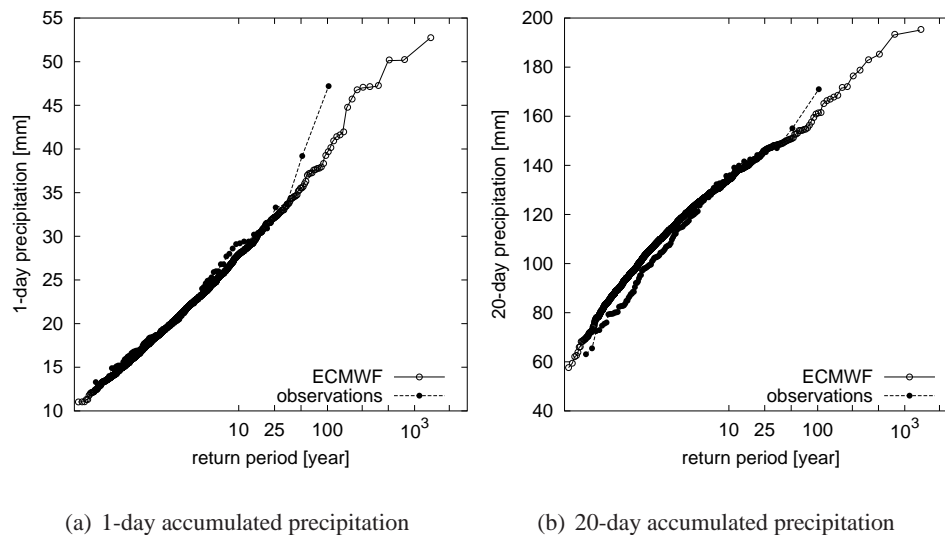
Extreme value theory is often required to find return values for return periods that amply exceed the record length. This implies extrapolation of the GEV fit to a domain outside the range of the observations. In our approach, the return value determination involves little extrapolation, as series length and return periods of interest T are about equal. This considerably reduces the uncertainty in the estimate.

5.3 ECMWF Model

a. Description

From September 2001 onward the European Centre for Medium-range Weather Forecasts (ECMWF) produces every month an ensemble of 40 global seasonal forecasts up to six months ahead, i.e., amply surpassing the 2-weeks horizon of weather predictability from the atmospheric initial state. Over the period 1987–2001, hindcasts with smaller ensembles have been performed to calibrate the system. The forecast system consists of a coupled atmosphere-ocean model (Anderson et al. 2003). The atmospheric component has a horizontal resolution of T95 (1.875°) and 40 levels in the vertical (Ritchie et al. 1995; Gregory et al. 2000; Anderson et al. 2003). The ocean component has a resolution of 1.4° and 29 vertical levels (Wolff et al. 1997). We combined all hindcasts and forecasts generated up to May 2004 into 1570 calendar years of data, all of them generated by the so-called System-2 (Anderson et al. 2003). The ECMWF dataset provides, among other fields, global fields of 6-hourly winds and 2m-temperatures, 12-hourly sea level pressures and temperatures, and 24-hourly precipitation amounts.

Figure 5.2: Gumbel plots of the 1-day (a) and 20-day (b) accumulated precipitation, for the average of 15 Dutch stations (1901-2001) and the corresponding ECMWF boxes (4.5° – 6° E, 52.5° N). See Figure 5.1 for the locations of the 15 stations.

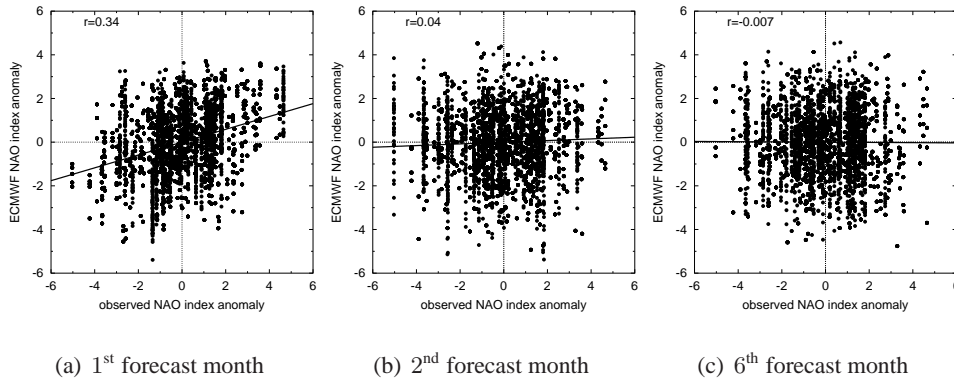


b. Verification

In order to model hydraulic extreme events correctly, especially the wind and precipitation should well be represented in the model. As it is difficult to verify the model winds directly (due to the relatively short (homogeneous) observational records over the North Sea), van den Brink et al. (2004b) validated the sea level pressure (SLP) instead: a direct model parameter which can easier be compared with observations than wind data, and which is a good measure of the capability of the model to produce deep depressions. They found a good agreement between the statistics of extremely low SLP's in the ECMWF model and the observations for coastal station Den Helder. Also the surge statistics for the coastal station Hoek van Holland are well reproduced by the ECMWF model (van den Brink et al. 2004b).

Figure 5.2 compares the extreme precipitation rates of the average of the two ECMWF boxes (4.5° – 6° E, 52.5° N) in the ECMWF data with the accumulated precipitation averaged over 15 stations in the Netherlands (indicated in Figure 5.1). Both the 1-day and the 20-day accumulated quantities are shown. Figure 5.2 shows that

Figure 5.3: Scatter plot of the NAO index anomaly (Dec-Mar) of the ECMWF seasonal forecast against the observed NAO, for first (a) second (b) and sixth (c) forecast month. The lines represent a least-square fit.



the statistics of extreme precipitation are well reproduced for both timescales.

In order to investigate the dependence between the ensembles and their initial states, we calculated the correlation between the observed (monthly mean) North Atlantic Oscillation (NAO) index and the calculated NAO-index from the ECMWF data. Figure 5.3 shows the scatter plots for different forecast months. For the first forecast month, there is a small correlation ($r = 0.34$) between the monthly-averaged NAO of the seasonal forecast and the observed NAO. This correlation is nearly zero ($|r| \leq 0.07$) for longer forecast times. This implies that the NAO index of ECMWF data set is (almost) independent of the initial NAO index, and thus is representative for a more general situation than for the 1987–2004 period only. A very similar version of the ECMWF model has also been shown to have very limited skill in predicting the NAO index (Palmer et al. 2004).

The constant variance of the modelled NAO index with forecast time, and the independence of fitted GEV parameters with forecast time indicate that the climatology of the system shows no detectable deterioration with forecast time.

We verified that the dependence between the ensemble members in the first weeks of the forecasts has negligible influence on the estimates of the GEV parameters, making the whole 6-month period usable for our purpose.

5.4 Four Applications

a. Rhine discharge

The dikes along the Dutch rivers are supposed to withstand a discharge with a return period of 1250 years. The Rhine discharge at the Dutch border and the accumulated n -day precipitation over the Rhine basin correlate well for $n=10-30$ (Fink et al. 1996). We concentrate on 20-day accumulated values (validated in section 5.3b).

We calculated the Rhine discharge at Lobith at the Dutch-German border (see Figure 5.1) with the following simple water balance equation:

$$Q = A + \sum_{j=0}^{19} \sum_i s_i \left(\text{LSP}_{i,j} + \text{CP}_{i,j} - \text{E}_{i,j} - \text{S}_{i,j} \right) \quad (5.4)$$

with $\text{LSP}_{i,j}$ the large-scale precipitation on the j^{th} -last day in grid box i , of which a surface area s_i (in m^2) belongs to the catchment of the Rhine. CP is the convective precipitation, E the evaporation and S the snow accumulation, all in meters water per second. The adjustment parameter A was determined empirically by tuning the location parameter μ of the GEV distribution (i.e. the once-a-year event) with its observed value at Lobith. A turns out to be $-4 \cdot 10^3 \text{ m}^3\text{s}^{-1}$.

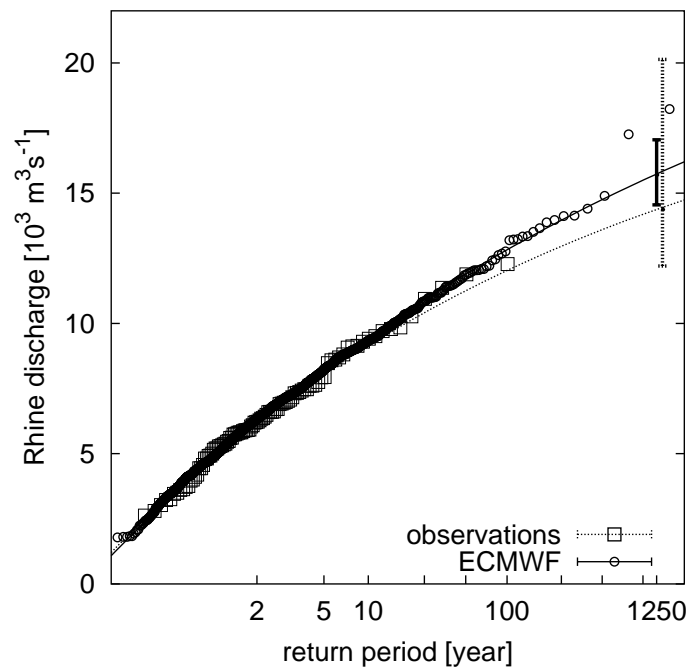
The Gumbel plot of the Rhine discharge according to the observational record at Lobith and to the ECMWF data (Eq. 5.4) are shown in Figure 5.4. The estimate from the observations for the 1250-year discharge ($14.3_{12.2}^{20.1} \cdot 10^3 \text{ m}^3\text{s}^{-1}$) is 9% smaller than the estimate from the ECMWF data ($15.7_{14.5}^{17.1} \cdot 10^3 \text{ m}^3\text{s}^{-1}$). The ECMWF estimate lies amply within the 95% uncertainty interval of the estimate from the observations. The application of the ECMWF data reduces the 95% confidence interval of the 1250-year level estimate by a factor three.

b. IJsselmeer sluicing

The IJsselmeer (Lake IJssel) in central Netherlands covers an area of 2000 km^2 , and is separated from the North Sea by the Afsluitdijk. To keep the level of the IJsselmeer at the preferred level of 0.45 m below mean sea level (MSL) in winter (and 0.25 m below MSL in summer) (Peilbesluit, 1992), the excess of IJsselmeer water is discharged into the North Sea during low tide by opening the Afsluitdijk sluices at Kornwerderzand and Den Oever (Low lower tide at Kornwerderzand: 1.23 m below MSL). During high tide, the sluice gates are closed. If a surge elevates the low-tide sea level above a value of 0.55 m below MSL, sluicing is not possible during an entire tidal cycle.

To examine the period that surges prevent sluicing, we calculated the sea level at every low tide by adding the surge to the astronomical low tide, where the 6-hourly calculated surge was linearly interpolated to the time of the astronomical low

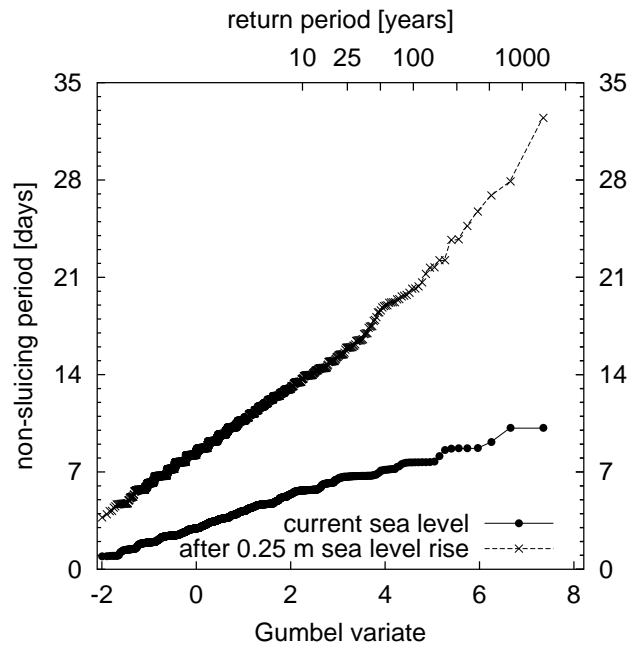
Figure 5.4: Gumbel plot for the 100 observed annual maximum Rhine discharges at Lobith (1900-2000) (\square) and for the 1569 annual maxima as derived from the ECMWF data via Eq. 5.4 (\circ). Also shown are the extrapolated GEV fits to 1250-year return periods and the 95%-confidence intervals to the observations and to the ECMWF data.



tide. The harmonical constituents of the astronomical tide at Kornwerderzand were obtained from Flater (1998). The surge was calculated from the ECMWF data by applying a simple surge model (see Eq. (1) in van den Brink et al. 2004b) to the nearby location Harlingen (see Figure 5.1).

Figure 5.5 shows a Gumbel plot of the time period of non-sluicing, both for the current sea level, and for the situation with a sea level rise of 0.25 m. This value is within the expected range of 5–32 cm in 2050 (Houghton et al. 2001), and is the estimate of the medium scenario for The Netherlands (Kors et al. 2000). Apparently, for the present-day sea level a one-week period of non-sluicing occurs every 25 years. With constant water management practice, a 0.25 m sea level rise would increase the length of the extreme duration of non-sluicing by at least a factor of two. A rise of 0.45 m (which is the extreme scenario for The Netherlands in 2050, Kors et al. 2000)

Figure 5.5: Gumbel plot of the period that surges prevent sluicing from the IJsselmeer into the North Sea, both for current mean sea level and for the situation after a sea level rise of 25 cm, expected for 2050.



would cause another factor three increase.

c. Storm surge barrier closure

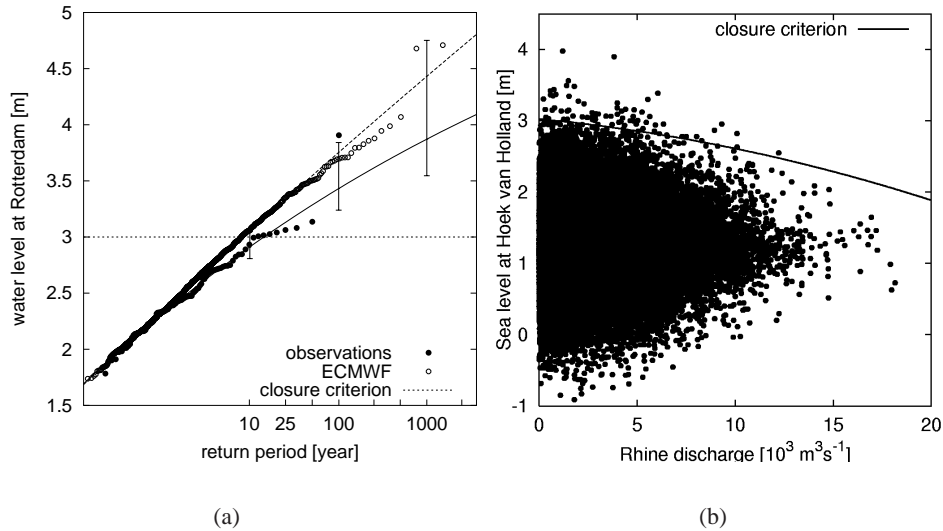
The 'Maeslantkering' is a storm surge barrier in the 'Nieuwe Waterweg' Rhine outlet near Hoek van Holland (see Figure 5.1), which automatically closes when the water level L_R at Rotterdam is expected to exceed a level of 3 m above MSL. The water level at Rotterdam is determined not only by the Rhine discharge, but also by the tidal motions of the sea and the surges.

The water level at Rotterdam L_R relates statistically to the sea level at Hoek van Holland L_{HvH} and the Rhine discharge at Lobith Q by:

$$L_R = L_{HvH} + aQ + bQ^2 \quad (5.5)$$

where a and b are constants. The average closure frequency of the Maeslantkering is not exactly known, as there has been some debate whether the extreme surges and discharges can be treated independently in the risk analysis.

Figure 5.6: Left: Gumbel plot of the water level with respect to MSL L_R at Rotterdam, both for the observational set and for the ECMWF set. Also shown are the closure criterion, the GEV fits, and the 95%-uncertainty intervals for return periods of 10, 100 and 1000 years for the observational set. The closure criterion of the Maeslantkering, $L_R = 3$ m, is indicated. Right: Scatter plot of the water level at Hoek van Holland L_{HvH} versus the Rhine discharge Q for all high-tide values of L_R of the ECMWF set, together with the closure criterion $L_R = 3$ m. According to our analysis, the closure criterion is exceeded once every 8.1 years.



We calculated the Rhine discharge according to Eq. 5.4, and the high-tide sea level at Hoek van Holland by calculating the high tide surge every 12 hours from the ECMWF data according to (Eq. (1) in van den Brink et al. 2004b), and adding that value to the astronomical high tide that occurred in the 12 preceding hours. A Gumbel plot of L_R is shown in Figure 5.7(a), both for the observations and for the ECMWF data. The scatter plot of the Rhine discharge and the sea level at Hoek van Holland for the annual maxima of L_R , as well as the closure criterion $L_R = 3$ m, are shown in Figure 5.7(b). According to the ECMWF data, the criterion is exceeded on average once in 8.1 years. Note that most of these events occur because of an extreme surge level rather than an extreme river discharge, due to the small sensitivity of the

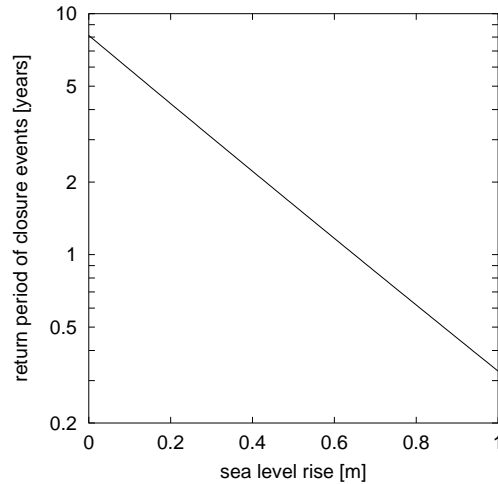


Figure 5.7: Effect of sea level rise on the frequency of closing the 'Maeslantkering'. The vertical scale is logarithmic.

criterion (Eq. 5.5) to the river discharge. Note also that no positive correlation is apparent between surges and discharges.

Figure 5.7 shows that the number of closure events increases exponentially with sea level rise. In this calculation, no greenhouse-effect on the tides, surges and Rhine discharges is taken into account. With the increase of number of closings, the average duration of closing will also increase.

d. Wave and sea level interaction

The "Pettemer zeekering" is a small stretch of sea dike that closes a gap in the natural coast protection formed by sand dunes near Petten. The design height of the dikes is determined not only by sea level elevations, but also by wave heights, because of run-up of waves. Extreme surges and sea wave heights are correlated, as they both tend to occur during strong North-Westerly winds. Failure of the "Pettemer zeekering" may occur if the dike load exceeds the design load (see e.g. de Haan and de Ronde 1998):

$$\text{dike load} \equiv L_P + 0.3 H > 7.6 [m] \quad (5.6)$$

with L_P the sea level at Petten and H the wave height. For the evaluation of Eq. 5.6, we consider the tidal station IJmuiden, located about 30 km south of Petten (Figure 5.1), for which wave data are also available. The surge was calculated from the

ECMWF data by applying the surge model (Eq. 1 in van den Brink et al. 2004b) to Petten/IJmuiden, and then transformed into sea level by adding the astronomical high tides.

The ECMWF data include deep-water wave heights, calculated by the WAM model (Komen et al. 1994). We scaled the ECMWF deep-water wave height to the depth-limited wave height using the following relation (based on Bouws. et al. 1998, by taking the limit of fully developed wind waves):

$$H_{\text{shallow}} = H_{\text{deep}} \tanh\left[0.63\left(\frac{h}{H_{\text{deep}}}\right)^{0.75}\right] \quad (5.7)$$

with H_{shallow} the depth-limited wave height, H_{deep} the ECMWF deep-water wave height and h the water depth (25 m for IJmuiden).

A Gumbel plot of the dike load $L_P + 0.3 H$ is shown in Figure 5.8(a) both for the observations and for the ECMWF data. The scatter plot of the wave height and the sea level, as well as the failure criterion at Petten, are shown in Figure 5.8(b). The estimate of the exceedance of the failure criterion is $1 \cdot 10^4$ years, i.e., in agreement with the design return period for coastal protection.

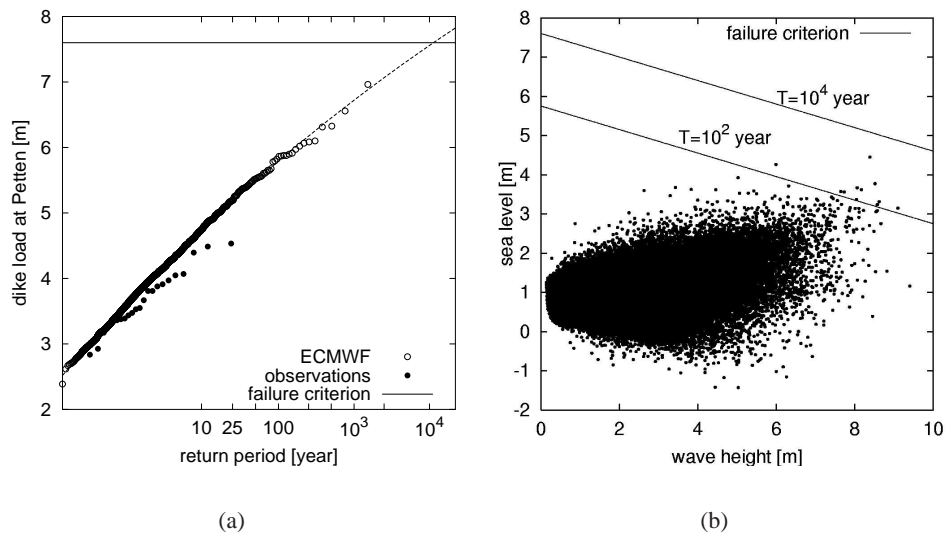
5.5 Discussion and conclusions

The ECMWF seasonal forecast ensembles provide a large data set which well reproduces the annual extremes of wind over the North Sea and of precipitation over the Rhine basin. This opens the possibility to semi-empirically estimate the return values with return periods up to 10^3 years, which is an order larger than what is possible from the observational sets, and to improve the accuracy of extrapolations to the 10^4 -year level.

Four applications are shown, all of them associated with hydraulic response to synoptic-scale meteorologic events. Checking the results with the extreme value analysis for observations shows good agreement for surges, waves, precipitation rates and Rhine discharge. This strengthens the belief that the ECMWF data can be considered as a realistic 'climate series' of extended length that is representative for the current climate on synoptic scale. This opens the possibility to study the extreme far tail from the climatological probability density function, a region that is of great importance for society but whose characteristics cannot be studied from observational records other than by huge extrapolation. The four applications show improved return value estimates. Two of the applications explore the correlation between violent events of different types.

The type of analysis explored here may be extended to other meteorological elements, such as temperature. However, the application has its limitations. Some of

Figure 5.8: Left: Gumbel plot of the dike load $L_P + 0.3H$ of the Pettemer zeewering, with L_P the sea level and H the wave height at Petten, for the ECMWF set (1569 years) and for the observational set (1979-2001). Also shown is the GEV fit to the ECMWF data. The failure level (7.6 m) is indicated by a horizontal line. Right: Scatter plot of L_P versus H is shown in (b) for all high-tide events in the ECMWF set. The failure area is reached with a return period of $1 \cdot 10^4$ years. Also shown is the line with a return period of 100 years.



the largest weather-related impacts on society are caused by synoptic-scale systems, but if meso-scale systems (order 10-100 km) are the driving force behind the events, the ECMWF set cannot represent them. Obvious examples are extreme showers and gusts. Another limitation of the present approach is the use of simple downscaling relations, e.g., the representations for the drag relation in the surge equation, the Rhine discharge (Eq. 5.4) and the bottom effects in waves (Eq. 5.7). In principle, these downscaling relations can be improved by using advanced models (see e.g., Gerritsen et al. 1995; van Deursen and Kwadijk 1993).

Despite the encouraging results of our analysis, the estimates of the extreme return values may have a limited validity. As the climate system for present day conditions may exhibit low frequency variability, this 17-year dataset may not be entirely

representative for the full spectrum of the present-day climate. In fact, the simulations only represent the extreme statistics associated to the single realization of the 1987-2004 period, where the simulations are initiated from.

In order to explore the extreme statistics of the climate in a wider time window, or for different climate conditions than the 1987-2004 window, one has to return to long simulations with climate models, but these lack the benefits mentioned in the introduction. A better alternative is to base the analysis on the seasonal prediction hindcasts, as recently produced for the 1958-2001 window in the "Demeter" project (Palmer et al. 2004).

It is fortunate that ECMWF archived these seasonal forecasts so carefully that a big dataset is available now for an application that was not envisioned at the starting time. As the length of the dataset will only be expanded in the future (with 20 years every month), it will allow for more accurate extreme value estimations under more general climatological circumstances than the present 1987-2004 baseline.

Chapter 6

Increased evidence for the existence of 'superstorms'

Abstract

The existence of a second population in the extreme wind speed, as detected in chapter 3, is confirmed by the output of an ensemble run with the NCAR-GCM, which has a higher complexity than ECBilt-Clio. The analyzed event shows similar characteristics (i.e., merging of two cyclones, a strong jet stream, and extreme precipitation) as the events analyzed in van den Brink et al. (2004a) (chapter 3).

6.1 Introduction

The existence in the real world of a second population in the extreme wind speed, as detected and described in chapter 3, is hard to verify from observational data. The reason is that we have not yet enough detailed understanding about the dynamical aspects of the second population to look for their characteristics in the observational data set. In other words, so far we can only detect second populations by a statistical technique. The point that makes the validation hard is that the observational records are far too short and the second population is far too rare to apply the statistical detection method.

At the moment, the only way to gain support for the results of chapter 3, is to find second populations in climate models more complex than EcBilt-Clio. This motivated us to redo the analysis of chapter 3 with the GCM ensembles data of the so called 'Challenge project'.

6.2 Model Description

In the Challenge project (Selten et al. 2004), the evolution of the climate system up to the year 2080 was simulated with version 1.4 of the Community Climate System Model (CCSM) of the National Center for Atmospheric Research (Ammann et al. 2004, and references therein). The model simulated the evolution of the coupled atmosphere-ocean-sea-ice-land system under prescribed climate forcings. The atmospheric component has a horizontal resolution of T31 (3.75°) and 18 levels in the vertical.

The simulations cover the period 1940-2080. Until 2000, historic forcings are used (Ammann et al. 2003, 2004), and from 2000 onwards, all forcing factors are kept at their year 2000 values, except for the concentrations of GHGs, which increase according to a 'business-as-usual' scenario (Dai et al. 2001) that is similar to the SRES-A1 scenario of the Intergovernmental Panel on Climate Change (IPCC) (Nakicenovic et al. 2000).

An ensemble of 62 simulations was produced, each covering the 141-year period. All initial ensemble fields are the same, apart from small random perturbations applied to the initial atmospheric temperature fields.

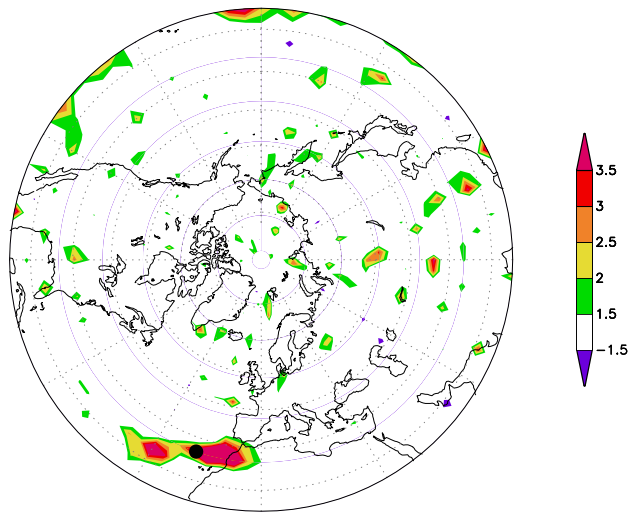
6.3 Presence of second population in wind speed

In chapter 3, we classified extreme winds to belong to a rare second distribution if the centennial extremes can not be described with the same GEV distribution as the annual extremes. We found that the meteorological circumstances of these events are characterized by the merging of two vortices into a single one, that this events is embedded in a very strong jet stream, accompanied by extreme precipitation.

We repeated both the statistical and meteorological analysis of chapter 3 with the Challenge data. The signal-to-noise ratio SN used for the detection of second populations (see Eq. 3.22 on page 46) is calculated for the whole 1941–2080 period, giving $62 \times 140 = 8680$ years. The small sensitivity of extreme winds on greenhouse forcing (see Section 6.4) justified our decision to use the entire set for our purpose.

Figure 6.1 shows SN applied to the five-year ($p = 5$ in Eq. 3.22) and centennial maxima ($p = 100$) for both periods. (We use $p = 5$ instead of $p = 1$ to get rid of the lower annual maxima, which do not converge to a GEV distribution, resulting in a 'kink' in the Gumbel plot around a 2-year return period, see Figure 6.2(a). This 'kink' is caused by the fact that the parent distribution can not be described by a Weibull distribution, and thus the annual extremes do not converge to a Gumbel/GEV distribution (see page 44). Taking $p = 1$ would erroneously lead to doubling of SN). A pattern with high SN -values is present over the North Atlantic, i.e., on more-or-

Figure 6.1: Signal-to-noise ratio SN for detection of a second population in the extreme wind speeds for the data of the Challenge project. Only areas with $|SN| > 1.5$ are plotted. According to the criterion of Eq. 3.22, $SN > 2$ is an indication for the existence of a second population. See section 3.3 for a more comprehensive description.



less the same location as in the control run of the ECBilt-Clio data (Figure 3.6 on page 52).

We now focus on the grid point ($19^{\circ}\text{W}, 35^{\circ}\text{N}$) in this area, indicated with a black dot in Figure 6.1(a), for which $SN = 4.53$. For this grid point, the Gumbel plot of the daily-averaged wind speed at the lowest sigma-level ($\sigma = 0.9925$) is shown in Figure 6.2(a). It shows that it is especially the largest wind event that deviates from the other extremes. If this most violent event were omitted from the calculation, then SN reduces from 4.53 to 1.5. This event, occurring in February 2021 of ensemble member 24, is not only extreme in the wind speed, but also in the SLP and vorticity. Indeed, the most extreme values in SLP and vorticity (Figure 6.2(b) and 6.2(c)) correspond to this same event, in which the SLP value truly represents an outlier. The Feb 2021/member 24 event is accompanied by a daily-averaged convective precipitation rate which is not the largest of all, but still with a 500-years return period (Figure 6.2(d)).

The evolution of the SLP pattern of the Feb 2021/member 24 event is shown in

Figure 6.2: Gumbel plots of the daily-average wind speed at $\sigma = 0.992$ (a), SLP (b), relative vorticity at $\sigma = 0.992$ (c) and convective precipitation (d) for the 1941-2080 period of the Challenge data. For all panels, the value belonging to the cyclone occurring in February 2021 of ensemble member 24 is indicated with an arrow.

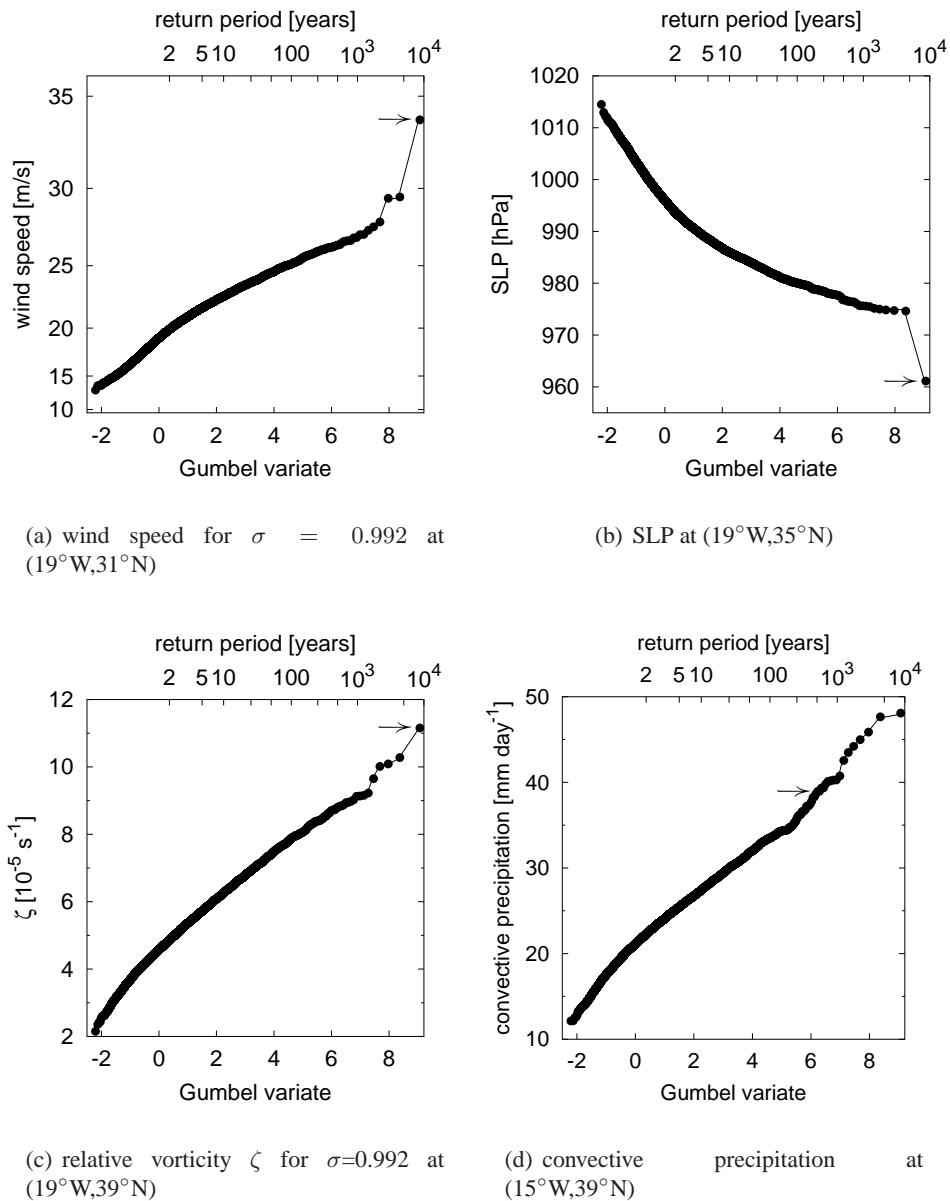


Figure 6.3: Evolution of SLP patterns of the storm leading to the most extreme wind speed in the Challenge data (Feb 2021/member 24) at position $19^{\circ}\text{W}, 31^{\circ}\text{N}$ (indicated with a black dot). This event occurs at panel f. The time step between the successive panels is 9 hours. Values below 1000 hPa are shaded.

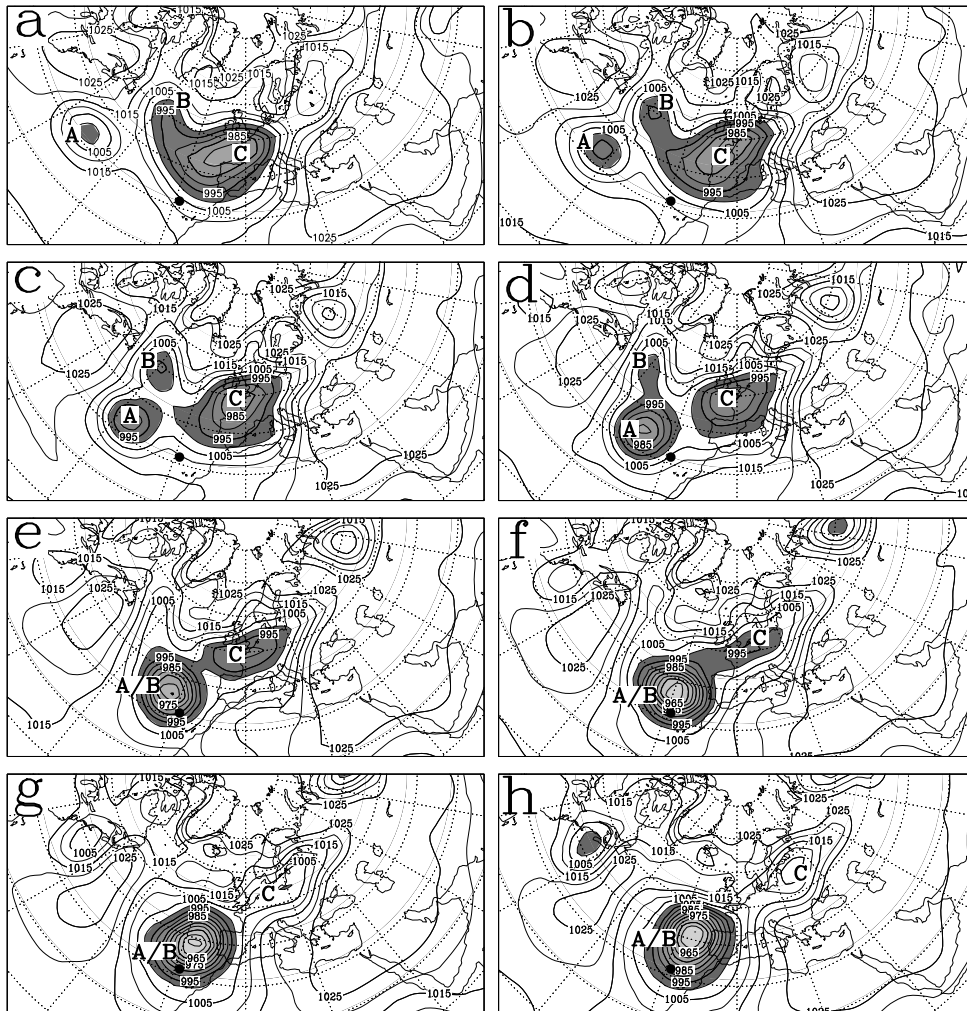


Figure 6.3. The time step between consecutive panels is 9 hours. It shows a cyclone

A and another B which separates from a third one, C , in panel c. In panel d, the cyclones A and B merge into a single one A/B . From this moment the deepening starts, from 978 hPa in panel d to 951 hPa just after panel g. The strong interactions between the vortices A and B , and possibly C , seem to enhance the deepening of the main vortex (lowest SLP 951 hPa, maximum wind speed 40.4 m s^{-1} at $\sigma = 0.992$, 46.3 m s^{-1} at $\sigma = 0.866$). This behavior – strong interactions between neighbouring vortices – is similar to what was found to be responsible for the second population in extreme wind speeds in ECBilt-Clio (chapter 3).

For a more detailed analysis of the Feb 2021/member 24 storm, we project (like in chapter 3) the geopotential height Φ of this single storm on that of 141 storms from the first population:

$$\begin{aligned}\Phi_{an} &= \Phi_b - \Phi_a & (6.1) \\ \Phi_a &= \frac{1}{141} \sum_{i=1}^{141} \Phi_{a,i} & \Phi_b = \Phi_{b,1}\end{aligned}$$

where $\Phi_{a,i}$ is the 7-day averaged pattern of the 500-hPa geopotential height for the region 80W–10E and 20N–65N for case i in the first population a , and Φ_b for the single event of the second population b . For the projection we use (see Eq. 3.25):

$$p_i = \frac{\langle \Phi_{a,i} - \Phi_a, \Phi_{an} \rangle}{\langle \Phi_{an}, \Phi_{an} \rangle} \quad (6.2)$$

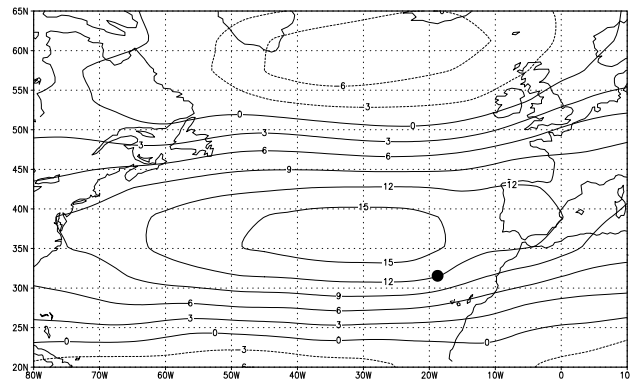
We applied this projection to the 500-hPa geopotential height field, and found that for the 141 cases of population a , the largest projection on population b is 0.83, i.e., considerably lower than unity. From extrapolation it follows that unity is exceeded about once in hundred years. This suggests that the background flow in which the event of population b developed is rare.

Applying the projection to other variables also results in small maximum projections for population a : The maximum projection for the 7-day averaged total precipitation is 0.51 (corresponding with a frequency of less than once in thousand years), and for SLP 1.01 (corresponding with a frequency of about once in hundred years).

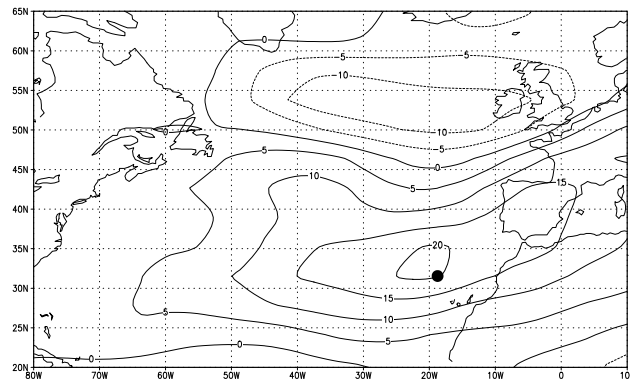
The zonal wind patterns at 0.866σ for population a and b are shown in Figure 6.4. The maximum zonal wind in the second population is stronger, and more eastward than in the first population. These results are also found in ECBilt-Clio (Figure 3.12 on page 58).

We conclude from this analysis that the single event that we examined in the Challenge data has similar characteristics as the events of the second population in the ECBilt-Clio data. This supports our hypothesis that the merging process, if embedded in a strong jet stream, and accompanied by extreme precipitation, can lead to

Figure 6.4: Time mean zonal wind at $\sigma = 0.866$ [m/s] of the first population (a) and the second population (b).

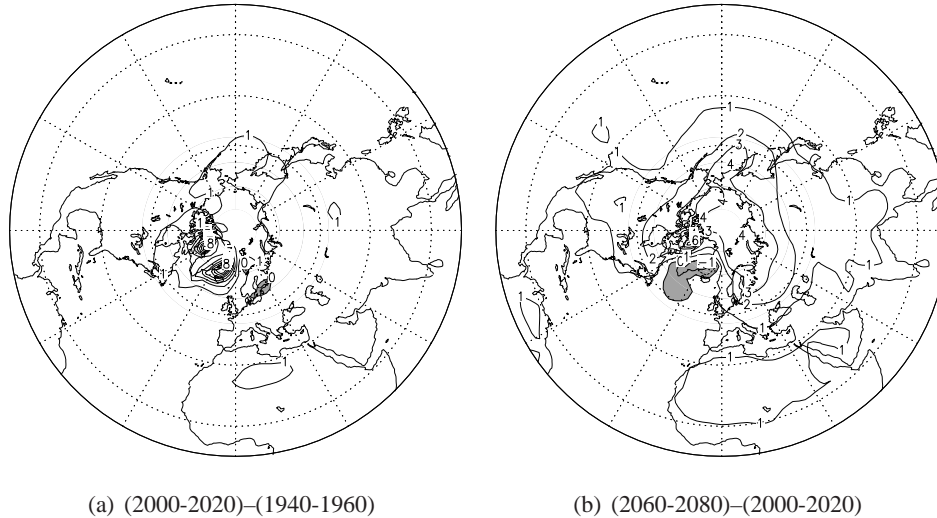


(a) mean 7-day averaged zonal wind speed at $\sigma = 0.866$ of the first population *a*



(b) mean 7-day averaged zonal wind speed at $\sigma = 0.866$ of the second population *b*

Figure 6.5: Change of the ensemble mean 2m-temperature in winter (Oct-Mar) averaged over 2000-2020 with respect to 1940-1960 (a) and 2080-2060 with respect to 2000-2020 (b). Units are °C. Negative values are shaded.

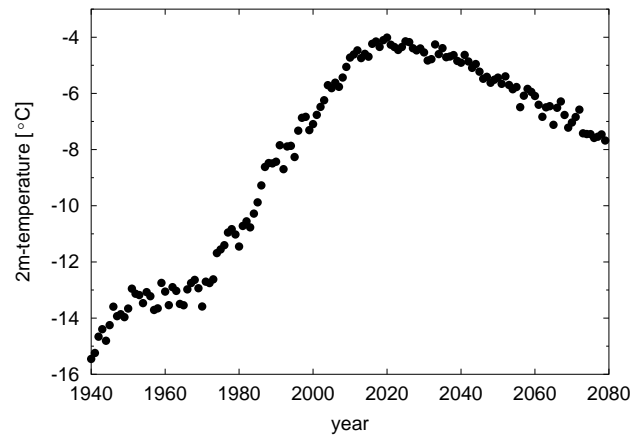


larger wind speeds than extrapolated from non-merging cyclones. The fact that the Challenge data reproduces the ECBilt-Clio results increases the belief that the existence of an earlier identified second population in the extreme wind speed is not a model artifact, but rather seems to be an existing feature that dominates the extreme value statistics for large return periods in the real world. Hence it represents an important feature to be counted with in safety design calculations in certain parts of the world.

6.4 CO₂ effect

As a final point of this study, we investigate the effect of the increased CO₂ concentrations. Figure 6.5 compares the ensemble mean 2m-temperature in winter (Oct-Mar) at the beginning, halfway, and at the end of the simulated period. It shows a warming over the whole NH up to the year 2020, and a further warming up to 2080, except for the area between Greenland and Iceland, where the strong warming of 10°C is followed by a cooling of 3°C (Figure 6.6). We attribute this local cooling to melting

Figure 6.6: Ensemble mean 2m-temperature in winter (Oct-Mar) at (30°W,65°N).



of the Arctic sea ice, which reduces salinity and stops the convection of (relatively warm) deep water around the year 2020 (see also Schaeffer et al. 2002).

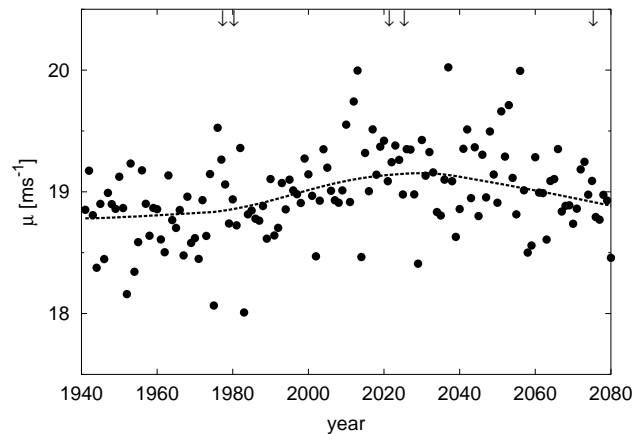
The time evolution of the once-a-year exceeded wind speed for the (19°W,31°N) grid point, which is the grid point analyzed in the previous section, is shown in Figure 6.7. We fitted a GEV distribution to the 62 annual maxima that are available for each year from the 62 ensemble members. The smoothed line (Cleveland 1979, using 70-year span) shows a variation of at most 3 % on the GEV location parameter for the $\sigma = 0.992$ wind speed. We hypothesize that the increase of the extreme wind speed up to 2020, and the decrease afterwards, is related to the temperature changes shown in Figures 6.5 and 6.6.

The arrows in Figure 6.7 indicate the occurrences of the five largest wind events in the whole set. No evidence is found that the magnitude of these largest events are influenced by the increased CO₂ concentrations.

6.5 Discussion and conclusions

The existence of a second population in the extreme wind speed as inferred from the ECBilt-Clio data, is confirmed in the ensemble run of the NCAR model. This increases the probability that the second population is a real feature that dominates the extreme value distribution of the wind in certain areas of the earth, including the extra-tropics. Evidence for this result requires a better understanding of the mechanism of these 'superstorms'. In particular, recognizing certain characteristics of this

Figure 6.7: Time series of the GEV location parameter μ of the $\sigma = 0.992$ wind speed for ($19^\circ\text{W}, 31^\circ\text{N}$), as estimated for each set of 62 annual extremes for every year in the Challenge data (1941-2080). The line is the Cleveland (1979) smoother with 70-year span. The arrows indicate the dates of the five largest wind events in the total set (Figure 6.2(a)).



population may enable in the future the identification of less violent members of this second population. Hopefully, this leads to an empirical estimation of the probability of occurrence in datasets as short as ERA40-reanalysis (Simmons and Gibson 2000). This challenging extension is beyond the scope of this thesis.

A second result of this preliminary GCM study on extreme winds is the non-trivial nature of the response of extreme winds on greenhouse forcing (Figures 6.6 and 6.7). It is encouraging that the present GCM ensemble experiment now produces a clear signal in changes of extreme winds. It is clear that the nature of this response needs further research in that direction.

Summary

This thesis deals with the problem of how to estimate values of meteorological parameters that correspond to return periods that are considerably longer than the length of the observational data sets.

The problem is approached by considering the output of weather- and climate models as pseudo-observations. These pseudo-observational records, which are one to two orders of magnitude longer than the observational records, open the possibility to reduce the large statistical uncertainty in the 10^4 -year estimate from observations, as well as to examine the assumption that all extremes (up to 10^4 -year return periods) are part from the same population.

In **Chapter 1** we quantify the statistical uncertainty in the 10^4 -year surge level if estimated from hundred-year records (as the observational records are). This is done by dividing the 5336-year long outputs of the climate model ECBilt-Clio into subsets of hundred year. This chapter shows that annual maxima of hundred-year surge records can generally, within the uncertainty, be described by a Gumbel distribution (a commonly applied distribution for annual hydrological extremes (see e.g., Katz et al. 2002)). However, the total 5336-year record of the control run (1960–1990) can clearly *not* be described by a single Gumbel distribution, but requires a GEV distribution instead. This implies that uncertainty ranges calculated from Gumbel distributions will produce numbers that are misleadingly low (see also Coles et al. 2003). The uncertainty in the estimate of the shape parameter of the GEV distribution on basis of hundred-year records results in a large uncertainty (~ 4 m) in the 10^4 -year surge estimate. For the grid point representing the North Sea, the greenhouse run (2050–2080) of ECBilt-Clio reveals a 'kink' in the distribution of the annual maxima if displayed on a Gumbel plot. The extremes with a lower probability than once in 250 years seem to originate from another distribution than the less extreme events. It is hypothesized that the super-extremes originate from a second population in the extreme wind speed distribution.

Chapter 2 deals with the optimal method of determining 10^4 -year surge estimates by statistical means. Next to the GEV analysis (that usually only considers the annual maxima) the so-called Peak Over Threshold (POT) method exists, which con-

siders all independent events above a certain threshold. These methods are evaluated with the ECBilt-Clio record of simulated surges in Delfzijl by first estimating the 100-year surge level and its uncertainty for all 116-year subsets, and then checking if these uncertainty intervals contain the correct realization, as determined directly from the total (7540-year) set. We found that in our experimental setting, the POT-method systematically underestimates the uncertainty in the 10^2 -year surge level, while application of the GEV distribution results in a unbiased estimate, making the last approach most appropriate for determining safety levels.

Chapter 3 focuses on the 'superstorms' detected in chapter 1. A statistical criterion is developed to determine whether all annual extremes can be described by a single GEV distribution or not. We found that for specific geographical locations in ECBilt-Clio, the extreme winds can not be described with a single GEV distribution, but requires a Generalized Two-Component Extreme Value (GTCEV) distribution. The meteorology resulting in the second component of the GTCEV distribution has the following characteristics: the extreme winds are related to situations in which two vortices merge into a single one. In addition, the cyclones are embedded in a strong jet stream, and extreme precipitation accompanies the development of the cyclone.

It is found that the area for which a second population is detected shifts due to the greenhouse effect from the North-Atlantic ocean to the European continent. This explains that in chapter 1 the 'superstorms' are only detected in the greenhouse run.

In **Chapter 4** we explore the suitability of the European Centre for Medium-Range Weather Forecasts (ECMWF) seasonal forecast archive for extreme value analysis of surges. The combined seasonal forecasts of the ECMWF cumulate to 1600 years. The high resolution in time and space and the more complete physics (even compared with state-of-the-art climate models) make these data highly appropriate to be analyzed with extreme value statistics. The results for the surge in Hoek van Holland shows good statistical agreement with the observed extremes. The long model record reduces the statistical uncertainty in the 10^4 -year estimate with no less than a factor four.

We demonstrate in **Chapter 5** that the archived ECMWF seasonal forecasts can also be used for extreme value estimates of other variables than wind and surge only. Four examples are presented, i.e., the Rhine discharge at Lobith, the sluicing of Lake IJssel water into the sea, the closure-frequency of the 'Maeslant'-barrier, and the (wave and sea level dependent) load on the Pettemer sea wall. The examples illustrate that the -still expanding- ECMWF data set offers unforeseen possibilities in modeling (hydrological) extremes. Especially, the simultaneous modeling of multiple extremes opens new perspectives.

Preliminary results obtained with the so-called Challenge data are presented in **Chapter 6**. The 'superstorm' that we analyzed in the Challenge data has similar char-

acteristics as the events in the ECBilt-Clio model. This result supports the idea that the earlier detected 'superstorms' are not a model-artifact, but rather seems to be indeed a phenomenon belonging to the real world.

Bibliography

- Ammann, C.M., G.A. Meehl, W.M. Washington, and C.S. Zender, 2003: A monthly and latitudinally varying volcanic forcing dataset in simulations of 20th century climate. *Geophys. Res. Lett.*, **30**, 1657–1660, doi:10.1029/2003GL016875.
- Ammann, C.M. et al., 2004: Coupled simulation of the 20th-century including external forcing. *J. Clim.*, *subm.*
- Anderson, D.L.T., T. Stockdale, M.A. Balmaseda, L. Ferranti, F. Vitart, P. Doblaser, R. Hagedorn, T. Jung, A. Vidard, A. Troccoli, and T. Palmer, 2003: Comparison of the ECMWF seasonal forecast systems 1 and 2, including the relative performance for the 1997/8 El Niño. Technical Report Technical Memoranda 404, ECMWF, Shinfield Park, Reading, U.K.
- Battjes, J. and H. Gerritsen, 2002: Coastal modelling for flood defence. *Philosophical Transactions of the Royal Society of London Series A*, **360**, 1461–1475.
- Beersma, J.J., K.M. Rider, G.J. Komen, E. Kaas, and V.V. Kharin, 1997: An analysis of extra-tropical storms in the north atlantic region as simulated in a control and 2xco₂ time-slice experiment with a high-resolution atmospheric model. *Tellus*, **49A**, 347–361.
- Bonekamp, H., G.J. Komen, A. Sterl, P.A.E.M. Janssen, P.K. Taylor, and M.J. Yelland, 2002: Statistical comparisons of observed and ECMWF modeled open ocean surface drag. *Journal of Physical Oceanography*, **32**, 1010–1027.
- Bouws., E., L. Draper, E.D.R. Shearman, A.K. Laing, D. Feit, W. Mass, L.I. Eide, P. Francis, D.J.T. Carter, and J.A. Battjes, 1998: *Guide to Wave analysis and forecasting*. WMO - No.702. World Meteorological Organization, Geneva, second edition, 168 pp.
- Brabson, B.B. and J.P. Palutikof, 2000: Tests of the Generalized Pareto Distribution for predicting extreme wind speeds. *Meteorological Applications*, **39**, 1627–1641.

- Buishand, T.A., 1991: Extreme rainfall estimation by combining data from several sites. *Hydrological Sciences Journal*, **36**, 345–365.
- Buishand, T.A. and C.A. Velds, 1980: *Neerslag en Verdamping*. Staatsdrukkerij, 's Gravenhage (NL).
- Charnock, H., 1955: Wind stress on a water surface. *Q.J.R. Meteorol. Soc.*, **81**, 639.
- Church, J.A., J.M. Gregory, P. Huybrechts, M. Kuhn, K. Lambeck, M.T. Nhuan, D. Qin, and P.L. Woodworth, 2001: Changes in sea level. *Climate Change 2001: The Scientific Basis. Contribution of Working Group I to the Third Assessment Report of the Intergovernmental Panel on Climate Change*, J. Houghton, Y. Ding, D. Griggs, M. Noguer, P. van der Linden, X. Dai, K. Maskell, and C. Johnson, eds., Cambridge University Press, 639–694.
- Cleveland, W.S., 1979: Robust locally weighted regression and smoothing scatterplots. *Journal of the American Statistical Association*, **74**, 829–836.
- Coles, S., 2001: *An Introduction to Statistical Modelling of Extreme Values*. Springer-Verlag, London, 208 pp.
- Coles, S., L. Pericchi, and S. Sisson, 2003: A fully probabilistic approach to extreme rainfall modeling. *Journal of Hydrology*, **273**, 35–50.
- Cook, N.J., 1982: Towards better estimation of extreme winds. *Journal of Wind Engineering and Industrial Aerodynamics*, **9**, 295–323.
- Cook, N.J. and R.I. Harris, 2001: Discussion on application of the generalized Pareto distribution to extreme value analysis in wind engineering by J.D. Holmes, W.W. Moriarty. *Journal of Wind Engineering and Industrial Aerodynamics*, **89**, 215–224.
- Cook, N.J., R.I. Harris, and R. Whiting, 2003: Extreme wind speeds in mixed climates revisited. *Journal of Wind Engineering and Industrial Aerodynamics*, **91**, 403–422.
- Dai, A., T.M.L. Wigley, B.A. Boville, J.T. Kiehl, and L.E. Buja, 2001: Climates of the twentieth and twenty-first centuries by the NCAR CSM. *J. Clim.*, **14**, 485–519.
- de Haan, L., 1976: Sample extremes: an elementary introduction. *Statistica Neerlandica*, **30**, 161–172.
- 1990: Fighting the arch-enemy with mathematics. *Statistica Neerlandica*, **44**, 45–68.

- de Haan, L. and J. de Ronde, 1998: Sea and wind: multivariate extremes at work. *Extremes*, **1**, 7–45.
- Deltacommissie, 1960: *Rapport Deltacommissie*. SDU uitgevers, Den Haag.
- Dillingh, D., L. de Haan, R. Helmers, G.P. Können, and J. van Malde, 1993: De basispeilen langs de Nederlandse kust; statistisch onderzoek. Technical Report DGW-93.023, Ministerie van Verkeer en Waterstaat, Directoraat-Generaal Rijkswaterstaat.
- Embrechts, P., C. Klüppelberg, and T. Mikosch, 1997: *Modelling extremal events*. Springer Verlag Berlin Heidelberg.
- Fink, A., U. Ulbrich, and H. Engel, 1996: Aspects of the January 1995 flood in Germany. *Weather*, **51**, 34–39.
- Flater, D., 1998: Xtide: Harmonic tide clock and tide predictor. <http://www.flaterco.com/xtide/>.
- Galambos, J., 1978: *The asymptotic theory of extreme order statistics*. John Wiley & Sons, New York.
- Garratt, J. R., 1992: *The atmospheric boundary layer*. Cambridge University Press, Cambridge.
- Gaza, R.S. and L.F. Bosart, 1990: Trough-merger characteristics over North America. *Weather Forecasting*, **5**, 314–331.
- Gerritsen, H., H. de Vries, and M. Philippart, 1995: The Dutch Continental Shelf Model. *Quantitative Skill Assessment for Coastal Ocean Models*, D. Lynch and A. Davies, eds., American Geophysical Union, volume 47 of *Coastal and Estuarine Studies*.
- Goosse, H. and T. Fichefet, 1999: Importance of ice-ocean interactions for the global ocean circulation: a model study. *Journal of Geophysical Research*, **104**, 23337–23355.
- Gregory, D., J.J. Morcrette, C. Jakob, A.C.M. Beljaars, and T. Stockdale, 2000: Revision of convection, radiation and cloud schemes in the ECMWF Integrated Forecasting System. *Quart. J. Roy. Meteor. Soc.*, **126**, 1685–1710.
- Hakim, G.J., L.F. Bosart, and D. Keyser, 1995a: The Ohio valley wave-merger cyclogenesis event of 25-26 January 1978. part I: Multiscale case study. *Monthly Weather Review*, **123**, 2663–2692.

- 1995b: The Ohio valley wave-merger cyclogenesis event of 25-26 January 1978. part II: Diagnosis using quasigeostrophic potential vorticity inversion. *Monthly Weather Review*, **124**, 2176–2205.
- Hall, N.M.J., B.J. Hoskins, P.J. Valdes, and C.A. Senior, 1994: Storm tracks in a high-resolution GCM with doubled carbon dioxide. *Quarterly Journal of the Royal Meteorological Society*, **120**, 1209–1230.
- Hosking, J.R.M., J.R. Wallis, and E.F. Wood, 1985: Estimation of the Generalized Extreme-Value distribution by the method of probability-weighted moments. *Technometrics*, **27**, 251–261.
- Houghton, J.T., Y. Ding, D.J. Griggs, M. Noguer, P.J. van der Linden, X. Dai, K. Maskell, and C.A. Johnson, 2001: *IPCC Working Group I Third assessment report*. Cambridge University Press.
- Jenkinson, A.F., 1955: The frequency distribution of the annual maximum (or minimum) values of meteorological elements. *Quarterly Journal Royal Meteorological Society*, **81**, 158–171.
- Kalnay, E., M. Kanamitsu, R. Kistler, W. Collins, D. Deaven, L. Gandin, M. Iredell, S. Saha, G. White, J. Woollen, Y. Zhu, M. Chelliah, W. Ebisuzaki, W. Higgins, J. Janowiak, K.C. Mo, C. Ropeliwski, J. Wang, A. Leetmaa, R. Reynolds, R. Jenne, and D. Joesph, 1996: The NCEP/NCAR 40-year reanalysis project. *Bulletin of the American Meteorological Society*, **77**, 437–471.
- Katz, R.W., M.B. Parlange, and P. Naveau, 2002: Statistics of extremes in hydrology. *Advances in Water Resources*, **25**, 1287–1304.
- Kharin, V.V. and F.W. Zwiers, 2000: Changes in the extremes in an ensemble of transient climate simulations with a coupled atmosphere-ocean GCM. *Journal of Climate*, **13**, 3760–3788.
- Kiktev, D., D.M.H. Sexton, L. Alexander, and C.K. Folland, 2003: Comparison of modeled and observed trends in indices of daily climate extremes. *Journal of Climate*, **16**, 3560–3571.
- Knippertz, P., U. Ulbrich, and P. Speth, 2000: Changing cyclones and surface wind speeds over the North Atlantic and Europe in a transient GHG experiment. *Climate Research*, **15**, 109–122.
- Komen, G.J., L. Cavaleri, M Donelan, K. Hasselmann, S. Hasselmann, and P.A.E.M. Janssen, 1994: *Dynamics and Modelling Ocean Waves*, volume 1. Cambridge University Press, 486 pp.

- Kors, A.G., F.A.M. Claessen, J.W. Wesseling, and G.P. Können, 2000: Scenario's externe krachten voor WB21. *Waterbeleid voor de 21^e eeuw, Advies van de Commissie Waterbeheer 21^e eeuw*, F. Tielrooij, J. van Dijk, J. de Blécourt-Maas, A. van den Ende, G. Oosterbaan, and H. Overbeek, eds., (in Dutch).
- Kotz, S. and S. Nadarajah, 2000: *Extreme value distributions: theory and applications*. Imperial College Press, London.
- Kysely, J., 2002: Comparison of extremes in GCM-simulated, downscaled and observed central-European temperature series. *Climate Research*, **20**, 211–222.
- Leadbetter, M.R., G. Lindgren, and H. Rootzén, 1983: *Extremes and Related Properties of Random Sequences and Processes*. Springer-Verlag, New York, NY.
- Nakicenovic, N. et al., eds., 2000: *Special Report on Emission Scenarios*. Cambridge University Press, 595 pp.
- Opsteegh, J.D., R.J. Haarsma, and F.M. Selten, 1998: ECBilt: A dynamic alternative to mixed boundary conditions in ocean models. *Tellus*, **50A**, 348–367.
- Opsteegh, J.D., F.M. Selten, and R.J. Haarsma, 2001: Climate variability on decadal timescales. Technical Report Report 410 200 060, Dutch National Research Programme on Global Air Pollution and Climate Change.
- Palmer, T. N., A. Alessandri, U. Andersen, P. Cantelaube, M. Davey, P. Délecluse, M. Déque, E. Diez, F. J. Doblas-Reyes, H. Feddersen, R. Graham, S. Gualdi, J.-F. Guérémy, R. Hagedorn, M. Hoshen, N. Keenlyside, M. Latif, A. Lazar, E. Maisonave, V. Marletto, A. P. Morse, B. Orfila, P. Rogel, J.-M. Terres, and Thomson M. C., 2004: Development of a European multi-model ensemble system for seasonal to inter-annual prediction (DEMETER). *Submitted to Bull. Am. Met. Society*.
- Palutikof, J.P., B.B. Brabson, D.H. Lister, and S.T. Adcock, 1999: A review of methods to calculate extreme wind speeds. *Meteorological Applications*, **6**, 119–132.
- Peilbesluit wateren IJsselmeergebied, 1992: Ministerie van Verkeer en Waterstaat, directoraat-generaal Rijkswaterstaat, directie Flevoland (in Dutch).
- Ritchie, H., C. Temperton, A.J. Simmons, M. Hortal, T. Davies, D. Dent, and M. Hamrud, 1995: Implementation of the semi-Lagrangian method in a high resolution version of the ECMWF forecast model. *Mon. Wea. Rev.*, **123**, 489–514.
- Rossi, F., M. Fiorentino, and P. Versace, 1984: Two-Component Extreme Value distribution for flood frequency analysis. *Water Resources Research*, **20**, 847–856.

- Schaeffer, M., F.M. Selten, and J.D. Opsteegh, 2003: Shifts of means are not a proxy for changes in extreme temperatures in climate projections. *Climate Dynamics* (submitted).
- Schaeffer, M., F.M. Selten, J.D. Opsteegh, and H. Goosse, 2002: Intrinsic limits to predictability of abrupt regional climate change in IPCC SRES scenarios. *Geophysical Research Letters*, **29**, 14, doi:10.1029/2002GL01524.
- Schubert, M., J. Perlwitz, R. Blender, K. Fraderich, and F. Lunkeit, 1998: North Atlantic cyclones in CO₂-induced warm climate simulations: frequency, intensity and tracks. *Climate Dynamics*, **14**, 827–837.
- Selten, F.M., G. Branstator, M. Kliphuis, and H.A. Dijkstra, 2004: Tropical origins for recent and future Northern Hemisphere climate change. *Geophys. Res. Lett.*, L21205, doi:10.1029/2004GL020739.
- Simiu, E., N. A. Heckert, J. J. Filliben, and S. K. Johnson, 2001: Extreme wind load estimates based on the Gumbel distribution of dynamic pressures: An assessment. *Structural Safety*, **23**, 221–229.
- Simmons, A.J. and J.K. Gibson, 2000: The ERA-40 project plan. Technical Report ERA-40 project report series No. 1, ECMWF, Shinfield Park, Reading, U.K.
- Smith, S.D., R.J. Anderson, W.A. Oost, C. Kraan, N. Maat, J. Decosmo, K.B. Katsaros, K.L. Davidson, K. Bumke, L. Hasse, and H. M. Chadwick, 1992: Sea surface wind stress and drag coefficients: The HEXOS results. *Bound.-Layer Meteorol.*, **60**, 109–142.
- Timmerman, H., 1977: *Meteorological effects on tidal heights in the North Sea*. Staatsdrukkerij, The Hague.
- van den Brink, H.W., G.P. Können, and J.D. Opsteegh, 2003: The reliability of extreme surge levels, estimated from observational records of order hundred years. *Journal of Coastal Research*, **19**, 376–388, (chapter 1 of this thesis).
- 2004a: Statistics of extreme synoptic-scale wind speeds in ensemble simulations of current and future climate. *Journal of Climate*, **17**, 4564–4574, (chapter 3 of this thesis).
- van den Brink, H.W., G.P. Können, J.D. Opsteegh, G.J. van Oldenborgh, and G. Burgers, 2004b: Improving 10⁴-year surge level estimates using data of the ECMWF seasonal prediction system. *Geophysical Research Letters*, **31**, L17210, doi:10.1029/2004GL020610, (chapter 4 of this thesis).

-
- van Deursen, W.P.A. and J. Kwadijk, 1993: RHINEFLOW: an integrated GIS water balance model for the river Rhine. *Application of Geographic Information System in hydrology and water resources management*, K. Kovar and H. Nachtnebel, eds., IAHS publ. 211, 507–519.
- van Montfort, M.A.J., 1969: Inleiding over de verdeling van extremen. *Statistica Neerlandica*, **23**, 97–111.
- Wolff, J.-O., E. Maier-Reimer, and S. Legutke, 1997: The Hamburg Ocean Primitive Equation model HOPE. Technical Report No. 13, Deutsches Klimarechenzentrum, Hamburg, Germany.

Samenvatting

In dit proefschrift wordt het probleem behandeld van het schatten van waarden van meteorologische grootheden die corresponderen met herhalingstijden die aanzienlijk langer zijn dan de periode waarover gemeten is. Deze moeilijkheid speelt sterk bij het bepalen van de hoogte van de zeedijken in grote delen van Nederland, die volgens de Wet op de Waterkering niet vaker dan eens in de 10000 jaar mogen bezwijken. Deze herhalingstijd is dus honderd keer zo lang als de lengte van de meetreeks van honderd jaar.

We benaderen dit probleem door de uitkomsten van weer- en klimaatmodellen te beschouwen als pseudo-waarnemingen. Deze reeksen, zijn tien tot honderd keer langer zijn dan de 'echte' waargenomen reeksen. Hiermee kan de grote statistische onzekerheid, die er in de schattingen van het 10^4 -jaar niveau vanuit de waarnemingen is, verkleind worden. Ook kan er met de pseudo-waarnemingen de aanname dat alle extremen (tot aan 10^4 -jaar herhalingstijden) tot een enkele populatie behoren, onderzocht worden.

In **Hoofdstuk 1** kwantificeren we de statistische onzekerheid in de 10^4 jaar stormvloedniveau (de zogenaamde 'opzet'), als deze geschat wordt uit een honderd jaar lange reeks (dit de lengte van de waargenomen reeksen). We doen dit door de 5336 jaar aan output van het klimaatmodel ECBilt-Clio, te verdelen in deelreeksen van elk zo'n 100 jaar. In dit hoofdstuk wordt aangetoond dat in het algemeen de jaar-maxima van opzet-reeksen van honderd jaar (binnen de onzekerheid), beschreven kunnen worden met een Gumbel verdeling (deze verdeling wordt vaak gebruikt om hydrologische jaarmaxima te beschrijven (zie bijv. Katz et al. 2002)). De totale reeks van 5336 jaar van het controle klimaat (1960–1990) kan echter *niet* door een enkele Gumbel verdeling worden beschreven; hiervoor is een GEV verdeling nodig. Dit impliceert dat onzekerheidsbanden die berekend worden met een Gumbel verdeling misleidend laag uit kunnen vallen (zie ook Coles et al. 2003). De onzekerheid in de schatting van de vormparameter van de GEV verdeling op basis van een honderd-jaar lange reeks resulteert in een grote onzekerheid (~ 4 m) in het geschatte 10^4 -jaar opzet-niveau. Voor het gridpunt van ECBilt-Clio dat de Noordzee representeert toont de 'broeikas-run' (2050–2080) een 'knik' in de verdeling van de jaarmaxima

bij weergave op een Gumbel plot. De extremen die zeldzamer optreden dan eens in de 250 jaar lijken te ontstaan vanuit een andere verdeling dan de minder extreme gevallen. Dit suggereert dat de super-extremen door een ander meteorologisch mechanisme worden voortgebracht dan de rest van de extremen.

Hoofdstuk 2 gaat over de optimale methode om de 10^4 -jaar opzet-niveaus statistisch te schatten. Naast de GEV analyse, waarin gewoonlijk alleen de jaarmaxima beschouwd worden, bestaat er de zogenaamde 'Peak Over Threshold' (POT) methode waarin alle onafhankelijke gevallen die boven een bepaalde drempel uitkomen, in de analyse meegenomen worden. Beide methoden worden geëvalueerd met de ECBilt-Clio reeks van gesimuleerde opzetten in Delfzijl. Hiertoe worden eerst de 100-jaar niveaus en hun onzekerheden geschat vanuit 116-jarige deelreeksen. Vervolgens wordt gekeken of de echte waarde (die eenvoudig is af te leiden uit de totale reeks) binnen het onzekerheidsinterval ligt. Het blijkt dat in ons experiment de POT-methode de onzekerheid in het 10^2 -jaar opzet-niveau systematisch onderschat, terwijl toepassing van de GEV verdeling in een zuivere schatting resulteert. Dit maakt deze laatste verdeling het best geschikt om veiligheidsniveaus te bepalen.

In **Hoofdstuk 3** richten we ons op de in hoofdstuk 1 gedetecteerde 'superstormen'. Hier wordt een statistisch criterium ontwikkeld om te bepalen of alle jaarmaxima met een enkele GEV verdeling beschreven kunnen worden of niet. Het blijkt dat in ECBilt-Clio er specifieke locaties zijn waar de extreme winden niet beschreven kunnen worden door een enkele GEV verdeling, maar een 'Generalized Two-Component Extreme Value' (GTCEV) verdeling nodig is. De meteorologie die resulteert in de tweede component van de GTCEV verdeling blijkt de volgende karakteristieken te hebben: De extreme winden horen bij situaties waarbij twee wervels samensmelten tot een enkele; Daarbij is de storm ingebed in een extreem sterke straalstroom, en gaat de ontwikkeling van de storm gepaard met extreme neerslag. Het geografische gebied waar een tweede populatie wordt gedetecteerd, verschuift onder invloed van het broeikas-effect van de Noord-Atlantische Oceaan naar het Europese continent. Dit verklaart dat in hoofdstuk 1 de 'superstormen' alleen in de 'broeikas-run' gedetecteerd worden.

In **Hoofdstuk 4** onderzoeken we of de langetermijnverwachtingen van het Europees Centrum voor Middellange Termijn Verwachtingen (ECMWF) geschikt zijn voor analyse van de extreme stormvloed. Momenteel vormen de gecombineerde langetermijnverwachtingen in totaal zo'n 1600 jaar. De hoge resolutie in tijd en ruimte, en de completere fysica (zelfs ten opzichte van state-of-the-art klimaatmodellen) maken dat deze reeksen uitermate geschikt zijn om geanalyseerd te worden via de statistiek van extremen. De resultaten voor Hoek van Holland laten een goede overeenkomst zien tussen de schattingen van de langetermijnverwachtingen en de waarnemingen. Door de grote totale lengte van de langetermijnverwachtingen wordt

de statistische onzekerheid in de 10^4 -jaar schatting met maar liefst een factor vier verkleind.

We laten in **Hoofdstuk 5** zien dat de langetermijnverwachtingen van het ECMWF ook voor andere grootheden dan wind en opzet kunnen worden gebruikt om extreme waarden schattingen te maken. Er worden vier voorbeelden gepresenteerd, nl. de Rijnafvoer bij Lobith, het spuien van IJsselmeerwater in de Waddenzee, de frequentie waarmee de 'Maeslantkering' in de Nieuwe Waterweg gesloten moet worden, en de belasting (die afhankelijk is van zowel golfhoogte en zeeniveau) van de Pettemer zeewering. Dit hoofdstuk illustreert dat de -nog steeds langer wordende- ECMWF reeks onvoorziene mogelijkheden biedt bij het modelleren van (hydrologische) extremen. Vooral het simultaan modelleren van meerdere, gelijktijdig optredende extremen biedt nieuwe perspectieven.

Voorlopige resultaten die verkregen zijn met de zogenaamde 'Challenge' data van het NCAR model worden gepresenteerd in **Hoofdstuk 6**. De 'superstorm' die we in de Challenge data geanalyseerd hebben, heeft dezelfde karakteristieken als de gevallen in het ECBilt-Clio model. Dit resultaat ondersteunt het idee dat de eerder gedetecteerde 'superstormen' niet een model-artefact zijn, maar juist een fenomeen zijn dat tot de werkelijkheid behoort.

Dankwoord

Met veel genoegen kijk ik terug op de tijd die ik op het KNMI aan dit proefschrift heb gewerkt. Dit kwam niet alleen door de inhoudelijke kant van het onderzoek, maar zeker ook door de collegialiteit die er op het KNMI is. Altijd was het mogelijk om naar een collega toe te stappen als je een vraag had: iedereen was bereid om je te helpen! Ik denk hierbij o.a. aan Gerrit Burgers, Olaf Klos, Geert Jan van Oldenborgh, Frank Selten, Peter Siegmund, Ilja Smits, Hans Theizhen, Hans de Vries, en zeker ook iedereen van de groep Klimaatanalyse, waar ik de afgelopen jaren bij hoorde. KA-ers, hartelijk bedankt voor de altijd goede sfeer en samenwerking.

In het bijzonder denk ik hierbij natuurlijk aan Günther Können, die als hoofd KA en als co-promotor met veel enthousiasme, kennis en betrokkenheid het onderzoek heeft begeleid. Günther, altijd was je bereid om mee te denken. Zelfs op zaterdagen (en een keer zelfs op zondag...) belde je me op omdat een detail jou te binnen schoot dat ik toch echt niet mocht vergeten. Toch was het niet zo wij alleen over de wetenschappelijke aspecten praatten. Heel vaak is muziek aan de orde gekomen, en bijna net zo vaak mijn gereformeerde denken en cultuur. Deze onderwerpen – extremen, muziek en religie – smolten samen in de Bach-schaal, een objectieve weergave van de kwaliteit van muziekstukken.

Theo Opsteegh, ook jou wil ik hartelijk bedanken voor het feit dat je promotor wilde zijn, en voor de altijd fijne samenwerking. Je stond op een iets grotere afstand dan Günther, maar je kon daarmee ook meer op de grote lijnen letten. Ik heb de gesprekken met jou altijd als stimulerend ervaren, niet in het minst de gesprekken van levensbeschouwelijke inhoud.

Stefan Meulemans en Anne Moggré wil ik bedanken voor de plezierige samenwerking tijdens jullie afstuderen. De EHBO-ers en BHV-ers, bedankt voor de altijd gezellige sfeer tijdens de oefensessies: dat is nog eens het nuttige met het aangename verenigen!

Het RIKZ bedank ik voor de financiële ondersteuning, waardoor dit onderzoek mogelijk werd gemaakt. Ik hoop dat de resultaten een bijdrage vormen aan de veiligheid van Nederland tegen overstromingen. Douwe Dilling, bedankt voor de begeleiding die je me hebt gegeven.

Ook mijn moeder, schoonouders, broers en zussen, schoonzussen en zwagers wil ik hartelijk bedanken voor jullie meeleven. Vooral tijdens mijn (mislukte) poging om een artikel in Nature gepubliceerd te krijgen, kreeg ik vaak de vraag: 'En... hoe staat het met je Nature artikel?' Ook al kon ik inhoudelijk niet veel vertellen, het meeleven heeft me altijd wel goed gedaan!

Lieve Joëlla, vooral jou wil ik bedanken. Het feit dat ik ging promoveren heeft ook jou heel wat inspanning bezorgd, omdat ik, zeker aan het eind, nog wel eens thuis er aan moest werken, en jij er dan alleen voor stond. Toch heb je er altijd achter gestaan dat ik ging promoveren.

Lieve kleine Lilian, ook jou wil ik bedanken. Al die moeilijke onderwerpen waren meteen uit m'n hoofd als ik thuis kwam en jij stond met je stralende snoet me op te wachten!

Het stemt mij tot dankbaarheid dat alle dingen uit de Vaderlijke hand van God ons toekomen. Dat geeft meer rust dan de hoogste dijken. God was het ook Die de achterliggende jaren de kracht en het inzicht gaf om dit boeiende en tegelijkertijd nuttige onderzoek te doen. Allein Gott in der Höh' sei Ehr!

Curriculum Vitae

Henk van den Brink is op 5 januari 1974 geboren te Amersfoort. Hij doorliep het VWO op het Van Lodensteincollege in Amersfoort, waar het diploma werd gehaald in 1992. Na een jaar Technische Informatica gestudeerd te hebben, begon hij in 1993 met de studie Technische Natuurkunde aan de Technische Universiteit in Delft. Na zijn afstuderen in 1998 werkte hij bij Crycle Cryogenic in Leimuiden en vervolgens bij Stork Product Engineering in Amsterdam. Op 1 december 1999 begon hij bij het KNMI aan een onderzoek waarin klimaatmodellen onderling werden vergeleken op het broeikas-sigitaal. Hij startte zijn promotie-onderzoek op 1 september 2001. Het resultaat hiervan hebt u nu in handen. Momenteel werkt hij bij het Instituut voor Marien en Atmosferisch Onderzoek Utrecht (IMAU) van de Universiteit Utrecht.

